Long-term interactions between vegetation and climate

- Model simulations for past and future -

Guillaume Schurgers

Hinweis

Die Berichte zur Erdsytemforschung werden vom Max-Planck-Institut für Meteorologie in Hamburg in unregelmäßiger Abfolge heraus- gegeben.

Sie enthalten wissenschaftliche und technische Beiträge, inklusive Dissertationen.

Die Beiträge geben nicht notwendigerweise die Auffassung des Instituts wieder.

Die "Berichte zur Erdsystemforschung" führen die vorherigen Reihen "Reports" und "Examensarbeiten" weiter.

Notice

The Reports on Earth System Science are published by the Max Planck Institute for Meteorology in Hamburg. They appear in irregular intervals.

They contain scientific and technical contributions, including Ph. D. theses.

The Reports do not necessarily reflect the opinion of the Institute.

The "Reports on Earth System Science" continue the former "Reports" and "Examensarbeiten" of the Max Planck Institute.

Long-term interactions between vegetation and climate
- Model simulations for past and future -

Dissertation zur Erlangung des Doktorgrades der Naturwissenschaften
im Departement Geowissenschaften der Universität Hamburg
vorgelegt von

Guillaume Schurgers
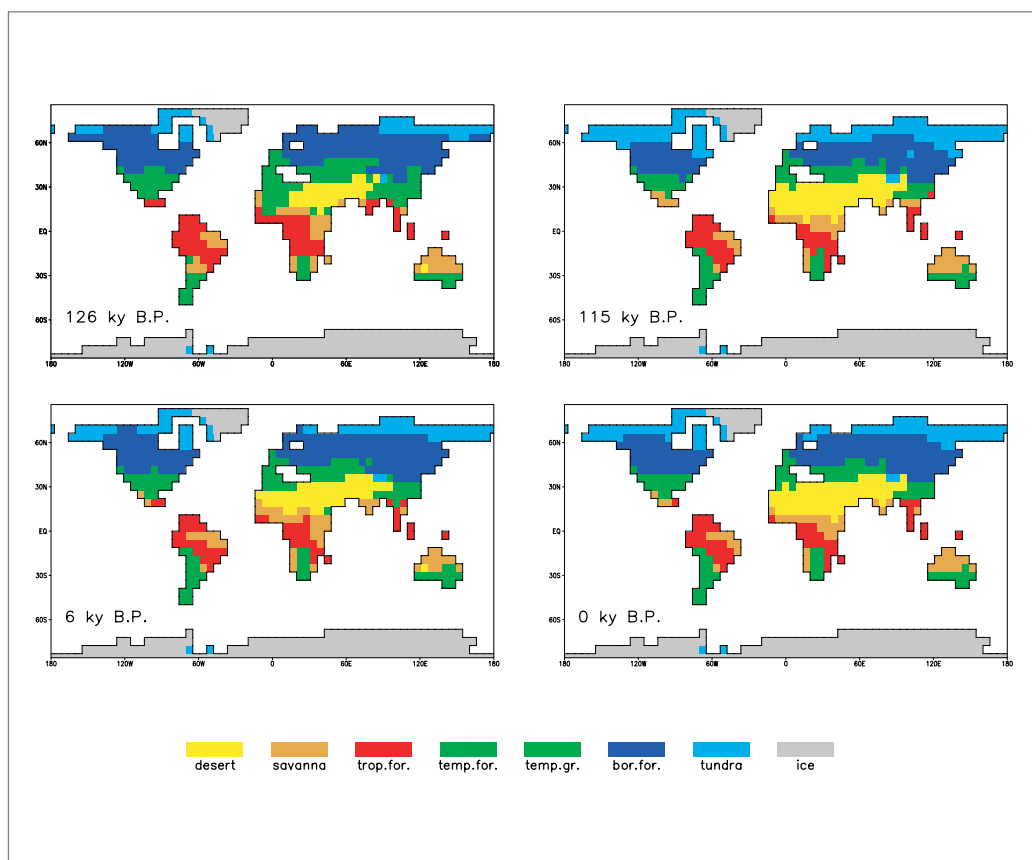aus Valkenswaard, Niederlande

Hamburg 2006

Guillaume Schurgers
Max-Planck-Institut für Meteorologie
Bundesstrasse 53
20146 Hamburg

Long-term interactions between vegetation and climate
- Model simulations for past and future -

Guillaume Schurgers

Hamburg 2006

Contents

Summary

The terrestrial biosphere interacts with the atmosphere on short as well as long timescales. It plays a biogeophysical role in the earth system with respect to the atmosphere, where the land surface represents the boundary conditions, and a biogeochemical role in the cycles of carbon and other nutrients. These interactions between the terrestrial biosphere and climate were studied with a long-term perspective using a complex earth system model, consisting of general circulation models for atmosphere and ocean, an ocean biogeochemistry model, a dynamic global vegetation model and a thermomechanical ice sheet model.

The long-term changes of the biogeophysical and biogeochemical roles of the terrestrial biosphere were studied with simulations for past and future climate. Simulations with paleoclimatic variations in the earth's orbit were performed for two interglacials: the Eemian (128–113 ky B.P.) and the Holocene (9 ky B.P.–present). Long-term simulations of anthropogenic climate change were performed using the IPCC SRES scenarios with an exponential decay of the emissions after 2100. Besides these experiments with the coupled model, several types of sensitivity studies were performed with the vegetation model only.

The paleoclimate experiments revealed an overall amplification of the orbitally induced climate change due to land surface changes. This was mainly caused by the positive feedback between forest growth, surface albedo and surface temperatures in the high latitudes of the northern hemisphere, and by the positive feedback between vegetation growth, surface albedo and moisture transport into the monsoon areas of northern Africa and southeast Asia. Changes in climate caused a gradual decrease of terrestrial carbon storage during both the Eemian and the Holocene, which resulted for both interglacials in an increase of the atmospheric CO_2 concentration. This increase caused only a weak negative feedback on the cooling of especially the northern hemisphere during the interglacials. Radiation changes and hydrological changes contributed to the decreasing carbon storage, temperature changes had two counteracting effects: both global photosynthesis and respiration were influenced, which have a positive and a negative effect on carbon storage respectively. The combination of these two effects causes a large uncertainty in the outcome.

The anthropogenic climate change experiments show a large positive effect of CO_2 increase on photosynthesis. This caused an increase in terrestrial carbon storage, which was partially reduced due to an increase in respiration related to global warming caused by the enhanced CO_2 concentrations. The positive feedback between forest growth, surface albedo and surface temperature, which affected the paleoclimate simulations as well, caused an additional warming up to 2 K in the high latitudes after 1000 years with the SRES A2 scenario.

The shift in type of the forcing from past to future climate (orbital forcing versus CO_2 emissions) causes a major shift of the role of the terrestrial biosphere in the earth system: from an amplifier of climate change due to biogeophysical feedbacks, and a cause of changes in the atmospheric CO_2 concentration, to a damper of the CO_2 increase and thus a damper of climate change.

Chapter 1

Introduction

Abstract

In this chapter the role of the terrestrial biosphere in the earth system is explained, and the biogeochemical and biogeophysical interactions between the terrestrial biosphere and the atmosphere are discussed, as well as the time scales of processes in the terrestrial biosphere. Different types of vegetation models are presented, focussing on the biogeographical, biogeochemical or biogeophysical properties of vegetation, as well as combinations of these, and their application to interactions between vegetation and climate on a long term is presented.

The last paragraph of the introduction provides a detailed outline of the thesis.

1.1   The terrestrial biosphere as part of the earth system

The terrestrial biosphere has always fascinated man. As the environment he lives in, changes in the biosphere had a strong influence on his life. Biosphere and climate have long been a single conception for man, reflecting the biotic and abiotic environment. Even in research, biosphere and climate was long treated as a whole: explorers like Alexander von Humboldt described the natural environment on the their voyages with both biotic and abiotic characteristics, and even the 20th century scientist Wladimir Köppen uses a distribution of climate zones (Köppen, 1931) that is very much related to vegetation occurrence.

Vegetation has often been considered as an inert component of the climate system, merely as a visualisation of the climate. Nevertheless, the effect of vegetation on climate, or the effect of vegetation in the climate system, has long been subject of studies. Current research focusses on two major roles of the biosphere: its role in the biogeochemistry of the earth, and its role in the physical processes occuring in the boundary layer of the atmosphere.

Biogeochemical studies of the terrestrial biosphere focus on the cycles of elements through the biotic and abiotic components of the earth system. Especially carbon has been studied often, for its potential as a greenhouse gas (Arrhenius, 1896), but other elements with importance for the biosphere (nitrogen, phosphorus, sulphur) have been studied as well.

Biogeophysical studies focus on the fluxes of water and energy at the surface. These are influenced by the properties of the surface: presence or absence and type of vegetation, and state of the vegetation and the soil. This influences local weather and climate, but it can have influence on a regional and global scale as well.

Biogeophysics and biogeochemistry were studied with laboratory and field scale experiments, as well as with model simulations.

1.2   Interactions between climate and vegetation: experimental studies

Climate and vegetation interact on different temporal and spatial scales. Micrometeorological conditions are influenced directly by the environment, but even on a mesoscale and a global scale the vegetation interacts with the environment. The most important interactions on a global scale are discussed below.

CO_2, photosynthesis and evaporation

CO_2 increase is assumed to increase photosynthesis on a global scale, as it is one of the molecules needed for photosynthesis and is usually one of the limiting factors. Its effect on photosynthesis has been studied in laboratory experiments as far back as the 18th century, showing enhanced photosynthesis under elevated CO_2 concentrations.

Field scale experiments with increased levels of CO_2 were performed in so-called FACE experiments (Free Air CO_2 Enrichment), in which larger areas (50–500 m^2) of natural ecosystems and cultivated areas were exposed to elevated CO_2 concentrations. Only a few of these large-scale experiments that were performed up to now have reported effects of increased atmospheric CO_2 concentration on production of the ecosystem or crop (Ainsworth and Long, 2005).

The effect of temperature on photosynthesis and respiration

Both photosynthesis and autotrophic and heterotrophic respiration are chemical reactions with a reaction speed depending on temperature. The description for the dependency of chemical conversions on temperature, proposed by Arrhenius at the end of the 19th century, assumes an exponential relation between temperature and reaction speed. The so-called Q_{10}-relation, in which Q_{10} is defined as the multiplication factor of the reaction speed in case of a temperature increase of 10 K, describes basically the same behaviour of reaction speed as the Arrhenius equation.

Although both the pathways of photosynthesis and respiration consist of far more than a single process, and both processes are extremely complex, especially on an ecosystem scale, temperature dependency is in most vegetation or biogeochemistry models still described with an Arrhenius equation or a Q_{10}-relation. This simple representation of temperature effects, without any distinction between ecosystem types or soil types, makes the simulation of temperature effects on carbon storage very uncertain on regional or global scales. The major subject of discussion is whether photosynthesis and respiration differ in their dependency on temperature on a global scale, and which process is more sensitive to temperature changes in case of a difference. Especially the reaction of soil organic carbon to changes in temperature is causing a large uncertainty, and this is an issue of debate at the moment (Knorr et al., 2005; Reichstein et al., 2005).

The effect of changes in solar radiation

Shortwave radiation provides the energy for performing photosynthesis in plants. The radiation is absorbed by chlorophyll in leaves. Moreover, many plant species regulate the timing of their growth and development by the daylength.

According to Churkina and Running (1998), radiation alone is only a minor factor in limiting vegetation growth. It is usually a combination of temperature and radiation that causes the limitation, especially in high latitudes. The difference in contribution of the direct and diffuse component of shortwave radiation is important for its effect on photosynthesis. An increase of cloud cover results in a decrease of direct radiation and an increase of diffuse radiation. The overall amount of incoming radiation will go down, but the increase in diffuse radiation might increase photosynthesis actually due to a more efficient use by the canopy (Roderick et al., 2001; Gu et al., 2003).

The effect of changes in water availability

Plants require water, not only to perform photosynthesis, but for transport as well. Water availability is crucial for vegetation growth in many regions. Except for the regions with tropical rainforest, water is the most important limiting factor for vegetation growth between 30°N and 30°S (Churkina and Running, 1998). Drought can have a severe impact on gross primary production. Ciais et al. (2005) estimate a reduction of 30% due to the extreme heat and drought event for Europe in 2003, for which especially the reduction in eastern Europe was caused by a precipitation deficit.

1.3   Interactions between climate and vegetation: modelling studies

Experimental studies result in understanding of vegetation effects on a local scale. To apply this knowledge to regional or global scales, modelling is the most effective tool. Vegetation modelling has concentrated in different themes, depending on the aim of the study field: biogeography, biogeochemistry and biogeophysics.

Biogeography

The field of biogeography studies the distribution of plant species or plant types over the earth. Models for simulating a biogeographical distribution usually use a set of conditions for each type of plant or ecosystem that constrain the type to certain climatic circumstances, the so-called bioclimatic envelopes. In relation to climate change, biogeographical models were used to study the impact of modelled or predicted changes in the climate on the distribution of plants.

Several models are available, such as BIOME (Prentice et al., 1992) and SIVM (Cosgrove et al., 2002). A lot of paleoclimate and paleovegetation research has been done with the BIOME model (Prentice et al., 1992). Experiments where performed using results from paleoclimate runs from gen-

eral circulation models as input, e.g. by Prentice et al. (1993b) for 21 ky B.P. (with input from the ECMWF model), by Harrison et al. (1995) for the beginning and ending of substage 5e (125-126 ky B.P. and 115 ky B.P., with input from CCM1) and by Harrison et al. (1998) for 6 ky B.P. (with input from several GCMs).

Biogeochemistry

The field of biogeochemistry studies the cycles of elements through the atmosphere, biosphere, hydrosphere and lithosphere. The major elements of interest are carbon, nitrogen, phosphorus and sulphur. Of these elements, the carbon cycle was studied most widely, because of the direct relation to the atmospheric CO_2 concentration and its importance as a greenhouse gas (Arrhenius, 1896).

Many models were developed that deal with the carbon cycle. In a first approach, models were developed that focus on the role of the terrestrial biosphere in the global carbon cycle. These models usually contain components for atmosphere and ocean as well, and focus on the sources and sinks of CO_2 (e.g. Björkström, 1979; Goudriaan and Ketner, 1984). Effects of changes in climate are not considered by these models. A second approach originates from forestry models (e.g. Prentice and Leemans, 1990; Leemans, 1991; Prentice et al., 1993a), which predict carbon cycling in a forest stand. These models focus on the role of climate on plant (forest) growth, and operate on a much smaller scale. Many of the principles from these forestry models are still used in models that combine biogeochemistry and biogeography.

Mainly models following the first approach were used to study long-term effects on the carbon cycle. Köhler and Fischer (2004) simulated the carbon cycle model with a box model, using paleoclimate records as input.

Besides these global models, there are many other models dealing with a certain subsystem of the biogeochemical cycles, e.g. dealing with peatland dynamics and carbon storage (Klinger et al., 1996; Hilbert et al., 2000).

Biogeophysics

Biogeophysical models, or land surface schemes, were developed to represent the land surface conditions in atmospheric models. The conditions of the land surface influence the fluxes of energy, water and momentum between the land surface and the boundary layer.

Fraedrich et al. (1999) and Kleidon et al. (2000) performed simulations to estimate the potential effect of land surface changes on the atmospheric circulation by prescribing a land surface as if completely covered by forest or completely covered by deserts.

In numerous studies on paleoclimate, vegetation has been a subject of

interest. The way vegetation is taken into account concerning its biogeo-physical effects, and the way that these effects were modelled, has differed. Henderson-Sellers and McGuffie (1995) distinguished five methods in which changes in vegetation distribution could be taken into account for the atmosphere, listed below:

(1) Ignore vegetation changes, simulate atmosphere with fixed surface parameters

(2) Simulate atmosphere with fixed surface parameters, and calculate the new equilibrium state vegetation afterwards

(3) Calculate equilibrium state vegetation and equilibrium state climate in a iterative way: calculate equilibrium vegetation, update surface parameters, calculate equilibrium climate, calculate new equilibrium vegetation, etc.

(4) Calculate equilibrium state climate from time to time in a transient climate, updating the surface parameters

(5) Couple a dynamic vegetation model and let climate and vegetation equilibrate or run transiently together

By then, coupling in atmosphere models reached till method 3, and method 5 was stated as optimum (Henderson-Sellers and McGuffie, 1995). At the moment, method 5 is common in several coupled atmosphere-biosphere or earth system models.

A land surface scheme in an atmosphere model allows for simulation of both short-term and long-term effects of the land surface. Among the paleoclimate studies, there are studies with atmosphere GCMs using reconstructed vegetation (e.g. from pollen) as input for the land surface scheme. This is done by Lynch et al. (2003), using a maximum and a minimum reconstructed vegetation cover with 11 ky B.P. conditions, or by Wyputta and McAvaney (2001) using a vegetation reconstruction by Adams and Faure (1997) for 21 ky B.P.

Combinations of biogeography, biogeochemistry and biogeophysics

Coupled models of biogeography and biogeochemistry were developed to study the long-term effect of climate change on vegetation. Changes in the carbon cycle can be studied taking changes in vegetation distribution into account. Examples of biogeography-biogeochemistry models, often referred to as dynamic global vegetation models, are IBIS (Foley et al., 1996) and LPJ-DGVM (Sitch et al., 2003).

Many studies were done in which a dynamic global vegetation model uses the input from a climate model to predict the vegetation state. Examples of these are Friedlingstein et al. (1992), François et al. (1998) and Otto et al. (2002), who all use a biosphere model with input from climate models to simulate the vegetation distribution of the Last Glacial Maximum (21–18 ky B.P.). Similar studies are done with the LPJ model, using a forcing from a climate model coupled to BIOME4. Kaplan et al. (2002) use the Hadley

Center Unified Model (UM) coupled to BIOME4 (biogeography model) to model the period from 21 ky B.P. to present in 1 ky steps. Outcome of this model is used to force LPJ (biogeography-biogeochemistry model).

The combination of a biogeographical model with a biogeophysical land surface scheme enables modelling the changes in distribution of plants together with their impact on climate. Rather than prescribing a distribution of ecosystem types for the land surface scheme, the ecosystem types are calculated using a biogeographical model.

In first experiments this was done with an iterative coupling to the atmosphere, as was mentioned before as method 3 in Henderson-Sellers and McGuffie (1995), e.g. in Kubatzki and Claussen (1998) for 21 ky B.P. (coupled with ECHAM4), in Claussen et al. (1998) for 6 ky B.P. and 21 ky B.P. (coupled with ECHAM3.2) and in De Noblet-Ducoudré et al. (2000) for 6 ky B.P. (coupled with ECHAM and with LMD). This iterative coupling was done by running the atmosphere for a few years, calculating an equilibrium vegetation corresponding to this climate, and using this equilibrium vegetation to derive new surface conditions, which were used to force the atmosphere again.

Later experiments were performed with a biogeography model coupled to an atmosphere model directly. The Hadley Center Unified Model (UM) was coupled to BIOME4 (Kaplan et al., 2002). Drawback of this method is that changes in the vegetation take place instantaneously, as it reflects an equilibrium vegetation. To encorporate dynamic changes of the vegetation, a biogeochemical component has to be added to simulate vegetation growth.

The combination of biogeochemistry and biogeophysics is often used for representation of CO_2 and water vapour exchange by vegetation. Because the exchange of both gases takes place through the stomata in leaves, and the resistance of these stomata depends on the water stress in plants, the exchange of both gases is closely connected. This is represented in biogeochemical-biogeophysical models. Lüdeke et al. (1994) presented a model with 32 vegetation types that can be prescribed.

Models that combine biogeography, biogeochemistry and biogeophysics can be considered as the state-of-the-art representation of vegetation for use within earth system models. Especially for long-term effects, the changes of vegetation distribution become important, and both land surface and carbon storage can change substantially over longer time scales, with considerable influence on climate.

Climate change experiments including all these aspects were performed for anthropogenic global warming studies by Cox et al. (2000) and Dufresne et al. (2002). Paleoclimate experiments including these three aspects were performed with earth system models of intermediate complexity (Claussen et al., 2002), for both time slices and transient experiments, and with complex earth system models, for time slices only.

The CLIMBER model was used to perform simulations for the mid-

Holocene (6 ky B.P., Ganopolski et al., 1998; Claussen et al., 2003) and time slice experiments for present-day and 8 ky B.P. together with a transient simulation from 8 ky B.P. to present (Brovkin et al., 2002). Cox et al. (2000) used the HadCM3 model combined with TRIFFID, feeding back both changes in the land surface parameters and changes in the carbon storage on land. The model was applied to the period 1850-2100. Doherty et al. (2000) performed time slice simulations for 6 ky B.P. and present for North-Africa with the GENESIS-IBIS model.

1.4   Time scales of the terrestrial biosphere

Interactions between plants and their environment take place on a range of temporal scales. Probably the smallest scale of interest for its influence on the environment is concerned with the opening and closure of stomata, which can take place rather abruptly, depending on the environmental conditions in the layer of air near the surface of the leaf, and influencing the composition of this layer as well. A next important time scale is one day. Plants react strongly to the diurnal cycle because of their light dependence, and thereby photosynthesis and the exchange of CO_2 have a clear diurnal cycle. This increase in temporal scale usually indicates an increase of spatial scale as well. The annual cycle is important in many regions outside the tropics. Either driven by light intensity, or by rain season occurrence, extratropical vegetation exhibits a clear annual cycle in many processes influencing the environment as well, including e.g. net ecosystem CO_2 exchange and albedo. Changes in the vegetation composition are important, as this can change both land surface properties and carbon storage of an ecosystem. The typical time scale for changes in the vegetation composition is 1–100 years. Soil formation or soil destruction take place on even longer time scales (100–1000 years). This will influence not only carbon storage, but the physical properties of soils play an important hydrological role: changes in the water retention of soils will alter evaporation and runoff. For even longer time scales (10,000-100,000 years), evolution of plants becomes important as a way to adapt to a changing environment.

For the studies presented in this thesis, time scales concerning the annual cycle and beyond are of interest. Changes in the annual cycle, changes in carbon storage in soils, and changes in plant composition of areas were taken into account. Not taken into account were soil formation and plant evolution.

1.5 Outline of this thesis

The biogeochemical and biogeophysical interactions between atmosphere and vegetation, as described in this chapter, were studied on long time scales. Up to now, these effects were studied only with complex models on shorter time scales, or with intermediate complexity models on (short as well as) long time scales. At the Max Planck Institute for Meteorology and the University of Wisconsin a new complex earth system model was developed, which was used to study these interactions on long time scales. The earth system model consists of components for atmosphere and ocean dynamics, ocean biogeochemistry, terrestrial vegetation, and ice sheets. This model framework is described in **chapter 2**, with special focus on the description and evaluation of the vegetation component, and its biogeochemical and biogeophysical interactions with the atmosphere.

Chapter 3 describes a short study on timescales in the terrestrial biosphere, with special attention for the possible effect of accelerating the insolation forcing for simulations of the terrestrial vegetation.

In **chapter 4** the earth system model is used to study the biogeophysical interactions for a period of the last interglacial (Eemian). Unaccelerated as well as accelerated experiments were performed with insolation changes as forcing. Climate change causes changes in the natural land surface, and the feedbacks of these changes on climate are studied.

The same period in the last interglacial is compared to the current interglacial (Holocene) in **chapter 5**, focussing on the biogeochemistry of the land surface. Experiments with the earth system model, as well as experiments with the vegetation model only, forced with climate data from the coupled experiments, were used to distuinguish the climatic factors that drive the carbon storage in the terrestrial biosphere during interglacials.

Biogeophysics and biogeochemistry of the interglacials are combined in a short comparison study in **chapter 6**. The effects and mutual influences of both types of interactions are discussed.

The biogeophysical and biogeochemical effects of vegetation under a different kind of forcing were studied in **chapter 7**: the anthropogenic effects caused by emissions of CO_2 were simulated. Climate and vegetation change, and their mutual influence, were studied in experiments with prescribed CO_2 emissions from 1750 to 2000 according to historical reconstructions, and from 2000 to 3000 according to different scenarios. Special focus of this study is the long-term effects of elevated CO_2 concentrations and global warming on terrestrial carbon storage.

General conclusions, and a comparison between experiments forced with changes in insolation and experiments forced with emissions of CO_2 are drawn in **chapter 8**.

Chapters 4 and 7 were submitted in a slightly altered form to *Climate Dynamics* and *Global and Planetary Change* respectively. Chapter 5 is in-

tended to be submitted to *Climate of the Past.* Co-authors for these manu-
scripts were mentioned on the title pages of the chapters. For each chapter,
the simulations used were summarized in a table. An overview of all expe-
riments used in this thesis is provided in the appendix (table A.1).

Chapter 2

Model description and model evaluation

Abstract
In this chapter, the earth system model and the dynamic vegetation model within it are introduced. The changes made to the original vegetation model are described. Biogeographical distribution and biogeochemical features of a pre-industrial control run vegetation are compared to estimates from observations and to other modelling studies. Special focus is put on the evaluation of the effects caused by changes in the vegetation parametrization. The parametrization of the biogeophysical feedbacks to the atmosphere is described and evaluated.

Note
Shortened versions of paragraph 2.3 and 2.6 were part of the manuscript on Eemian land surface changes (chapter 4), submitted to *Climate Dynamics*, as: Schurgers, G., Mikolajewicz, U., Gröger, M., Maier-Reimer, E., Vizcaíno, M., Winguth, A. The effect of land surface changes on Eemian climate.
Paragraph 2.4 was part of the manuscript on interglacial carbon storage (chapter 5), to be submitted to *Climate of the Past*, as Schurgers, G., Mikolajewicz, U., Gröger, M., Maier-Reimer, E., Vizcaíno, M., Winguth, A. Changes in terrestrial carbon storage during interglacials: a comparison between Eemian and Holocene.

2.1   The earth system model

An earth system model for long-term climate studies was developed. The model contains the most important components for studies on long-term climate change: atmosphere and ocean dynamics, ice sheet dynamics, terrestrial vegetation and ocean biogeochemistry. The atmosphere is modelled with the general circulation model ECHAM 3.6 (DKRZ, 1993), the ocean with the ocean general circulation model LSG 2 (Maier-Reimer et al., 1993), the ice sheets with SICOPOLIS (Greve, 1997), the terrestrial vegetation, both for land surface properties and for carbon storage, with the dynamic global vegetation model LPJ (Sitch et al., 2003) and the ocean biogeochemistry with HAMOCC (Maier-Reimer, 1993). A detailed description of the earth system model is given by Mikolajewicz et al. (submitted), and the single model compartments were described in the respective publications. Main features of the model are given in this paragraph.

The atmosphere general circulation model ECHAM 3 is a spectral model, used here with a T21 resolution (roughly $5.6° \times 5.6°$), 19 vertical levels and a time step of 40 minutes. The prognostic variables are vorticity, divergence, temperature, humidity, surface pressure, and cloud water. The land surface is represented with five soil layers regarding temperature, and with a single layer regarding water for each gridcell. Land surface properties are used as input for the model, and affect the energy and water balance at the surface.

The ocean general circulation model LSG 2, an improved version of the LSG model (Maier-Reimer et al., 1993), is used here on an Arakawa E-grid with an effective resolution of roughly $4.0° \times 4.0°$, with 22 vertical levels and a time step of 5 days, and a time step of 1 day for the thermodynamics of the surface layer. A simple dynamic sea ice model is incorporated in the ocean model. The coupling between the atmosphere and the ocean in the atmosphere-ocean general circulation model ECHAM-LSG is described in Mikolajewicz et al. (submitted). The atmosphere provides heat fluxes and water fluxes to the ocean, the ocean calculates surface temperature and sea ice distribution, which are passed to the atmosphere model.

The marine biogeochemistry model HAMOCC3 (Maier-Reimer, 1993) uses the same grid as the ocean model, and has a time step of 1 month. Most important tracers in the ocean are simulated, including CO_2, particulate organic carbon and $CaCO_3$, all with 3 carbon isotopes, as well as alkalinity, phosphate and silicate. It uses radiation and wind data from the atmosphere model, advection takes place with the same advection scheme as used in the ocean model for temperature and salinity. A sediment module was added in order to represent long-term storage of $CaCO_3$ in sediments.

The ice sheet model SICOPOLIS (Greve, 1997) calculates dynamics and thermomechanics of the land-based ice masses. It provides the atmosphere with orography and glacier mask, and the ocean with runoff and glacier calving. The model was used with a grid of 80×80 km and 21 ice layers

and 11 lithosphere layers, and with a time step of 1 year.

The dynamic global vegetation model LPJ (Sitch et al., 2003) uses the same horizontal grid as the atmosphere, and has a time step of 1 year, although certain processes are calculated using monthly or even daily time steps. The model provides the atmosphere with changes in the land surface, which will be discussed in paragraph 2.3.
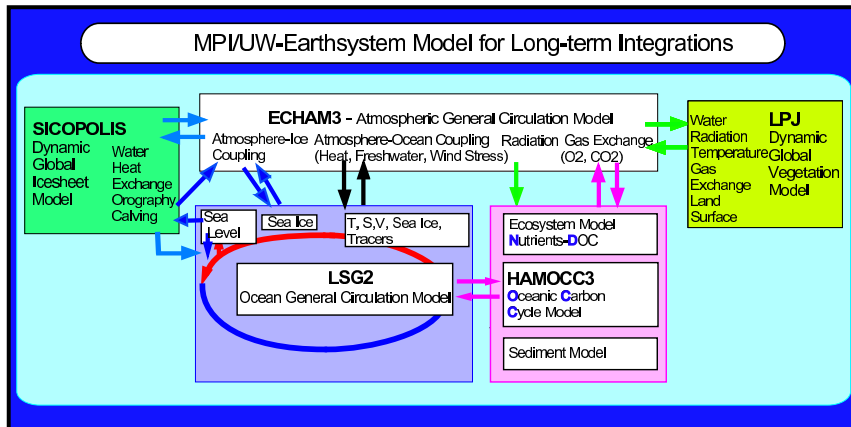
Figure 2.1: *Overview of the earth system model.*

The atmospheric CO_2 concentration is calculated from fluxes of CO_2 between the terrestrial biosphere and the atmosphere and between the ocean and the atmosphere. It is modelled as a global average, assuming that mixing in the atmosphere causes a relatively homogeneous distribution of CO_2. An overview of the earth system model is given in figure 2.1. State-of-the-art general circulation models for the atmosphere and the ocean are typically used for experiments up to a few hundred years. As the aim of the earth system model is simulation of long-term climate change for both paleoclimate periods and future climate change, several compromises have been made to allow for timespans one to two orders of magnitude longer than used in the state-of-the-art models.

A periodically-synchronous coupling technique was applied, (synchronous) periods of typically two years with the fully coupled model were followed by longer (asynchronous) periods in which the ocean model was driven with fluxes from a nonlinear energy balance model at the ocean surface. During these periods, the vegetation model and the ice sheet model were driven with climate data that were stored from previous synchronous periods. The length of this climate archive was 8 years for all experiments performed, corresponding to a typical length of the asynchronous period. For some of the experiments, the length of the asynchronous period was fixed at 8 years, for other experiments it was calculated depending on the deviation of the heat

flux from its previous synchronous state (see Mikolajewicz et al., submitted, for more details).

For the studies described in this thesis, the model was used in two different setups, using all components or all except the ice sheet model. For chapters 4, 5 and 6 the model is used without the ice sheet model. The experiments in these chapters were driven by changes in the orbital forcing. For the experiments in chapter 7, the model was used including the ice sheet model. The experiments in these chapters have a fixed orbital forcing, and were driven by anthropogenic emissions of CO_2 into the system. Chapters 3, 5, 6 and 7 contain experiments in which the vegetation model was used in an offline mode, forced with climate data from other experiments with the earth system model.

2.2 The dynamic vegetation model

The terrestrial vegetation is modelled with the Lund-Potsdam-Jena dynamic global vegetation model (LPJ-DGVM, Sitch et al., 2003). This model describes the terrestrial vegetation with ten plant functional types (PFTs), which can exist jointly in one gridcell. Within each of these PFTs in the gridcell the carbon cycle is described with four living biomass pools and three litter pools. Each gridcell has another two soil carbon pools. An overview of the carbon cycle with the main fluxes is given in figure 2.2.
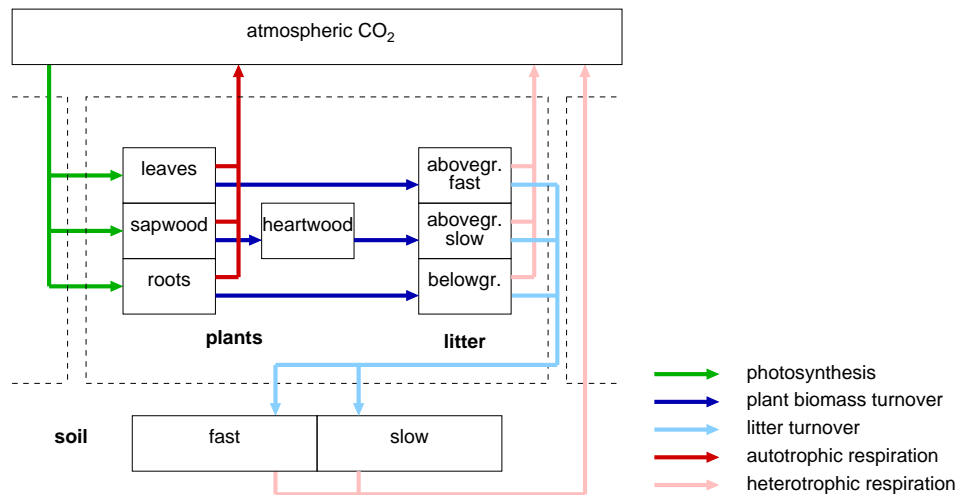
Figure 2.2: *Overview of the main pools and fluxes of carbon within a gridcell. The dashed square indicates a single plant functional type.*

The LPJ model that was coupled to the other components in the earth system model was developed using a version of the original LPJ model from

Sitch et al. (2003) that was adapted to model isotopes, as used in Kaplan et al. (2002) and Scholze et al. (2003). A detailed description of the processes in LPJ can be found in Sitch et al. (2003). The main features for application in the earth system model will be discussed here, and the changes as made compared to the versions in Sitch et al. (2003), Kaplan et al. (2002) and Scholze et al. (2003) will be discussed.

2.2.1   Climate input

The original LPJ model (Sitch et al., 2003) uses temperature, precipitation and sunshine fraction as input. Temperature is a control factor in the biogeographic distribution of plant functional types, as well as a major control on numerous biogeochemical processes. Precipitation is used to drive the water cycle in the model. Sunshine fraction is used to calculate the actual amounts of solar radiation from the potential amounts that are calculated in the model. In the adapted version, the use and calculation of climate parameters was changed. Because more climate data are available from the ECHAM model than the few mentioned above, part of the climate parameters were replaced by more detailed parameters (e.g. temperature). In some other cases, the calculation of climate parameters that was done in LPJ was replaced by parameters calculated in ECHAM (e.g. soil moisture or radiation).

Temperature

The original LPJ uses surface air temperature as driver for most of the temperature-dependent processes. For below-ground processes (root respiration, decay of soil organic matter), a soil temperature was derived, which was calculated from air temperature with a dampening on the annual cycle and a lag depending on depth and soil texture according to Campbell and Norman (1998). For the temperature conditions at the surface, the ECHAM model produces surface air temperature, surface temperature and five levels of soil temperature. As input for the LPJ model, several of these temperatures are used. For the bioclimatic limits, as well as for all aboveground processes such as photosynthesis and respiration, near-surface air temperature (2 meter temperature) is applied. Surface temperature is used for the decay of aboveground litter, a process that takes place at or near the surface. Soil temperature is used for decay of belowground litter, as well as for maintenance respiration in roots. It is taken as a weighted average of the temperatures of the upper three soil layers in ECHAM, reflecting the temperature of the upper one meter of soil.

Hydrology

The original LPJ model contains a hydrological cycle, which is linked to the carbon cycle with the relation between photosynthesis and evaporation. Because hydrological parameters are provided by the atmosphere model as well, the hydrological part in LPJ was removed, and replaced by input data from ECHAM. The new model uses soil wetness from ECHAM, which is used in the calculation of photosynthesis and water stress, allocation of produced carbon over the living biomass pools, carbon turnover rates in soils, and fire probability. Besides that, precipitation from ECHAM is used, which is used only as a limitation for plant establishment.

For soil moisture, the ECHAM3 model uses a single box approach with a depth of 0.5 m for each gridcell. Changes in soil moisture are driven by input into and output from this box, i.e. by precipitation, evapotranspiration and runoff (DKRZ, 1993). Precipitation has two components in the ECHAM3 model: convective precipitation and large-scale precipitation. The evapotranspiration calculation has components for evaporation from wet vegetation, soil moisture, and snow. The evaporation of soil moisture depends on vegetation fraction, horizontal wind speed, humidity, temperature and pressure (DKRZ, 1993). Excess precipitation, mainly when the soil moisture box is close to filled, is transported as runoff into the ocean, spatially depending on the catchment area.

Using the original ECHAM calculation for evapotranspiration rather than a calculation as performed in LPJ has the disadvantage that the coupling between photosynthesis and water loss, as was available in LPJ (Sitch et al., 2003), is not taken into account. This coupling is based on the fact that both photosynthesis and transpiration take place through the same stomata and have thus closely linked resistances. However, the description as used in ECHAM has a better link to the actual meteorological situation, taking wind speed and drag coefficients into account.

Radiation

The original LPJ model calculates incoming shortwave radiation from the radiation reaching the top of the atmosphere (calculated with use of the orbital parameters), multiplied by the cloud-free fraction of air. As incoming radiation at the surface is calculated in ECHAM, it is used directly for the calculation of photosynthesis and potential evapotranspiration. Besides a more accurate estimate of the amount of incoming radiation, this has the advantage that changes in the orbital parameters, as were used for the paleoclimate experiments that will be described, are considered and can influence photosynthesis in a consistent way.

2.2.2   PFT parameters

Because the control run climate of ECHAM3-LSG showed particularly cold regions for the high latitudes in Asia, the vegetation model needed adaptation to changes in this climate. One approach would have been to apply anomalies of the control run climate to a climatology the LPJ model was tuned for. Rather than applying this method, the parameters of the vegetation model were adapted slightly, allowing for more vegetation growth in high latitudes. The 'anomalies' method is only valid as long as the behaviour of the system is linear. The large changes that will be applied to the model for studying the long-term effects might prohibit this. The parameters for the boreal PFTs, as well as for the C_3 herbs, were adapted (table 2.1). Besides these changes, the minimum amplitude needed for the occurrence of boreal needleleaf summergreen trees, which was used in the original model to get a realistic distribution of *Larix spp.* and which was set at 43°C empirically (Sitch et al., 2003), was removed.

Table 2.1: *Adapted parameters for the PFTs.*

PFT	$T_{min,CO2}$ ($^\circ$C)		$T_{min,phot}$ ($^\circ$C)		GDD_{base} ($^\circ$C)	
	orig.	adap.	orig.	adap.	orig.	adap.
Boreal needleleaf evergreen trees	-4.	-6.	15.	10.	5.	2.
Boreal needleleaf summergreen trees	-4.	-6.	15.	10.	2.	-1.
Boreal broadleaf summergreen trees	-4.	-6.	15.	10.	5.	2.
Temperate herbaceous plants	-4.	-8.	10.	5.	5.	-1.

Disadvantage of the changes in the parametrization is that the changes made apply to plant presence and plant growth, but not to respiration of carbon. For this reason, carbon storage will increase in the latitudes that are affected, due to an increase of photosynthesis, whereas respiration will be low due to the low temperatures. This will be discussed in more detail below.

2.3   Land surface parametrization

Biogeophysical feedback from the land surface to the atmosphere has long been neglected. With the awareness that large-scale changes in land cover can influence the balances of water and energy, the land surface was parametrized, and experiments were performed changing these parameters. The land surface parameters used by the the atmosphere model ECHAM3 are surface background albedo and forest fraction for the calculation of surface albedo, vegetation fraction for the calculation of evaporation, and roughness length for calculation of the drag coefficients for energy, water and momen-

tum exchange. In the newly developed earth system model these parameters are derived from the results of the vegetation model LPJ.

The albedo of the land surface has a large impact on the energy balance. It is determined by the type of vegetation cover, the visibility and colour of the bare soil and the presence and smoothness of a snow cover. For the calculation of the background albedo (albedo of the surface without snow cover), the gridcell area is divided over several sub-grid parts: a part that is covered by leaf-covered vegetation, a part that is covered by leafless vegetation and a part that is covered by bare soil. The grid-cell albedo is a weighted average of the albedo values assigned to these compartments:

$$\alpha = c_v \cdot \alpha_{veg,l} + (c_{v,max} - c_v) \cdot \alpha_{veg,nl} + (1 - c_{v,max}) \cdot \alpha_{soil} \qquad (2.1)$$

In this equation, c_v is the leaf-covered vegetation fraction, $c_{v,max}$ is the maximum vegetation fraction, and $\alpha_{veg,l}$, $\alpha_{veg,nl}$ and α_{soil} are the albedos for leaf-covered vegetation, leafless vegetation and soil. The leaf-covered vegetation albedo is constructed from the albedos of the plant functional types. Each plant functional type was assigned an albedo value (see table 2.2), and the values are averaged according to the fraction of (leaf-covered) vegetated area they cover:

$$\alpha_{veg} = \frac{\sum_i (\phi_i \cdot c_{v,i} \cdot \alpha_i)}{\sum_i (\phi_i \cdot c_{v,i})} \qquad (2.2)$$

in which ϕ_i is the phenology state (between 0 and 1, see Sitch et al., 2003), $c_{v,i}$ is the maximum cover fraction and α_i is the albedo of the plant functional type i. The albedo values α_i in table 2.2 were derived from Claussen (1994), with albedos for 17 biomes, and Claussen et al. (1994), with albedos for 13 simple surface types.

Table 2.2: *Albedo (α) and roughness length (z_0) assigned to the plant functional types*

PFT	description	α_i	$z_{0,i}$
1	tropical broad-leaved evergreen	0.12	2.00
2	tropical broad-leaved raingreen	0.12	2.00
3	temperate needle-leaved evergreen	0.13	1.00
4	temperate broad-leaved evergreen	0.13	1.00
5	temperate broad-leaved summergreen	0.16	1.00
6	boreal needle-leaved evergreen	0.13	1.00
7	boreal needle-leaved summergreen	0.16	1.00
8	boreal broad-leaved summergreen	0.16	1.00
9	temperate herbaceous	0.20	0.03
10	tropical herbaceous	0.20	0.03

The values are in agreement with albedo values given in Wilson and Henderson-Sellers (1985), Hagemann et al. (1999) and Milly and Shmakin

(2002). A constant albedo for non leaf-covered area of all plant functional types $\alpha_{veg,nl} = 0.16$ was used. The bare soil albedo is dependent on the soil colour (which is given as input) and on the soil water content (Wilson and Henderson-Sellers, 1985). It is calculated as

$$\alpha_{soil} = w \cdot \alpha_{j,wet} + (1 - w) \cdot \alpha_{j,dry} \qquad (2.3)$$

in which w is the relative moisture content of the soil, and $\alpha_{j,wet}$ and $\alpha_{j,dry}$ are the albedos for wet and dry soil of soil colour j. The soil colour map that is used as input (fig. 2.3a), as well as the albedo values for dark, medium and light soil (table 2.3), were derived from Wilson and Henderson-Sellers (1985). In ECHAM, the total surface albedo is calculated from background albedo and snow cover albedo. For the calculation of the snow cover albedo, the forest fraction from LPJ is used. It is calculated as the sum of maximum cover fractions $c_{v,i}$ for all tree PFTs. Snow cover albedo for forested areas lies between 0.3 and 0.4, snow cover albedo for unforested areas lies between 0.4 and 0.8, dependent on surface temperature (Kukla and Robinson, 1980; DKRZ, 1993).

Table 2.3: *Albedo values for wet and dry soil, according to Wilson and Henderson-Sellers (1985).*

soil colour	$\alpha_{j,wet}$	$\alpha_{j,dry}$
dark	0.07	0.15
medium	0.10	0.20
light	0.18	0.35

The surface roughness is defined as the height above the ground that is obtained when the logarithmic wind profile from well above the canopy is extrapolated to the point where the wind speed would have been 0, thereby ignoring changes in the profile next to the surface. It is used in ECHAM to calculate drag coefficients for the fluxes for water, energy and momentum (DKRZ, 1993). Surface roughness is constructed from the orography roughness and the vegetation roughness length (Claussen et al., 1994):

$$z_0 = \sqrt{z_{0,oro}^2 + z_{0,veg}^2} \qquad (2.4)$$

The vegetation roughness is determined by the amount of vegetation and the type of vegetation. The roughness lengths per plant functional type $z_{0,i}$ were derived from Claussen (1994) and Claussen et al. (1994), and are shown in table 2.2. The vegetation roughness length is calculated from the averaged drag coeffcients (Claussen, 1991; Claussen et al., 1994), which uses a blending height z_b:

$$\frac{1}{ln^2(\frac{z_b}{z_{0,veg}})} = \sum_i \frac{c_{v,i}}{ln^2(\frac{z_b}{z_{0,i}})} + \frac{1 - c_{v,max}}{ln^2(\frac{z_b}{z_{0,soil}})} \qquad (2.5)$$
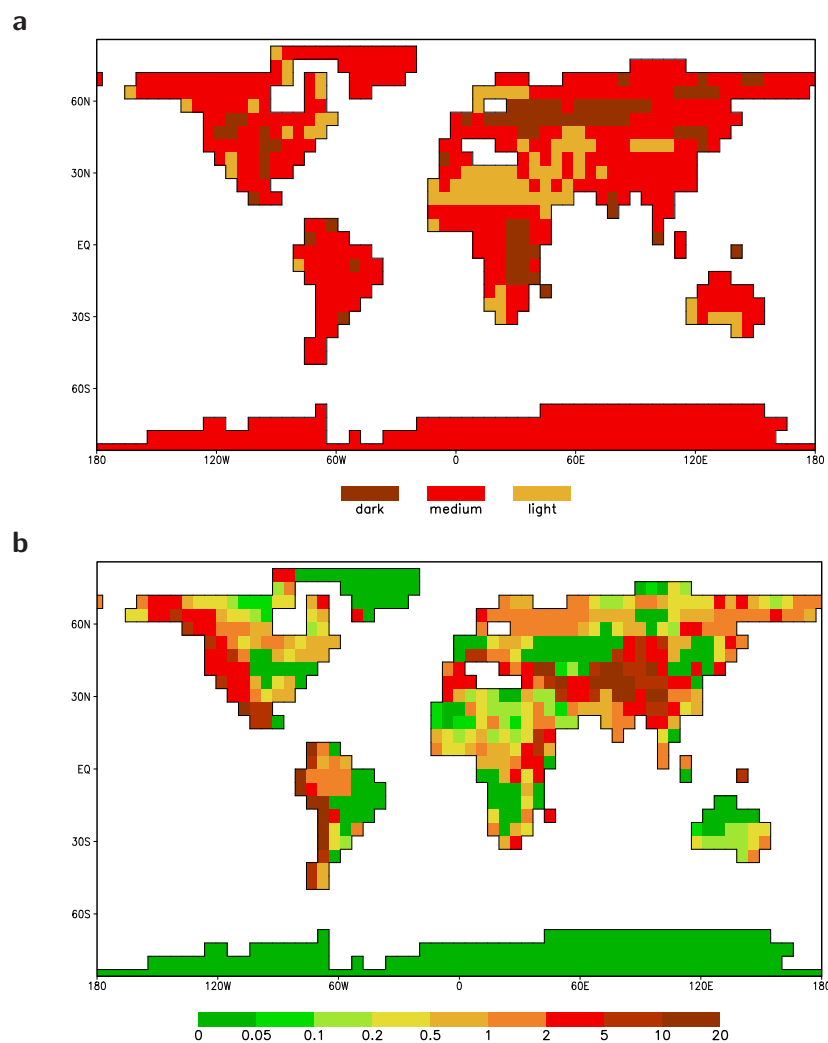
Figure 2.3: *(a) Soil colours for the soil albedo calculation, interpolated from a $1° \times 1°$ data set by Wilson and Henderson-Sellers (1985), and (b) orography rougness length (m) used in the roughness length calculation, derived from the original ECHAM3 input fields.*

The last part of the equation calculates the contribution of bare soil to the vegetation roughness length. Soil roughness $z_{0,soil} = 0.005$ m and the blending height $z_b = 100$ m, as taken from Claussen et al. (1994). The orography roughness $z_{0,oro}$ (equation 2.4) is given as input, and was derived from the original ECHAM roughness length field (fig. 2.3b).

The amount of vegetation influences evaporation. ECHAM uses the vegetation fraction (the fraction of a gridcell covered with vegetation) to calculate evaporation (DKRZ, 1993). This fraction is the sum of all individual PFT covers, corrected with the phenology state of each PFT. Vegetation fraction, as well as surface background albedo, feature a seasonal cycle.

2.4 Biome description

As a tool for evaluation of the vegetation distribution, a scheme was developed to represent the regular output of the vegetation model in so-called biomes or macro-ecosystems. In order to compare the modelled distribution of plant functional types with vegetation reconstructions for the past, the combinations of plant functional types as were simulated by LPJ are converted into seven biome classes. Several schemes have been described in literature, the classes that are proposed here are (1) able to present the major conversions that take place on longer time scales, (2) are structured in a way that is understandable and (3) can be derived from the LPJ output, without putting in too much uncertainty, but with enough distinction between them to show shifts of vegetation over long time scales. The scheme that is used here uses the fractions of coverage from the ten plant functional types from the output of the vegetation model, together with the soil temperature from the atmosphere model. The distribution is explained in table 2.4.

Table 2.4: *Conditions used to distinguish biomes.*

c_f		c_v	c_{v} comp	biome	
$c_f > 0.8$	$c_{f,trop} > c_{f,temp}$ $c_{f,trop} > c_{f,bor}$			Tropical forest	
	$c_{f,temp} \ge c_{f,trop}$ $c_{f,temp} > c_{f,bor}$			Temperate forest	
	$c_{f,bor} \ge c_{f,trop}$ $c_{f,bor} \ge c_{f,temp}$			Boreal forest	c_f
$c_f \le 0.8$	$\sum n_{T<273K} < 8$	$c_v \le 0.2$		Desert	
		$c_v > 0.2$	$c_{v,C4} \ge c_{v,C3}$	Savanna	
			$c_{v,C3} > c_{v,C4}$	Temperate grassland	
	$\sum n_{T<273K} \ge 8$			Tundra	

c_f forest fraction (sum of cover of all tree PFTs); $c_{f,trop}$ tropical forest fraction (sum of cover of all tropical tree PFTs); $c_{f,temp}$ temperate forest fraction; $c_{f,bor}$ boreal forest fraction; c_v vegetation fraction (sum of cover of all PFTs); $\sum n_{T<273K}$ number of months with average soil temperature below 273 K; $c_{v,C4}$ C$_4$ herbs fraction; $c_{v,C3}$ C$_3$ herbs fraction.

2.5   Evaluation of the vegetation model

The earth system model and the vegetation model as part of this were evaluated with several types of experiments. A control run was performed with the earth system model, for which the biogeographic distribution of the ecosystems as well as regional and global carbon storage were compared to other studies. Besides that, the sensitivities of the vegetation model for temperature and CO_2 changes were compared to the sensitivity of the model with the original parametrization and hydrological calculations.

2.5.1   Method

A pre-indrustrial control run of 10,000 years from the coupled earth system model, including atmosphere and ocean dynamics, terrestrial biosphere and ocean biogeochemistry, was used for model evaluation. The experiment was performed applying a periodically synchronous coupling, with a synchronous period applying the fully coupled model of 2 years, followed by an asynchronous period in which the atmosphere was replaced by an energy balance scheme, of which the length depends on the deviation of the ocean surface from its synchronous state. A spinup was performed with a fixed CO_2 concentration of 280 ppm, in order to equilibrate the carbon pools in the terrestrial biosphere and the ocean. For the pre-industrial control run, CO_2 concentration was calculated prognostically. Two control run with shorter asynchronous periods were performed to compare the effect of the introduction of the new land surface parametrization on climate: one of these experiments has a dynamic land surface ($ACTL^+$), the other has the land surface prescribed to the original ECHAM3 parametrization ($ACTL^-$).

2000 years from the climate data of the lon control run (CTL^+) were used for offline sensitivity experiments with the vegetation model only. The sensitivities of the model for changes in temperature and atmospheric CO_2 concentration were tested by enhancing or decreasing the temperature globally, or by prescribing the CO_2 concentration at higher or lower levels than 280 ppm. Results from these sensitivity experiments were compared with results from a similar set of sensitivity experiments with the model with original parametrization (see table 2.1), driven with NCEP reanalysis 2 data[1]. For these experiments, soil moisture was calculated in the vegetation model itself according to the original model (Sitch et al., 2003), rather than using the soil moisture from the reanalysis, because the provided soil moisture differs widely from the one used in the coupled experiments due to different parametrizations.

Both biogeographical and biogeochemical parameters from the terrestrial biosphere in the pre-industrial control run were compared with esti-

---

[1]NCEP Reanalysis 2 data were provided by the NOAA-CIRES Climate Diagnostics Center, Boulder, Colorado, USA. http://www.cdc.noaa.gov

mates from inventories in the literature and with other modelling studies. Results of the sensitivity experiments were compared to the sensitivities of the original LPJ model and to other models. All experiments used in this chapter are summarized in table 2.5.

**Table 2.5:** *Overview of the experiments used in this chapter*

CTL$^+$	control run with present-day insolation and interactive land surface (10 000 years)
ACTL$^+$	control run with present-day insolation and interactive land surface, length of the asynchronous periods reduced compared to CTL$^+$
ACTL$^-$	control run with present-day insolation and prescribed (present-day) land surface
SENST_O	temperature sensitivity experiments (global anomalies applied of -5 K, -2 K, 0 K, +2 K, +5 K) with the old parametrization and hydrology, forced with 20 years of NCEP reanalysis data (1980–1999, Kanamitsu et al., 2002)
SENST_N	temperature sensitivity experiments (global anomalies applied of -5 K, -2 K, 0 K, +2 K, +5 K) with the new parametrization and hydrology, forced with 20 years of the CTL$^+$ experiment
SENSC_O	CO_2 sensitivity experiments (prescribed concentrations applied of 200 ppm, 280 ppm, 360 ppm, 520 ppm, 840 ppm) with the old parametrization and hydrology, forced with 20 years of NCEP reanalysis data (1980–1999, Kanamitsu et al., 2002)
SENSC_N	CO_2 sensitivity experiments (prescribed concentrations applied of 200 ppm, 280 ppm, 360 ppm, 520 ppm, 840 ppm) with the new parametrization and hydrology, forced with 20 years of the CTL$^+$ experiment

2.5.2   Results

Biogeographic distribution of vegetation

The distribution of the main biomes is shown in figure 2.4 (the method applied to derive biomes from the cover fractions of plant functional types is described in paragraph 2.4).

The areas covered by these biomes are compared to estimates from the IPCC Third Assessment Report (Houghton et al., 2001) in table 2.6. It should be noted that the modelled vegetation from the pre-industrial control run does not take any human influence (land use, deforestation) into account, whereas the estimates in the table are based on observations. This can be illustrated most clearly with the area of cropland, roughly 15×10^6 km^2, which is not included in the simulation. Table 2.6 shows that the area of savanna is underestimated by the model, and the areas of tropical forest, temperate grassland, boreal forest and tundra are overestimated. For both boreal forest and tundra this is due to an extension of the area too far
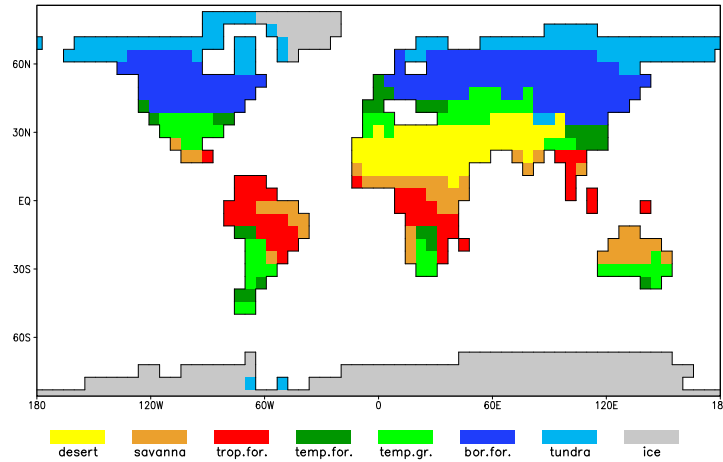
Figure 2.4: *Global distribution of biomes as calculated from PFT cover fractions in LPJ, average for the pre-industrial control run. For description of the biome calculation see paragraph 2.4.*

southward in the simulation (fig. 2.4). Temperate grassland is presently often replaced by cropland.

Because biases in the biome distribution can be either due to biases in the vegetation model, or to biases in the climate that is simulated to drive the vegetation model, a comparison is made with the distribution of Köppen's climate zones (Köppen, 1931). Köppen's distribution is widely used, and constructed in a way that is good for comparing the results with: the distribution of climatic zones is closely related to vegetation zones, and it is easily derived from key climatic parameters (temperature and precipitation).

Figure 2.5 displays the distribution of the climatic zones according to Köppen (1931) for the control run and for an average of 20 years from NCEP Reanalysis (1980–1999, Kanamitsu et al., 2002). Except for some small-scale features which are not resolved in the earth system model, most climate zones from the pre-industrial control run show a fair agreement with the NCEP Reanalysis data for the low latitudes (fig. 2.5). The area of *Af* (tropical rainforest) climate is slightly underestimated, and oppressed by the *Aw* (savanna) climate. The high latitudes are in general too cold compared to the NCEP reanalysis data, which results in a large overestimation of the area of the *ET* (tundra) and *EF* (snow) climate and an underestimation of the area of *Df* and *Dw* climate (humid and winter dry land climate). This is likely to have caused the overestimation of boreal forest and tundra area (table 2.6).

The slight overestimation of tropical rain forest (table 2.6) that occurred in the control run is not represented in the Köppen classification of the

Table 2.6: *Estimated and simulated areas and carbon stocks for the main biome types. Estimates come from the IPCC Third Assessment Report (Houghton et al., 2001), simulated values from the pre-industrial control run (CTL).*

| | Area (10⁶ km²) | | | Carbon density (kg C m⁻²) | | | | | | NPP (kg C m⁻² y⁻¹) | | |
| | | | | Vegetation | | | Soil | | | | | |
	Simulated	IPCC-AR3[a]		Simulated	IPCC-AR3[a]		Simulated	IPCC-AR3[a]		Simulated	IPCC-AR3	
Tropical forest	19.8	17.6	17.5	12.8	12.0	19.4	10.2	12.3	12.2	1.14	0.78	1.25
Temperate forest	9.0	10.4	10.4	10.5	5.7	13.4	19.5	9.6	14.7	0.86	0.63	0.78
Boreal forest	32.8	13.7	13.7	13.6	6.4	4.2	59.5	34.4	24.7	0.80	0.23	0.19
Savanna	17.6	22.5	27.6	3.6	2.9	2.9	4.6	11.7	9.0	0.44	0.79	0.54
Temperate grassland	20.0	12.5	17.8	2.3	0.7	1.3	10.7	23.6	9.9	0.43	0.42	0.39
Tundra	12.7	9.5	5.6	0.6	0.6	0.4	9.3	12.7	20.6	0.05	0.11	0.09
Desert	23.0	45.5	27.7	0.2	0.2	0.4	0.4	4.2	5.7	0.02	0.03	0.13
Croplands[b]	–	16.0	13.5	–	0.2	0.3	–	8.0	12.2	–	0.43	0.30
Wetlands[b]	–	3.5	–	–	4.3	–	–	64.3	–	–	1.23	–
Ice[c]	14.2	–	–	–	–	–	–	–	–	–	–	–

[a] The IPCC Third Assessment Report provides two estimates: the first is from WBGU (1988), the second is from Mooney et al. (2001).
[b] Not available from the earth system model.
[c] Not provided by the IPCC Third Assessment Report.
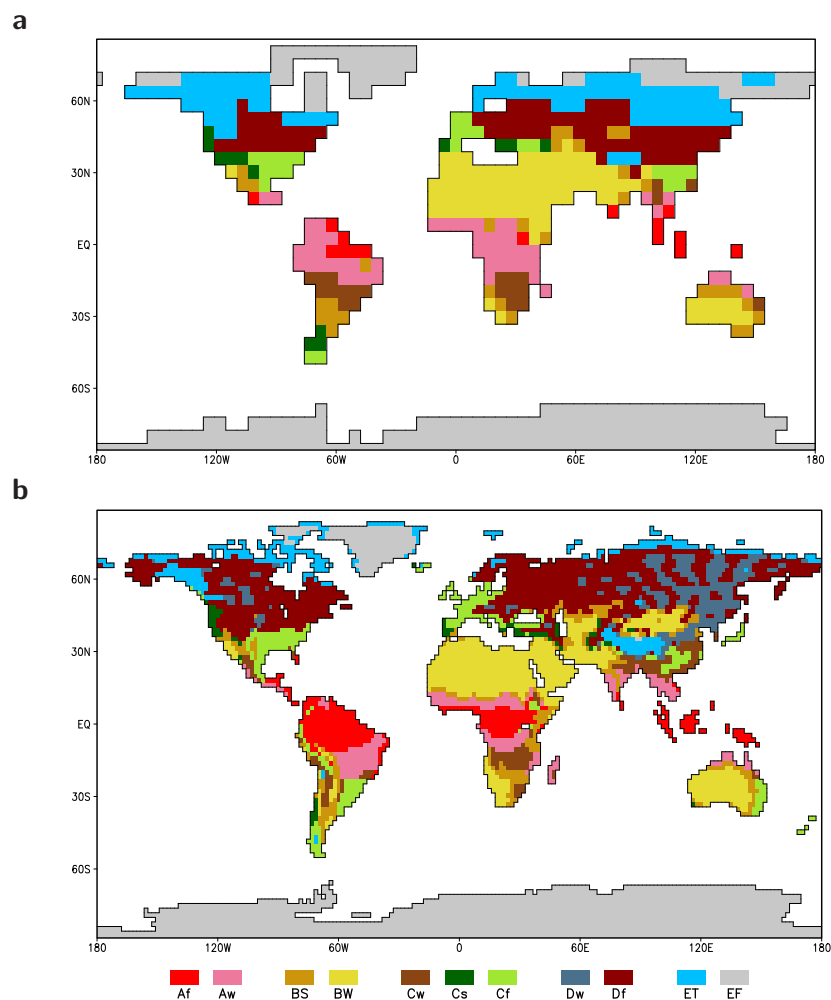
Figure 2.5: *Comparison of the distribution of climatic zones according to Köppen (1931) for (a) the pre-industrial control run with (b) the distribution derived from NCEP Reanalysis data (1980–1999, Kanamitsu et al., 2002). Köppen's classification: Af tropical rainforest climate; Aw savanna climate; BS steppe climate; BW desert climate; Cw warm winter dry climate; Cs warm summer dry climate; Cf humid temperate climate; Dw winter dry cool climate; Df winter humid cool climate; ET tundra climate; EF ice climate.*

control run climate, this bias is most likely a feature of the vegetation model rather than of the climate model. The cold bias in the high latitudes is present in the Köppen classification as well as in the vegetation estimates, this is a feature of the climate model.

Carbon storage and Net Primary Production

Table 2.6 compares the simulated areas and carbon storage in the biome types with estimates from the IPCC Third Assessment Report. Simulated carbon storage in vegetation per area is in most cases rather similar to the estimates from the Third Assessment Report (Houghton et al., 2001). Boreal forests shows a remarkably higher simulated amount, slightly higher amounts are simulated for savanna and temperate grassland.

These differences cause a large positive anomaly in total carbon storage in the experiments compared to estimates from literature, which is caused almost completely by the too high carbon storage in boreal forests and the overestimation of the area covered by these forests. The simulated carbon storage for the control run is compared to estimates of carbon storage from other studies in table 2.7.

Living biomass in the control run (CTL^+) is high, but this is generally the case for the LPJ model. Litter and soil carbon storage show a wide range of estimates, which reflects the uncertainty about global carbon storage in soils. Nevertheless, the control run gets clearly out of the range of other estimates, which is caused by the changes in parametrization, as explained above. As these changes in total carbon might influence the results of the studies presented in this thesis, a sensitivity analysis was performed to see how the terrestrial carbon storage in the model reacts to changes in temperature and CO_2 concentration. Due to the high carbon storage in soils, total terrestrial carbon storage is overestimated in the CTL^+ experiment as well, compared to other models.

Model sensitivity

The changes made to the parametrization of the vegetation model, as shown in table 2.1, were tested by comparing sensitivity results of the new model to changes in temperature and CO_2 concentration to the sensitivity of a model with the original parametrization (table 2.1) and soil hydrology calculations, driven with NCEP reanalysis 2 data.

The sensitivity of changes in vegetation carbon storage, litter and soil carbon storage, and net primary production (NPP) were compared in figure 2.6.

The sensitivity of both models for atmospheric CO_2 concentration is rather similar. Both for NPP and for carbon storage in vegetation and litter and soil, the original model seems to be slightly more sensitive. Tempera-

Table 2.7: *Estimates of carbon storage for pre-industrial and present-day inventories and modelling studies.*

reference	model	type	NPP (Pg C y^{-1})	living biomass (Pg C)	litter and soil (Pg C)	total carbon (Pg C)
Bolin et al. (1979)		inventory	63	592	1672	2264
Schlesinger (1991)		inventory	60	560	1500	2060
Cramer et al. (1999)	17 models	veg. model	39.9–80.5 (54.9)			
Cramer et al. (2001)	16 models	veg. model	45–60	500–950	850–1200	
Delire et al. (2003)[a]	IBIS	veg. model	54	634	1336	1970
Sitch et al. (2003)1	LPJ	veg. model	64	923	1841	2764
Gerber et al. (2004)	LPJ	veg. model	66	897	1795	2693
Krinner et al. (2005)[b]	ORCHIDEE	veg. model	64/74	641	1533	2174
Björkström (1979)[c]		coupled model	38–86	560–1090	1400–3000	1960–4090
Goudriaan and Ketner (1984)[d]		coupled model	62	650	2000	2650
Cox et al. (2000)	TRIFFID	coupled model	60	493	1180	1673
Delire et al. (2003)	IBIS	coupled model	54	621	1516	2137
this study[e]	LPJ	coupled model	74	906	2741	3647

[a] provides results from the vegetation model only as well as from the vegetation model coupled to an atmosphere model

[b] first estimate for NPP and carbon pool estimates with a prescribed vegetation pattern, second estimate for NPP with a dynamic vegetation pattern.

[c] different cases were provided: 'large and slow', 'average' and 'small and fast'

[d] 1980

[e] pre-industrial estimate
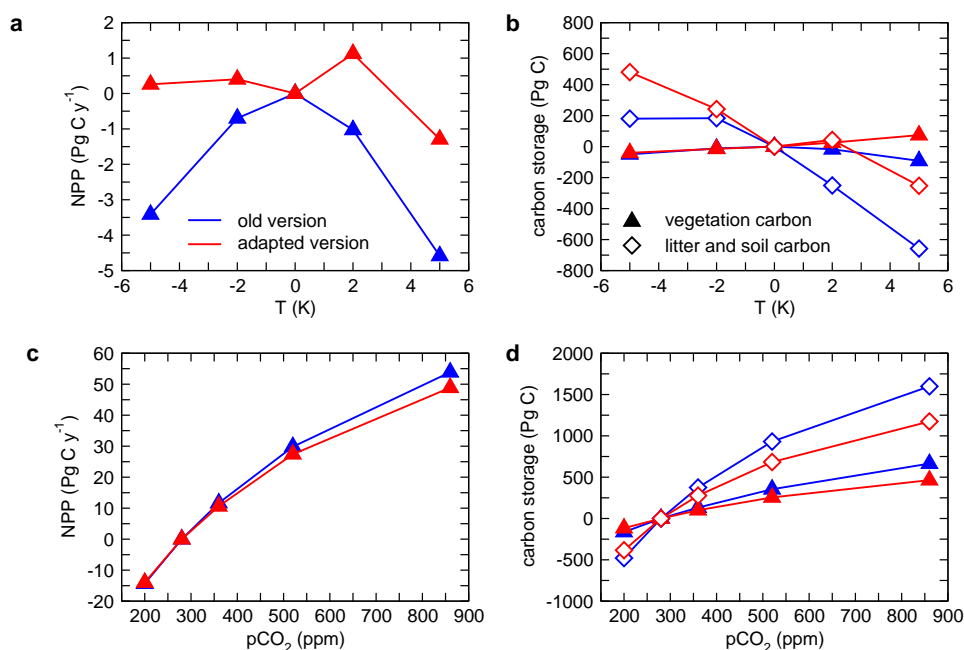
Figure 2.6: *Sensitivity of NPP and terrestrial carbon storage in the old and adapted version of LPJ to changes in temperature and CO_2 concentration. Anomalies of NPP (a, c) and carbon storage (b, d) from a control run with the new model and 20 years of climate data from the control run (CTL^2) and with the old model and 20 years of NCEP reanalysis 2 forcing (1980–1999 Kanamitsu et al., 2002), for different temperature anomalies (a, b, experiments SENST_o and SENST_n) or different atmospheric CO_2 concentrations (c, d, experiments SENSC_o and SENSC_n).*

ture changes cause larger differences between both models in sensitivity than the atmospheric CO_2 concentration. The sensitivity of NPP differs substantially: whereas in the original model NPP goes down rapidly with either an increase or a decrease of temperature, the new model decreases much slower or in case of cooling, hardly at all. Nevertheless, the sensitivity of carbon storage is more similar. Both model versions show a decrease of litter and soil carbon storage with increasing temperatures. The original model reacts more strongly towards higher temperatures, whereas the new model reacts more strongly towards low temperatures. Vegetation carbon storage reacts much less, with a slightly decreased storage for warmer or cooler climate for the original model, and a slightly increased storage with warmer and a slightly decreased storage with cooler climate for the new model.

The sensitivity of the model has changes compared to the original parametrization and hydrology, but the effect is merely a dampening of the storage anomalies towards higher temperatures or higher CO_2 concentration. Carbon storage in the new model is only more sensitive to changes in

temperature in case of a cooling.

2.6 Evaluation of the land surface parametrization

2.6.1 Method

Two additional experiments were performed as control runs: one with the old ECHAM3 land surface parametrization (ACTL$^-$), and one with the new dynamic land surface derived from the vegetation model LPJ (ACTL$^+$). The $^+$ denotes an interactive coupling, the $^-$ a fixed coupling, as will be used in chapters 4 and 6 as well. ACTL$^+$ differs slightly from the CTL$^+$ control run, as it has shorter asynchronous periods due to a smaller cutoff criterion for the periodically synchronous coupling (Mikolajewicz et al., submitted). Both experiments run with a present-day insolation, and CO_2 is calculated prognostically. A spinup was performed using an atmospheric CO_2 concentration of 280 ppm.

The land surface parametrization will be discussed by comparing the average land surface conditions of the control run (CTL$^+$) with original ECHAM3 surface parameters (as used for the ACTL$^-$ experiment). The ECHAM3 surface parameters were mainly derived from satellite measurements, which depicts the situation as influenced by man. The vegetation and land surface as modelled from the dynamic vegetation model do not take human influence (e.g. deforestation, land use) into account. It describes a 'present-potential' vegetation.

2.6.2 Results

Vegetation cover, as well as surface background albedo is simulated with an annual cycle. Figure 2.7 compares the yearly average surface conditions from the control run (vegetation and forest cover fraction and background albedo) with the yearly values of the original ECHAM3 parametrization. For both vegetation and forest cover fraction, model results differ substantially from the original input. For the vegetation cover in figure 2.7b, it should be noted that the original ECHAM3 model does not consider a yearly cycle for the vegetation cover, whereas the newly coupled version does, and that vegetation cover is corrected with a dependence on soil moisture content in the ECHAM3 parametrization, which was taken into account for figure 2.7a. The simulated vegetation cover shown here is the maximum cover that is obtained throughout the year.

Large differences in vegetation and forest fraction are due to the use of the observed vegetation (as derived from satellite measurements) in the original ECHAM3 parametrization, whereas the modelled vegetation in the earth system model is a 'present-potential' vegetation, human influence (land use, deforestation) is thus not taken into account here.
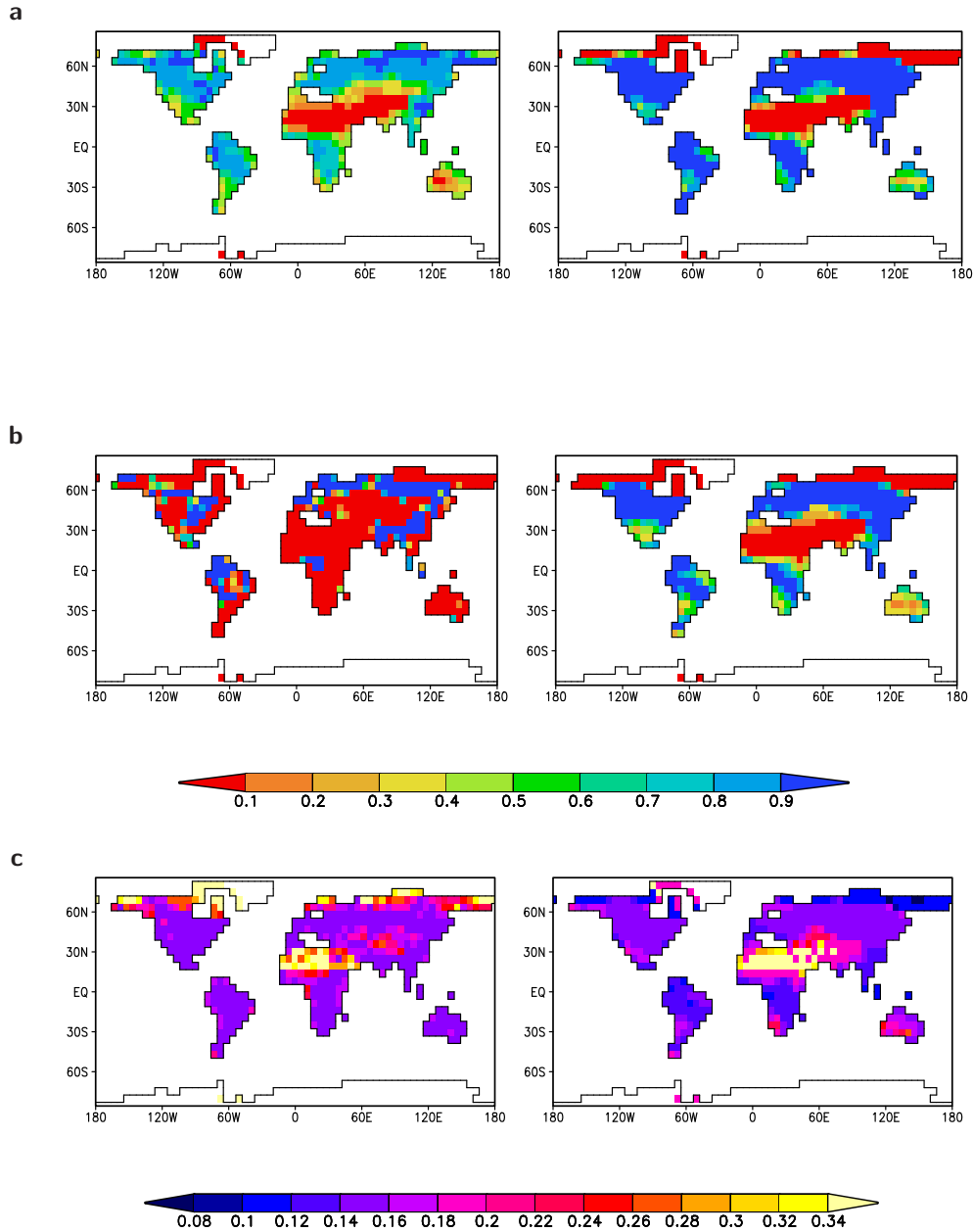
Figure 2.7: *Land surface parameters in ECHAM3 (left) and average of the control run (CTL$^+$) from the new parametrization (right): (a) Vegetation cover (in ECHAM3 corrected for soil wetness, for the CTL$^+$ experiment average growing season vegetation cover is shown), (b) forest cover, (c) surface background albedo (for the CTL$^+$ experiment the yearly average is shown).*

Although vegetation and forest cover differ substantially, albedo changes only moderately for most regions with the newly introduced parametrization (fig. 2.7c). Large differences occur in the highest latitudes, where the original parametrization shows high albedo values, whereas the modelled land surface shows a particularly low albedo, due to the presence of dark soils. The original parametrization could be biased here due to snow cover (the snow albedo correction is done in the atmosphere model, background albedo does not include snow influences), and the modelled values could be too low, because they are based on bare soils, whereas vegetation exists here, which is not simulated by the model. For the rest of the earth, the albedo matches quite well. Over tropical forest, the modelled albedo is slightly lower than from the original parametrization, the temperate and boreal regions show good agreement, as well as the desert regions in North Africa and Southern Asia.

The control runs with and without interactive land surface vary only slightly in climate. Global surface air temperature is 286.2 K for both control runs ($ACTL^-$ and $ACTL^+$), with a standard deviation of 0.27 K for the experiment with fixed land surface ($ACTL^-$) and a standard deviation of 0.18 K for the experiment with interactive land surface ($ACTL^+$). Local changes in annual temperature averaged over the control runs due to the interactive coupling range from -2 K for Central Asia and Northwest Africa to +3 K for Arabia, mainly caused by changes in the background albedo (fig. 2.7c). Even slightly higher differences can be observed near Antarctica due to changes in the ocean convection. The precipitation pattern does not show large changes due to the newly introduced land surface coupling, only over India and Southeast Asia the monsoon pattern expands slightly northward, thereby extending the land surface area that is affected. A slight decrease in precipitation was simulated over Northern Africa.

2.7   Conclusions and discussion

A complex earth system model was presented that allows for long-term transient experiments. With this model, transient experiments were performed for longer periods, experiments which were so far only performed with intermediate complexity models.

The earth system model, and the vegetation model within it, were introduced, and the parametrization of the land surface influencing the atmospheric energy and water balance was described. Results from a pre-industrial control run were compared to estimates based on measurements and other modelling studies.

The areas covered by the biomes derived from the plant functional types showed a fair agreement with estimates from the IPCC report (Houghton et al., 2001), as did the derived Köppen climate zones. Boreal forest and

tundra areas, and the area of the *ET* (tundra) climate zone from Köppen's classification, were overestimated, and expanded too far southward.

The carbon storage, in particular the storage in litter and soils, was higher than the usual range given from inventories and modelling studies. Despite this increase in soil carbon storage, the sensitivity of the simulated carbon storage to increases in temperature and CO_2 concentration were lower than for the model with original parametrization and hydrology. Only temperature decrease caused a higher sensitivity for the new model compared to the original one.

A parametrization for land surface properties was presented, which is used to model the effect of changes in the land surface on climate in the earth system model. The newly calculated vegetation and forest fraction differ substantially from the original input as used for the ECHAM3 atmosphere general circulation model. This bias is related to the difference between the observed vegetation as was used for ECHAM3 and the present-potential vegetation as modelled in this earth system model. However, the control run with interactive land surface did not differ widely in albedo values and climate from the control run with prescribed ECHAM3 parameters.

Chapter 3

On timescales in the terrestrial biosphere

Abstract

A common technique to speed up paleoclimatic modelling experiments is to accelerate the insolation forcing. Before doing this with the earth system model, it is important to know on what timescales the terrestrial biosphere reacts to changes in forcing. This was tested with experiments in which the climatic forcing was changed instantaneously to a higher CO_2 concentration and/or a corresponding climate. Time coefficients of changes of different parameters were determined, and conclusions with respect to experiment acceleration were drawn.

3.1 Introduction

Accelerating insolation experiments is an interesting feature for paleoclimatological modelling. As general circulation models become time and resource consuming when run for thousands of years, transient insolation experiments can be accelerated to save computation time. This has been done for coupled atmosphere-ocean experiments (e.g. by Lorenz and Lohmann, 2004), and will be used for some of the experiments described in this thesis as well. Here we try to find the timescales that are important for coupling the terrestrial biosphere, both for land surface parameters (biogeophysical coupling) and for carbon storage (biogeochemical coupling). The possibilities for acceleration of the terrestrial biosphere will be discussed.

3.2 Theory

A system that is shocked (e.g. by changes in climatic conditions) could move towards a new (stable) equilibrium. Ecological systems in which negative feedbacks drive this conversion do this often according to an exponential adaptation (Leffelaar, 1999):

$$y = y_{eq} - (y_{eq} - y_0) \cdot \mathrm{e}^{-\frac{t-t_0}{\tau}} \tag{3.1}$$

in which y is a certain parameter with initial value y_0 and maximum value y_{eq}, t is time, with initial value t_0 and τ is the time coefficient (units of time) that specifies the reaction time of the parameter.

The time coefficient τ can be interpreted as the time necessary to reach equilibrium y_{eq}, given a constant rate of change y'_t for any t (see fig. 3.1)[1]. Equation 3.1 is valid both for $y_{eq} > y_0$ and for $y_{eq} < y_0$, so both for an increasing and for a decreasing function.

3.3 Method

The model used here is an offline version of the coupled LPJ as described in chapter 2. This model was driven with data from an experiment with three times the pre-industrial CO_2 concentrations, as well as with data from a pre-industrial control run (Winguth et al., 2005), both performed with the earth system model presented in chapter 2. The experiments were divided in a spinup phase and two reaction phases. The spinup phase is a spinup with a control run forcing, and is common for all experiments. In the first reaction phase, climate and CO_2 concentration were altered instantaneously, and the vegetation in the model can adapt to the new forcing, moving towards a new

---

[1]Because the rate of change is not constant, equilibrium will not be reached. After $\Delta t = \tau$, y will reach $y_0 + \frac{1}{e}(y_{eq} - y_0)$, which is roughly 37% of its final value.
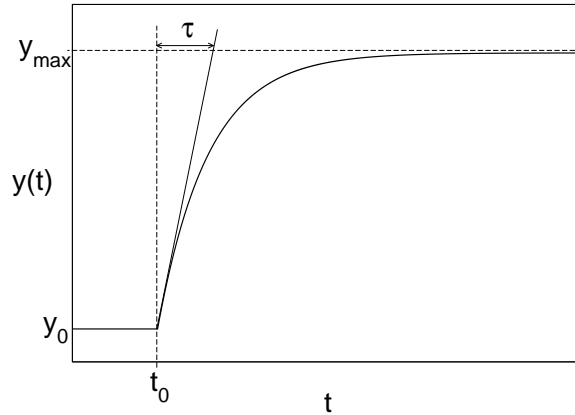
Figure 3.1: *Representation of equation 3.1.*

equilibrium state. In the second reaction phase, the forcing is returned to that of the control run, and the model can recover to its control run state. To be sure that the model reaches (near to) equilibrium in each phase, all phases were run for 5000 years. The control run forcing is a CO_2 concentration of 280 ppm together with 50 years from a pre-industrial control run. For the first reaction phase, climate and CO_2 concentration from the $3 \times$ pre-industrial CO_2 experiment are used as forcing (i.e. a CO_2 concentration of 840 ppm and 50 years of climate data from a coupled experiment with 840 ppm CO_2 as radiative forcing). The second reaction phase has the same forcing as the spinup phase, to test how fast the biosphere can recover to its old state, and whether increase and decrease show a symmetric behaviour.

For each of the reaction phases, an ensemble of three experiments was performed, and the average time series of these ensemble members was used for fitting a curve of the form of equation 3.1. Especially for the analysis of forest fraction, this averaging leads to a clear reduction of the variability in the time series, and thereby to a better result of the fitting. The ensemble members were forced with the same set of climate data, but the starting point within this set was altered with steps of 10 years for the different ensemble members.

Two parameters of the terrestrial biosphere are of major interest for the coupling with the atmosphere. The slowest biogeophysical parameter is the forest fraction. It was analysed for six zones (60°–90°N, 40°–60°N, 20°–40°N, 20°N–20°S, 20°–40°S and 40°–60°S). For the biogeochemical relation with the atmosphere, total carbon in the terrestrial biosphere was considered, because this will indicate how fast the terrestrial biosphere and the atmospheric CO_2 equilibrate. Because the reaction of total carbon in the terrestrial biosphere depends heavily on both climate change and CO_2

concentration, two dependencies that do not necessarily have similar time scales, the experiments were repeated using only climate change or only CO_2 changes as forcing for the first reaction phase.

Curves of the form of equation 3.1 were fitted to the modelled time series of forest fraction and total carbon storage with a least square fitting procedure, and the explained variance (R^2) for the fitting was calculated. For the fitting of forest fraction, the first 200 years of the time series after the change of forcing were used, for the fitting of total carbon storage the first 2000 years after the change were used. As the time series for total carbon storage showed often a behaviour as if two time scales play a role, caused by the difference in response time of vegetation and soil carbon stocks, the short time scales were estimated by repeating the exercise with a the first 50 years after the change of forcing. The average of the last 1000 years of the previous period was used as y_0, and the average of the last 1000 years of the current period was used as y_{eq}.

3.4 Results

3.4.1 Forest fraction

Figure 3.2 shows the time series of forest fraction together with the fitted curves for forest fraction of the experiments with combined climate and CO_2 forcing. Several time series show a reasonable accordance with equation 3.1, but for some time series fitting was not possible. Sometimes the variability was too high, limiting the possibilities to fit a curve. In cases of more or less instantaneous adaptation, with values for $\tau < 1$ year, the fitted curve was not very informative either, because this is below the time step of the vegetation model. These occurrences were removed from the analysis.

Table 3.1 gives the values for the time constants for forest fraction of the experiments with climate change and CO_2 change, together with the R^2 values for the fitting. For the fitted forest fraction curves, the increasing curves showed better accordance than the decreasing curves: forest expansion appears to be more gradual than forest decrease. Forest decrease shows often a sudden collapse of the forest fraction followed by a gradual recovery. The recovery is often related to the growth of different plant functional types. The time constants for forest fraction are up to 70 to 80 years for the high latitudes of the northern hemisphere, and up to 130 years for the southern hemisphere (table 3.1).

3.4.2 Carbon storage

The time series of carbon storage in the terrestrial biosphere, together with the fitted curves, are shown in figure 3.3 for all experiments. The fitted time constants τ are given in table 3.2, together with R^2 values for the fitting.
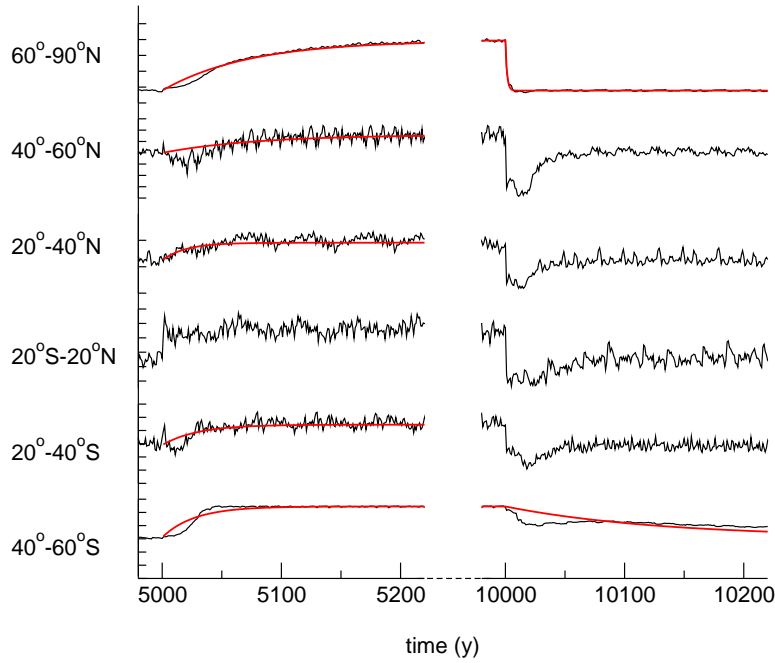
Figure 3.2: *Modelled forest fraction and fitted curves according to equation 3.1 for the CO$_2$ incease and climate change experiment. The marks along the y-axis have a 0.05 interval.*

Table 3.1: *Time constants of fitted curves for forest fraction, for the experiments with climate change and CO$_2$ together (1. Phase with climate change, 2. Recovery phase). In brackets whether the parameter has an increase (+) or a decrease (-) during this phase, and the R^2 for the fitting.*

	1.		2.	
60°–90°N	72.5	(+, 0.99)	1.3	(-, 0.84)
40°–60°N	79.1	(+, 0.68)	–	
20°–40°N	19.8	(+, 0.41)	–	
20°N–20°S	–		–	
20°–40°S	29.3	(+, 0.56)	–	
40°–60°S	27.1	(+, 0.89)	130.3	(-, 0.83)
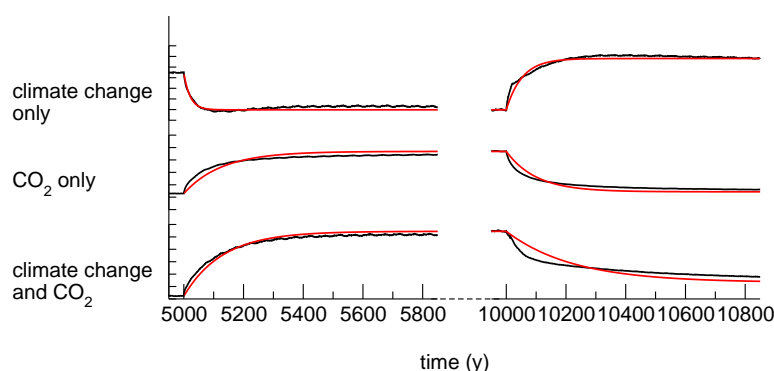
Figure 3.3: *Modelled total carbon and fitted curves according to equation 3.1 for all experiments, from the analysis using 2000 years of data for fitting. The marks along the y-axis have a 200 Pg interval for all plots.*

Table 3.2: *Time constants of fitted curves for all experiments (1. Phase with climate change and/or increased CO_2, 2. Recovery phase) for the total terrestrial biosphere carbon pool. In brackets the increase or decrease of carbon storage during this phase (Pg C), and the R^2 for the fitting.*

experiment	2000 year analysis		50 year analysis	
	1.	2.	1.	2.
Climate change only	21.3 (-348, 0.15)	53.1 (+482, 0.87)	22.0 (-348, 0.99)	38.7 (+482, 0.98)
CO_2 increase only	126.9 (+1699, 0.74)	100.0 (-1628, 0.74)	68.0 (+1699, 1.00)	53.9 (-1628, 1.00)
Climate change and CO_2 increase	129.9 (+1045, 0.93)	229.2 (-825, 0.80)	87.0 (+1045, 1.00)	98.0 (-825, 1.00)

Fitting of the curves for carbon storage was probably more successfull than for forest fraction, although some curves still show a low fraction of explained variance. The adaptation of total carbon storage to climate change is fastest, the adaptation to the combination of climate change and CO_2 is slowest. Largest time constants for adaptation are around 230 years. The analysis in which only the first 50 years were used shows remarkably smaller time constants than that with 2000 years of the time series used, especially for the effect of CO_2 increase and of climate change and CO_2 increase. There is clearly a difference in time scales within the terrestrial biosphere, which is related to the different life times of carbon between living biomass and soil organic carbon.

3.5   Conclusions and discussion

For forest fraction, curve fitting was reasonably successful. The fitting for forest fraction gives R^2 values over 0.5 for almost all increases in forest cover. Fitting of decreasing forest fraction was less succesful, which was mainly caused by rapid decreases that were not captured by the fitting procedure. The time coefficients τ differ both between zones. In general, high latitudes react more slowly than low latitudes. The values for the time coefficients are up to 80 years in the northern hemisphere and up to 130 years in the southern hemisphere for forest fraction.

For total carbon storage, fitting is slightly more succesful. The curves showed a reasonable agreement in most cases, and time coefficients vary between 20 years in case of only climate change to 230 years for climate change and CO_2 increase. An additional analysis using only the first 50 years of the time series showed that especially in case of (climate change and) CO_2 changes there is a faster component involved, which is assumed to be the living biomass. Soil carbon storage has a much slower turnover, and has a larger time coefficient.

Drawbacks of this method is that the fitting is not always good, sometimes other curves than of the form of equation 3.1 could be imagined. Especially curves that increase slowly in the beginning, and are more of logistic form (e.g. the second 40°-60°S curve in figure 3.2), are poorly represented by equation 3.1. Another drawback is that several regions, especially for the faster processes, get in equilibrium too fast to fit a curve to. Time constants of less than 1 year are meaningless in this context, as the model timestep is one year and the model cannot resolve these faster processes. This is especially true for a decreasing forest fraction. For total carbon storage there are often two or more processes involved with different time scales. Fitting of a function that allows for this (an addition of several components of the form of equation 3.1) would probably give better results, although the number of parameters that has to be estimated increases. Nevertheless, the method used here gives in general a proper representation for most of the curves, and even if the fitting is not perfect, the time coefficients give a fair indication of the time scales that are important for the processes.

For modelling studies with accelerations, it is important to be aware of these time scales. A time coefficient of 130 years, which was the time coefficient for an increase of total carbon storage due to climate change and CO_2 changes, leads to 300 years needed to reach 90% of the final value, or 600 years to reach 99%. Of course the 99% value is too pretentious, because the time series do not follow a perfectly exponential form, but the 90% level might be a proper estimate for a reasonable reaction time needed for the system.

Assuming the terrestrial biosphere needs 300 years to get reasonably close to an equilibrium state, a forcing with typical time scales of the order

of 10,000 years, as the changes in the earth's orbit have, are not problematic for the terrestrial biosphere, and the system will always be close to the equilibrium state at a certain moment. However, the climate system as a whole might react much more abrupt than the gradual changes in insolation, thereby reducing the time scales of interest. Nevertheless, time scales in the terrestrial biosphere will not obstruct a moderate acceleration of up to 10 times. However, for other pools in the earth system, where longer time scales play a role, this might be more problematic. Especially oceanic and cryospheric processes can be up to one order of magnitude slower than the processes in the terrestrial biosphere.

Chapter 4

The effect of land surface changes on Eemian climate

Abstract

Transient experiments for the Eemian (128-113 ky B.P.) were performed with the complex, coupled earth system model presented in chapter 2. Land surface parameters (background albedo, vegetation and forest fraction and roughness length) were either prescribed or modelled interactively, in order to investigate their impact on the climate of the Eemian. The experiments show that the influence of land surface on climate is mainly caused by changes in the albedo. For the Northern Hemisphere high latitudes, land surface albedo changed partially due to the direct albedo effect of the conversion of grasslands into forest, but the indirect effect of forests on snow albedo appears to be the major factor influencing the total absorption of solar radiation. The Western Sahara region experienced large changes in land surface albedo due to the appearance of vegetation between 128 and 120 ky B.P. These local land surface albedo changes can be as much as 20%, thereby affecting the local as well as the global energy balance. On a global scale, latent heat loss over land increased more than 10% for 126 ky B.P. compared to present-day, which was partially counterbalanced by a decrease of sensible heat loss.

4.1   Introduction

The effect of land surface changes on climate has long been excluded from climate model experiments. Growing awareness of the importance of land surface for climate resulted in a number of studies with changes in land surface conditions: first to study the sensitivity of a model to these changes, later to quantify the importance of realistic land surface changes for climate. Many of the studies were performed with paleoclimatic settings, because of the remarkable changes for the land surface that have been recorded for the past (e.g. as reported by Prentice and Webb III, 1998). The overview below briefly illustrates the richness of types of previous studies, and tries to group them by the approach used for studying the land surface effects.

Many studies were performed considering the importance of taiga and tundra in the high latitudes, starting with experiments prescribing albedo changes by Otterman et al. (1984). In later studies, deforestation was usually prescribed for certain regions (e.g. Bonan et al., 1992; Thomas and Rowntree, 1992; Douville and Royer, 1997). Experiments were performed as well for the Mid-Holocene (6 ky B.P.) prescribing forest expansion in the north (e.g. Foley et al., 1994; TEMPO, 1996), as was reported from proxy data for this epoch. These studies usually focus on the enhancement of the climate effect of prescribed insolation changes due to a biogeophysical feedback from the land surface: expansion of forests causes a decrease of the land surface albedo, an increase of the amount of absorbed radiation and thereby an increase in temperature. This increase in temperature from this feedback would favour the growth of vegetation.

Later, paleoclimate reconstructions of lake levels and vegetation from proxy data were used to drive general circulation models (Coe and Bonan, 1997; Crowley and Baum, 1997; Diffenbaugh and Sloan, 2002). This is a step in the direction of realistic modelling of the past and the effect of land surface changes can be estimated from the difference between these experiments and experiments with a present-day land surface, however feedbacks between land surface and climate are not taken into account.

To consider these feedbacks, simulated vegetation changes have been included in paleoclimate simulations and analysis (TEMPO, 1996). The feedback between atmosphere and land surface was studied in the Sahara desert region with an equilibrium vegetation model iteratively coupled to a dynamic atmosphere model for the Mid-Holocene by Claussen (1997), Claussen and Gayler (1997), Texier et al. (1997), Claussen et al. (1998) and De Noblet-Ducoudré et al. (2000). The greening of the Sahara desert was reported in many studies, and is mainly related to changes in the surface albedo. This change causes two associated effects that play a role in greening of the Sahara desert: (1) an increase in the absorption of shortwave radiation causes an increase in heat loss to the atmosphere, and thereby an increase in ascending air and in convection (Charney, 1975; Charney et al., 1975,

1976), and (2) an increased temperature contrast between the ocean and the land promotes the transport of moisture into the North African continent (Eltahir, 1996; Braconnot et al., 1999). Both processes cause an increase in precipitation, which is the key limiting factor for plant growth in the Sahara region, but the first explanation focusses more on local differences in surface albedo, whereas the second explanation takes regional circulation changes into account, focussing more on the role of the ocean as the source of water vapour.

Later, the coupling was performed with more sophisticated models for the vegetation and land surface. Complex coupled atmosphere-vegetation models (or atmosphere-ocean-vegetation models) were used, which simulate the state of vegetation directly, and are usually applied for time slices of interesting epochs. The Last Glacial Maximum (21 ky B.P.) was studied by Levis et al. (1999) and Crucifix et al. (2005), the Mid-Holocene was studied by Gallimore et al. (2005). Some of the studies mentioned above took the role of decreased CO_2 concentration into account, e.g. for the Last Glacial Maximum (Crowley and Baum, 1997; Levis et al., 2000; Crucifix et al., 2005).

Longer transient simulation of paleoclimatic time periods with earth system models are up to now only performed using intermediate complexity models (EMICS, Claussen et al., 2002), since the use of fully coupled atmosphere-ocean general circulation models is limited by the computational resources. Claussen et al. (1999) and Brovkin et al. (2002) used the CLIMBER-2 model to study the Holocene (from 9 ky B.P. to present), Calov et al. (2005) used the same model, now including ice sheets, to study the Eemian and the glacial inception (126 to 100 ky B.P.). The period between 126 ky B.P. and 115 ky B.P. was studied as well with the MoBidiC model by Crucifix and Loutre (2002). Performing longer transient simulations with atmosphere-ocean GCMs has so far only been done by accelerating the insolation forcing, e.g. as was done by Lorenz and Lohmann (2004).

For this study transient simulations with the complex earth system model as presented in chapter 2 were performed, instead of an intermediate complexity model. The earth system model consists of general circulation models for atmosphere and ocean, and models for the terrestrial biosphere and ocean biogeochemistry. The use of a rather coarse resolution, combined with a periodically-synchronous coupling (Sausen and Voss, 1996), enabled to perform experiments with unaccelerated as well as accelerated insolation forcing for longer transient periods, focussing in this study on the Eemian and the beginning of the transition into the last glacial. The experiments were used to study the effect of land surface changes on climate. In this chapter we will focus on the biogeophysical effects, the biogeochemistry will be discussed in chapter 5. By varying the coupling between fixed parameters and dynamic vegetation, the biogeophysical effects of changes in land surface on Eemian climate were studied.

4.2 Method

4.2.1 Model

The coupled earth system model, consisting of the atmosphere and ocean general circulation model, the ocean biogeochemistry model and the dynamic global vegetation model, was used to study the effect of changes in the land surface on the climate of the Eemian. The model was described in chapter 2. The atmospheric CO_2 concentration was calculated prognostically from the fluxes between atmosphere, terrestrial biosphere and marine biogeochemistry.

Coupling between the atmosphere and the terrestrial biosphere is performed yearly with monthly data. The vegetation model uses climate parameters from the atmosphere for its calculations, the main parameters are temperature, soil moisture content and radiation. The land surface parameters for the feedback to the atmosphere include parameters influencing both the energy balance (albedo, forest fraction) and the water balance (vegetation fraction, roughness length). A detailed description of the coupling with these parameters is given in paragraph 2.3. By varying these parameters between active coupling and prescribed values, the magnitude of their effects can be determined.

Due to the yearly coupling between atmosphere and land surface, a lag of one year emerges between the changes in climate and the land surface response to these. However, because the time scales of interest for the land surface processes are much longer for this study, this will not have a substantial influence on the land surface effects.

4.2.2 Experiments

An experiment was carried out in which insolation was prescribed for the time period 128 to 113 ky B.P. (15 000 years) according to Berger (1978). A 1000-year spinup run was performed for this experiment, starting from present-day conditions and running with an insolation forcing according to 129-128 ky B.P. In addition, a control run of 10 000 years with present-day insolation was carried out. Besides these two long runs, a set of experiments for the same period were performed with an accelerated insolation forcing, in order to study the influence of the land surface in detail. These experiments were performed with either an interactive or a prescribed (present-day) land surface, as well as two 'partially interactive' experiments: one in which the land surface was only interactive for forest fraction, and one in which the land surface was interactively coupled except for the land surface background albedo. In this set of accelerated experiments, insolation changes were accelerated with a factor 8, so that the model was integrated for 1875 years. Two additional control runs were performed with present-day insolation (one with a completely interactive land surface, one with a

completely prescribed land surface), with the same parameter settings as in the accelerated experiments. Interactive land surface coupling is denoted with $^+$, fixed land surface parameters with $^-$ for the experiments, accelerated experiments (as well as the control runs to the these experiments) are preceded by 'A'. The experiments are summarized in table 4.1.

Table 4.1: *Overview of the experiments*

CTL$^+$	control run with present-day insolation and interactive land surface (10 000 years)
EEM$^+$	insolation experiment (15 000 years)
ACTL$^+$	control run with present-day insolation and interactive land surface, shorter asynchronous periods than CTL$^+$
ACTL$^-$	control run with present-day insolation and prescribed (present-day) land surface
AEEM$^+$	insolation experiment, with interactive land surface (accelerated)
AEEM$^-$	insolation experiment, with prescribed land surface (accelerated)
AEEM$^+$A$^-$	insolation experiment, with interactive land surface, but with prescribed albedo (accelerated)
AEEM$^-$F$^+$	insolation experiment, with prescribed land surface, but with interactive forest fraction (accelerated)

Coupling between the atmosphere and the other components was done with a periodically-synchronous coupling technique (Sausen and Voss, 1996). In contrast to the original version, where the fluxes were kept constant during the period without interactive calculation of the atmospheric GCM, an energy balance model is applied here to get an appropriate feedback on sea surface temperature and sea ice. Details are given in Mikolajewicz et al. (submitted). For the accelerated experiments, the maximum length of the asynchronous period and the cutoff value for the heat flux anomaly, which determine the length of the asynchronous coupling period (Mikolajewicz et al., submitted), were reduced compared to the unaccelerated experiments. The control runs to these experiments (ACTL$^+$ and ACTL$^-$) were performed with the same settings.

For the experiments with a prescribed land surface, the vegetation model was still included for analysis of the vegetation changes, but changes in the vegetation were not allowed to affect the atmosphere model. The atmosphere and vegetation model run on a T21 grid (roughly $5.6° \times 5.6°$), the ocean and ocean biogeochemistry on an Arakawa E-grid (effectively $4.0° \times 4.0°$).

4.3 Results

4.3.1 Climate change

The coupled experiment (EEM$^+$), as well as the accelerated coupled experiment (AEEM$^+$), show a gradual cooling of the northern hemisphere earth surface during the Eemian of nearly 1.5 K (fig. 4.1). The southern hemisphere shows a very moderate warming in the beginning of the experiment, followed by a gradual cooling in the second half, but the variability is much higher than in the northern hemisphere for both the insolation runs and the control run (standard deviations for the control run CTL$^+$ are 0.15 K for the northern hemisphere and 0.42 K for the southern hemisphere). This high variability is caused by variations in the convection in the Weddell Sea and Ross Sea (see Mikolajewicz et al., submitted). For the accelerated experiments, variability is higher, especially in the southern hemisphere, which is related to a smaller set of atmosphere years due to the acceleration.
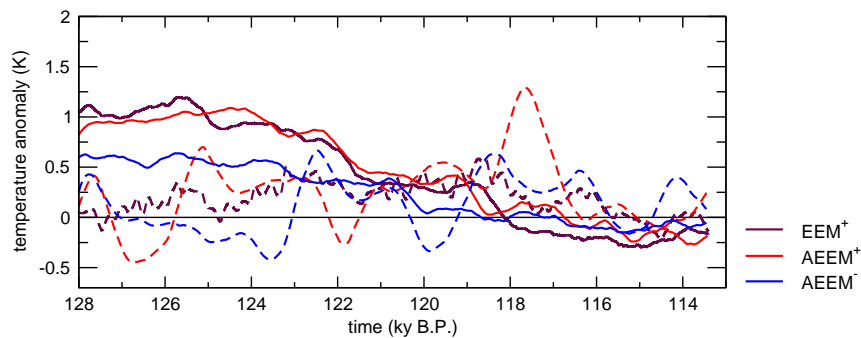
Figure 4.1: *Average surface air temperature anomalies (K) for the EEM$^+$, AEEM$^+$ and AEEM$^-$ experiments for the northern (full line) and southern (dashed line) hemisphere. Shown are 0.8 ky running means.*

The warming shown in the northern hemisphere for the first half of the experiment is mainly taking place during summer. Surface temperatures increase stronger over the land surface than over the ocean, with a strong positive anomaly for the whole northern hemisphere. The northern hemisphere monsoon regions (north Africa, southeast Asia) are remarkable exceptions, with a cooling of up to 5 K for the period 127-125 ky B.P. (fig. 4.2a). Changes in the circulation pattern in the subtropics cause an enhancement of rising air over the land surface and an enhancement of sinking air over the ocean, leading to an enhanced summer monsoon. The increase in precipitation in the monsoon belt over north Africa and southeast Asia is accompanied by an increase in evaporation due to increased soil wetness and increased vegetation cover. The precipitation increase is associated with an increase in cloud cover (fig. 4.2b). The decrease of incoming solar radiation

due to increased cloud cover, and the increase of evaporative cooling, cause
the negative temperature anomaly shown in figure 4.2a.
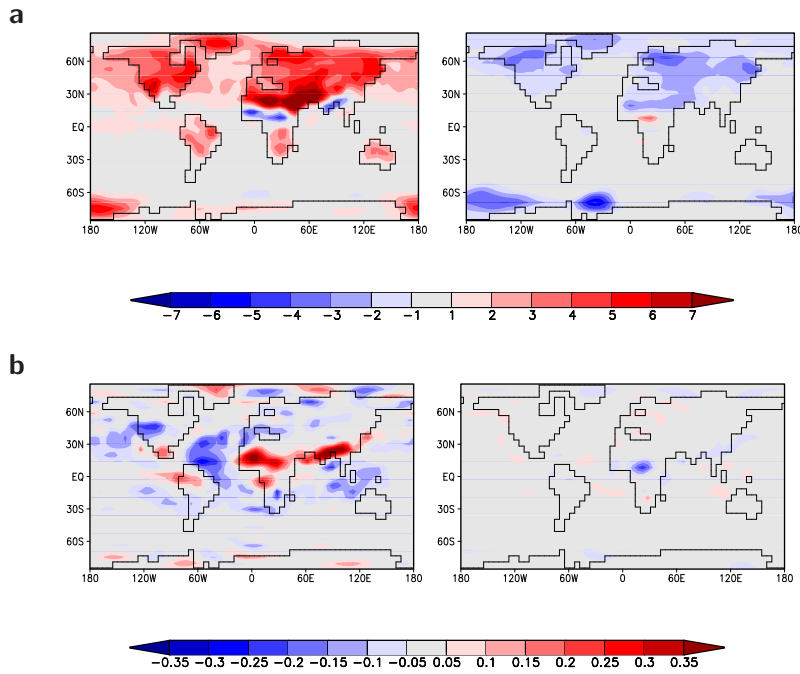
Figure 4.2: *(a) Surface air temperature anomaly (K) and (b) cloud cover anomaly (-)
for summer months (JJA) of 127-125 ky B.P. (left) and 116-114 ky B.P. (right) of the
coupled experiments (EEM$^+$-CTL$^+$).*

For 116-114 ky B.P., the temperature anomalies compared to the control
run are smaller (fig. 4.2a). During summer, a cooling was simulated over
the northern hemisphere land surface up to 4 K, with a small warming and
a small increase in cloud cover (fig. 4.2b) over the Sahel zone, which is the
opposite effect of that discussed for 127-125 ky B.P.

The CO_2 concentration increases during the coupled experiment EEM$^+$,
from around 270 ppm for the beginning (128 ky B.P.) to around 290 ppm
around 116 ky B.P. This increase is mainly related to a decrease of terres-
trial carbon storage. These effects will be described in chapter 5. For the
accelerated experiments, the increase in CO_2 concentration is smaller, and
the changes are delayed compared to the unaccelerated experiment.

4.3.2   Land surface changes

The results shown above are simulated for the accelerated experiments with
and without coupling as well, although the magnitude of the effects differ.

In general, there is much more similarity between the two experiments with interactive land surface (EEM$^+$ and AEEM$^+$) than between the two accelerated experiment (AEEM$^+$ and AEEM$^-$). The latter two experiments show remarkable differences, both in simulated vegetation and in simulated climate (fig. 4.3). The temperature pattern as shown for the EEM$^+$ experiment in summer for the period 127-125 ky B.P. (fig. 4.2a) dominates the yearly average for the two accelerated experiments as well, but both the warming in the high latitudes of the northern hemisphere and the cooling in the monsoon area, as described above, are larger for the experiment with interactive land surface (AEEM$^+$) than for the experiment with prescribed land surface (AEEM$^-$, fig. 4.3a). A similar amplification can be observed for precipitation (fig. 4.3b).

Changes in the surface albedo are considered to be the main cause of these amplifications. Figure 4.3c shows the albedo changes compared to the respective control runs. For the AEEM$^-$ experiment, background albedo was prescribed, so changes in surface albedo are only caused by changes in the snow cover and changes in sea ice cover. Over land, minor changes in surface albedo can be observed for the high latitudes. However, if the changes in vegetation cover are allowed to influence the albedo, as in the interactive experiment (AEEM$^+$), large areas with a decreased albedo can be observed for the high latitudes, as well as for northwest Africa. These changes are related to changes in the vegetation cover (fig. 4.3d), which themselves are often amplified by the coupling as well. Positive feedbacks between vegetation and climate cause this amplification of the changes due to changes in insolation in the high latitudes of the northern hemisphere and in the monsoon areas over north Africa and southeast Asia.

These local changes in the land albedo, and to a lesser extent changes in the vegetation cover, cause changes in the energy balance of the earth, not only in the areas that are directly subject to these changes, but in other parts of the earth as well, as discussed below.

High latitude boreal forest and tundra

Over the high latitudes in the Northern Hemisphere, boreal forests cover large areas up to the Arctic Ocean in the beginning of the transient experiments. Over the time span of the experiment, they show a gradual decrease in cover, which can be interpreted as a southward retreat of the treeline for most of the Northern Hemisphere regions. Between 128 ky B.P. and 120 ky B.P., temperate forests are present as well in higher latitudes, but they show a substantial southward retreat afterwards. Grasses stay constant or increase slightly for some boreal areas, occupying the area that is abandoned by boreal trees.

For all insolation experiments, the land surface between 60° and 90°N is simulated to be warmer than for the control runs (fig. 4.4c), causing

a

b

c

d
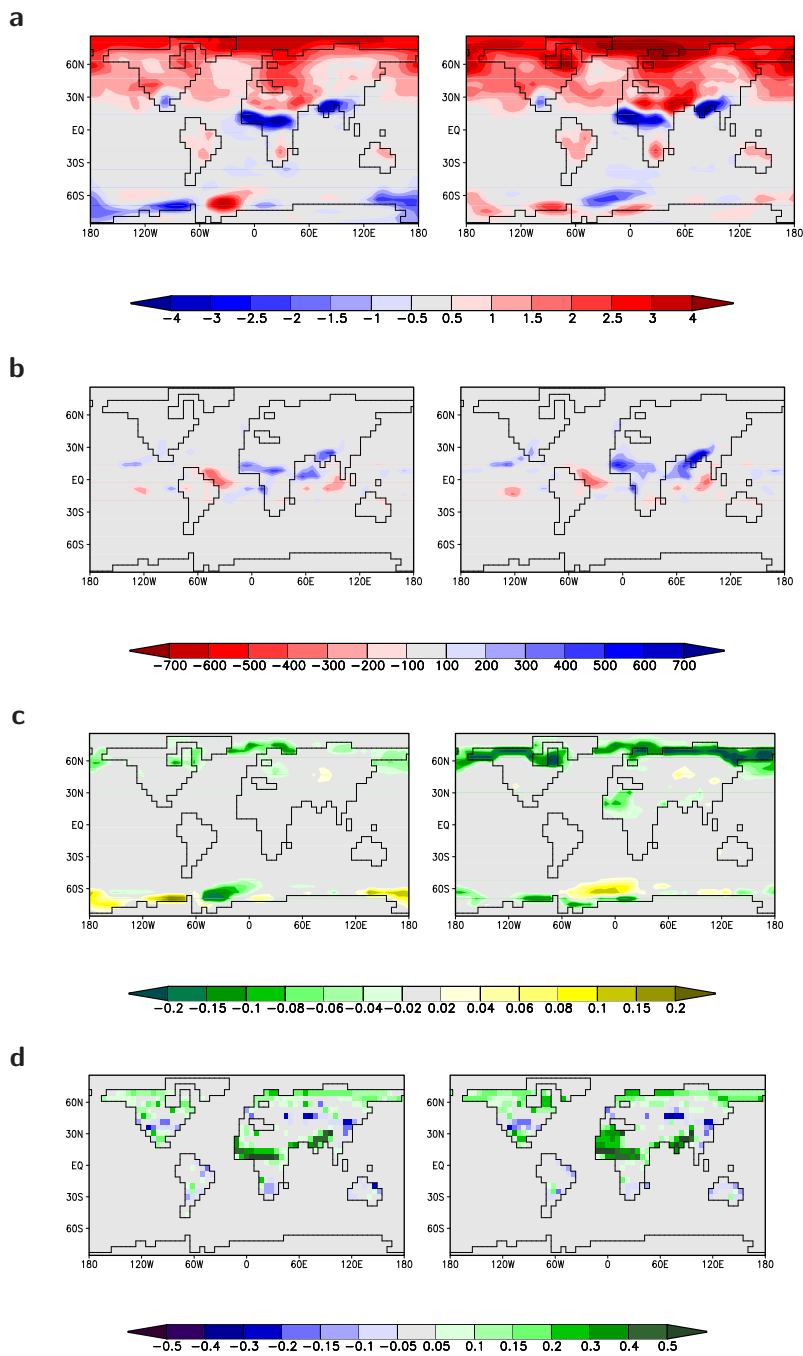
Figure 4.3: *126 ky B.P. yearly anomalies of (a) surface air temperature (K), (b) precipitation (mm y^{-1}), (c) surface albedo (-) and (d) average vegetation cover (-), for the experiment with fixed land surface (AEEM^{-}-ACTL^{-}, left) and the experiment with interactive land surface (AEEM^{+}-ACTL^{+}, right).*

these changes in vegetation. For the experiment with fixed land surface (AEEM$^-$), a maximum difference between control run and insolation run of 1.5 K is simulated, which is due to an increase in incoming shortwave radiation, and which is only very slightly enhanced by a snowcover-induced albedo decrease (fig. 4.4b). This effect is enhanced in the experiments with interactive land surface (EEM$^+$ and AEEM$^+$), because changes in forest fraction (fig. 4.4a) and background albedo cause a decrease in surface albedo (fig.4.4b). For the period 120 to 113 ky B.P., the opposite can be observed, with enhanced albedo increase and surface temperature decrease due to land surface changes. Two explanations are important for the decrease of surface albedo for the period 128 to 120 ky B.P.: (1) the albedo for forest is lower than for grasses, and (2) the albedo for a snow-covered forest is lower than for a snow-covered tundra, due to a more irregular covering of the surface. The additional experiment AEEM$^-$F$^+$, in which background albedo is prescribed, but forest fraction is used interactively, can help distinguishing the importance of the two explanations. In this experiment, surface albedo changes are caused only by changes in the snow cover.
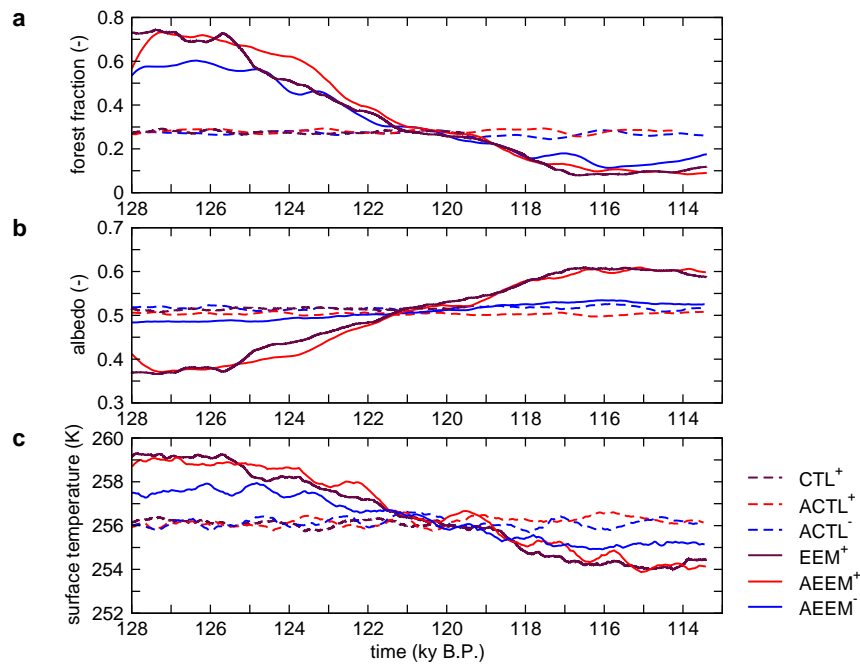
Figure 4.4: *(a) forest fraction, (b) surface albedo and (c) surface air temperature for the land surface 60°-90° N (excluding ice sheets). Shown are 0.8 ky running means from the unaccelerated experiments (CTL$^+$ and EEM$^+$), the control runs (ACTL$^-$ and ACTL$^+$) and the accelerated insolation experiments (AEEM$^-$ and AEEM$^+$).*

The annual cycle (fig. 4.5a) for albedo in the AEEM$^-$F$^+$ experiment is

similar to the experiment with interactive land surface (AEEM$^+$) during winter and spring, and similar to the experiment with fixed land surface (AEEM$^-$) during summer. Changes over winter are larger than over summer. However, because the incoming radiation is much higher during summer, the summer albedo changes are in general of more importance. Figure 4.5b shows that the insolation curve for the EEM$^-$F$^+$ experiment differs mostly from the AEEM$^-$ experiment in spring. The yearly total absorbed solar energy for the land surface 60°–90°N is 2.58×10^{22} J for the AEEM$^-$, 2.85×10^{22} J for the AEEM$^+$ and 2.76×10^{22} J for the AEEM$^-$F$^+$ experiment, which sets the increase in absorbed shortwave radiation due to forest fraction induced snow albedo changes to two third of the total yearly increase due to land surface changes, leaving one third for vegetation albedo changes and possible synergetic effects.
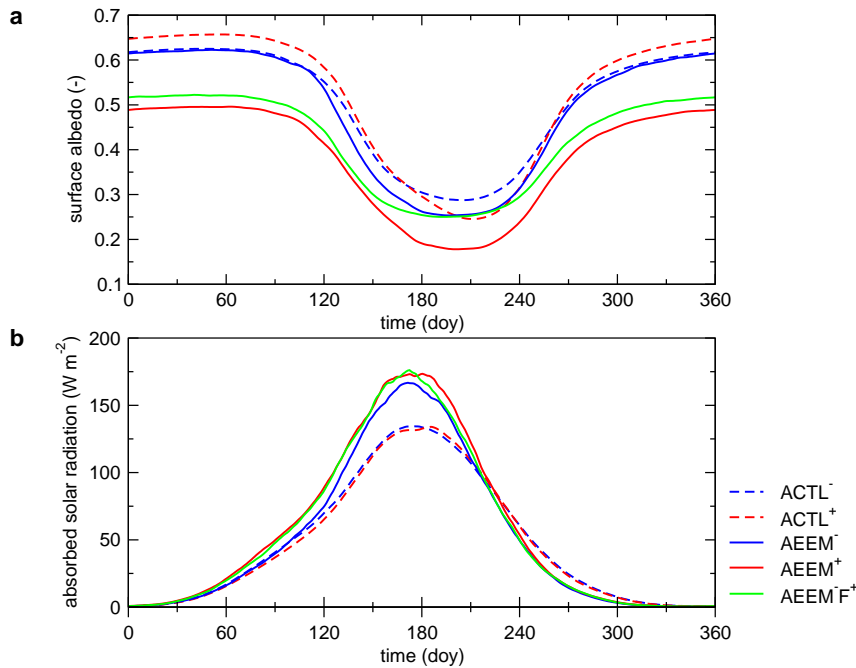
Figure 4.5: *Seasonal cycle of (a) land surface albedo and (b) absorbed shortwave radiation by the land surface for the northern hemisphere high latitudes (60°-90° N) for 127-125 ky B.P. Shown are 10-day running means.*

Sahara desert

During the first half of the coupled experiment (EEM$^+$), major changes in the vegetation pattern occur for Northern Africa. Evergreen trees, both tropical and temperate, increase in the area between 5°N and 15°N, and

herbaceous plants are reduced slightly. Further north, herbaceous plants expand clearly. A slight increase in evergreen trees is simulated here as well.

This increase in vegetation cover, accompanied by an increase in precipitation, is simulated for the period 128 ky B.P. to 120 ky B.P. in all insolation experiments. The diagnostic simulation of vegetation for the uncoupled transient run (AEEM$^-$) has a clear increase of both vegetation and precipitation compared to all control runs (CTL$^+$, ACTL$^-$ and ACTL$^+$, fig. 4.6). Changes in the insolation due to changes in the earth's orbit cause a heating of the land surface in the subtropical and temperate regions, and thereby an increased temperature gradient between the large land masses and the ocean, thereby enhancing the atmospheric moisture transport of the monsoons. Besides that, positive feedbacks cause a clear amplification of this effect for the coupled transient runs (EEM$^+$ and AEEM$^+$), related to a decrease of the surface albedo for this period (fig. 4.6b).
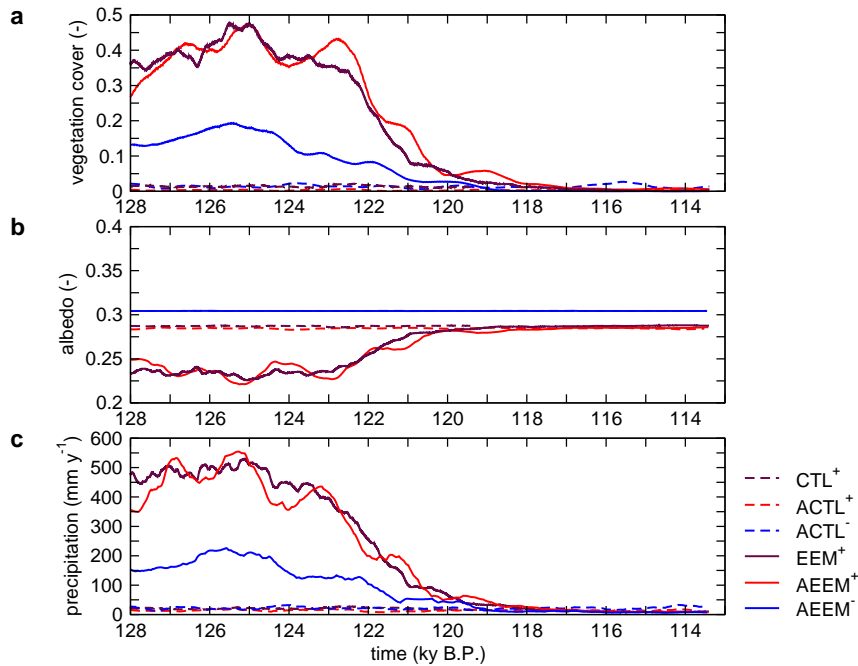
Figure 4.6: *Vegetation cover, albedo and precipitation for the Sahara region (10° E-20° W, 10°-30° N). Shown are 0.8 ky running means from the unaccelerated experiments (CTL$^+$ and EEM$^+$), the control runs (ACTL$^-$ and ACTL$^+$) and the accelerated insolation experiments (AEEM$^-$ and AEEM$^+$).*

The wind and atmospheric moisture patterns for the summer months for 127-125 ky B.P. are shown in figure 4.7 for the monsoon area over north Africa and India. There are clear differences between the experiment with prescribed (AEEM$^-$) and the experiment with interactive (AEEM$^+$) land

surface: Over west Africa the southwesterly winds coming from the Atlantic Ocean are stronger in case of interactive land surface coupling, thereby bringing more moisture into the western Sahara region. The continental winds coming from the north are clearly weaker. This results in an increase in atmospheric moisture, especially over large parts of western Africa.
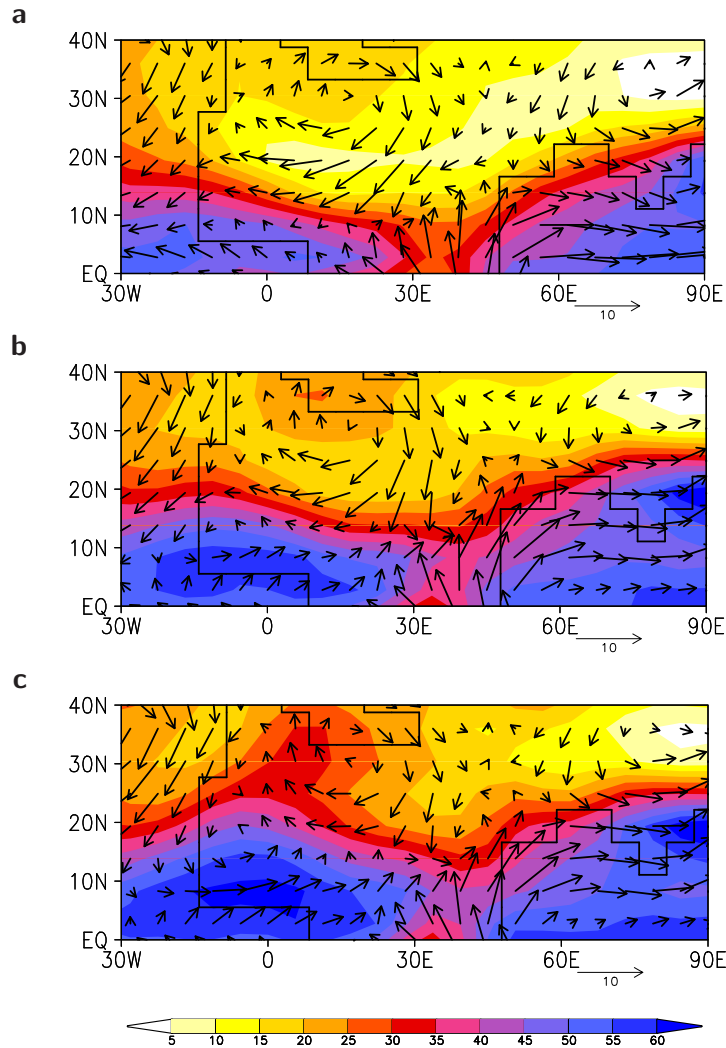
Figure 4.7: *Summer (JJA) average winds at pressure level 850 hPa (vectors, indicated is 10 m s^{-1}) and summer average integrated water content of the atmosphere (kg m^{-2}, colours) for (a) the uncoupled control run (ACTL$^-$) and for 127-125 ky B.P. (b) with fixed land surface (AEEM$^-$) and (c) with interactive land surface (AEEM$^+$).*

The positive feedback between vegetation and precipitation is supposed to be driven by changes in albedo. Charney (1975) presented a mechanism

which links a decrease in albedo to an increase in convection and thereby an increase in precipitation. According to Eltahir (1996) and Braconnot et al. (1999) the increased moisture transport from the ocean into northern Africa is driving this feedback. It is hard to distinguish between them, because both approaches are in principle arguing for an enhancement of the monsoon circulation, but the change in albedo, as shown in figure 4.6b is supposed to be the main driver of the change in circulation pattern in figure 4.7. To verify this, the additional experiment $AEEM^+A^-$ was performed.

In figure 4.8, the $AEEM^+A^-$ experiment is compared with the $AEEM^+$ and $AEEM^-$ experiments. The intensification of the monsoon for the period around 126 ky B.P. is shown clearly, both the uncoupled and the coupled experiments show a northward expansion of the precipitation pattern in summer, and in general higher precipitation rates. The $AEEM^+A^-$ experiment has roughly the same pattern as the $AEEM^-$ (compare figs. 4.8c, 4.8d and 4.8e), whereas the $AEEM^+$ experiment expands much further northward. This confirms that background albedo is the main factor in the enhanced precipitation due to dynamic vegetation changes.

4.3.3   Effect of land surface changes on the global energy balance

The total annual amount of incoming solar radiation at the top of the atmosphere is only slightly higher under Eemian conditions than under present-day conditions, with a small change over the period from 128 ky B.P. to 113 ky B.P. (0.11 to 0.13 PW more than present, fig. 4.9a). The large changes that occur in the climate over this period are caused by changes in the spatial and temporal distribution of the radiation (figs. 4.9b and 4.9c).

Figure 4.10 shows an overview of the global energy balance in the control run, and the anomalies for 126 ky B.P. and 115 ky B.P. As was discussed above, the globally and annually integrated incoming radiation changes only slightly between the control run, 126 ky B.P. and 115 ky B.P., with the anomalies for 126 ky B.P. and 115 ky B.P. being quite similar. However, the changes in the spatial and temporal distribution cause larger anomalies for other components of the energy balance, that are in most cases significant (fig. 4.10). These changes are up to one order of magnitude larger than the changes in annually integrated global incoming radiation, which indicated that these spatial and temporal changes are more important. For 126 ky B.P., total cloud cover is higher due to increased evaporation in the monsoon areas (fig. 4.2b), causing the solar radiation reflected and absorbed by the atmosphere to increase, and the solar radiation reaching the earth surface to decrease. Reflection of solar radiation shows a clear increase in the monsoon area over southeast Asia, Africa and the Arabian Sea, where cloud cover increased (see fig. 4.2), and a slight decrease in the high latitudes of the northern hemisphere, where albedo decreased due to land surface changes.
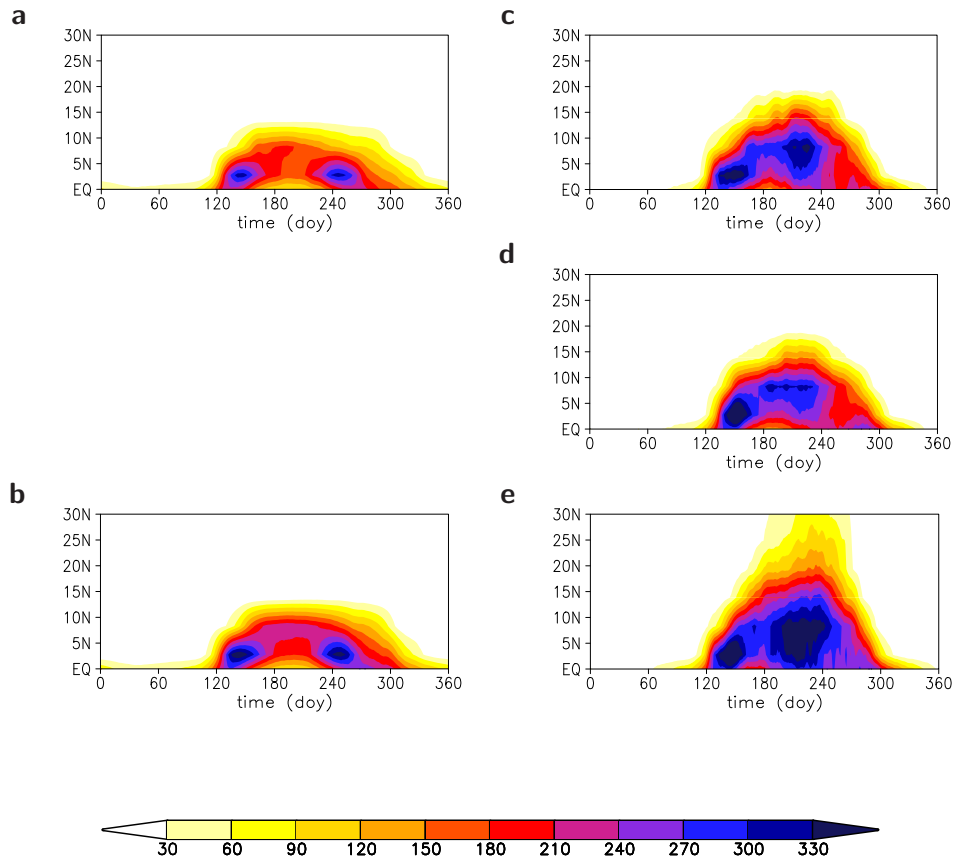
Figure 4.8: *Zonal average of the annual cycle of precipitation on land (mm month^{-1}) for a region in the Western Sahara (10° E-20° W). Displayed are the annual cycles of the control runs ACTL$^-$ (a) and ACTL$^+$ (b), and the average annual cycles for 127–125 ky B.P. for the insolation experiments: AEEM$^-$ (c), AEEM$^+$A$^-$ (d) and AEEM$^+$ (e). All figures are 10-day running means.*

Due to a lower albedo of the ocean (caused by a decrease of sea ice cover) and land (caused by the 'greening' of the Sahara region and the extention of boreal forests in high latitudes), the amount of solar radiation reflected by the surface decreases, especially for the land surface (-7.6%). For 115 ky B.P., the changes are much smaller. Cloud cover changes much less (fig. 4.2b), it is only very slightly decreased compared to the control run, therefore the anomalies in incoming radiation are much smaller and changed sign compared to 126 ky B.P. Due to a general warming, especially of the land surface, for 126 ky B.P. and a slight cooling for 115 ky B.P. (fig. 4.2a), the incoming and outgoing thermal radiation at the surface increased slightly for 126 ky B.P. and decreased slightly for 115 ky B.P., with in general stronger effects for the land than for the ocean, caused by larger temperature anomalies.

a

b

c
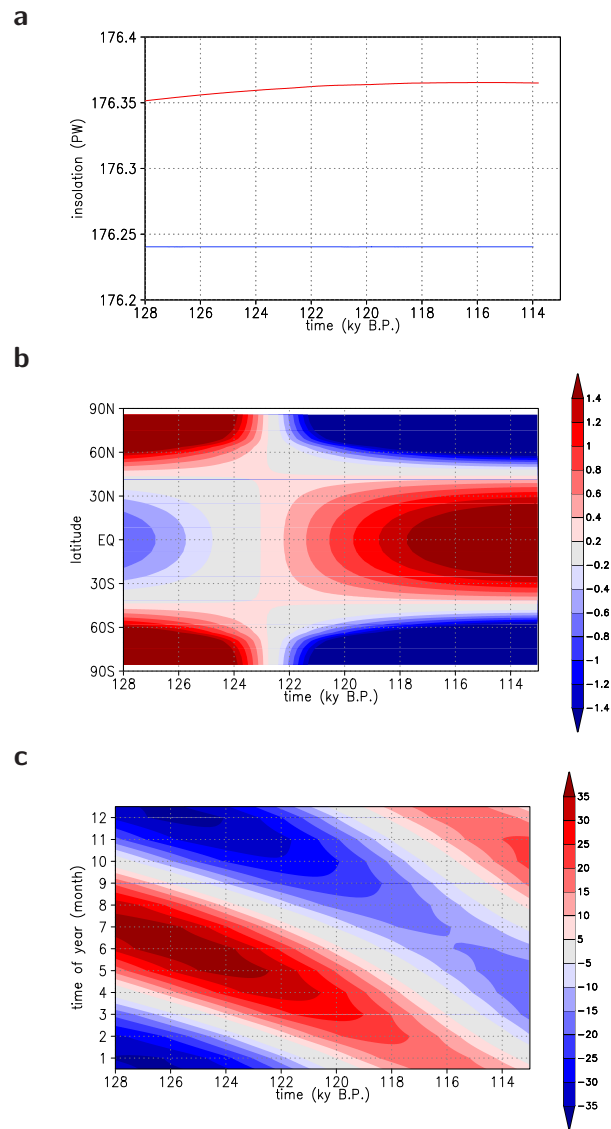
Figure 4.9: *Total incoming solar radiation at the top of the atmosphere over the period 128-113 ky B.P. (in red, with present-day value in blue, a) and anomalies in the distribution of the incoming solar radiation (W m^{-2}) over latitude (b) and over the time of the year (c) for the given period.*

Latent and sensible heat show a large effect for 126 ky B.P. compared to the control run, mainly for the land surface. Due to higher temperatures, and an increase of vegetation cover and soil wetness mainly in the Sahara region, evaporation increased drastically, causing a large increase in latent heat loss for the land surface (+13.8%). This is partially counterbalanced by a decrease in sensible heat loss (-4.2%). The main changes in latent and sensible heat loss took place in the tropics (fig. 4.11), with a dominant role for north Africa.
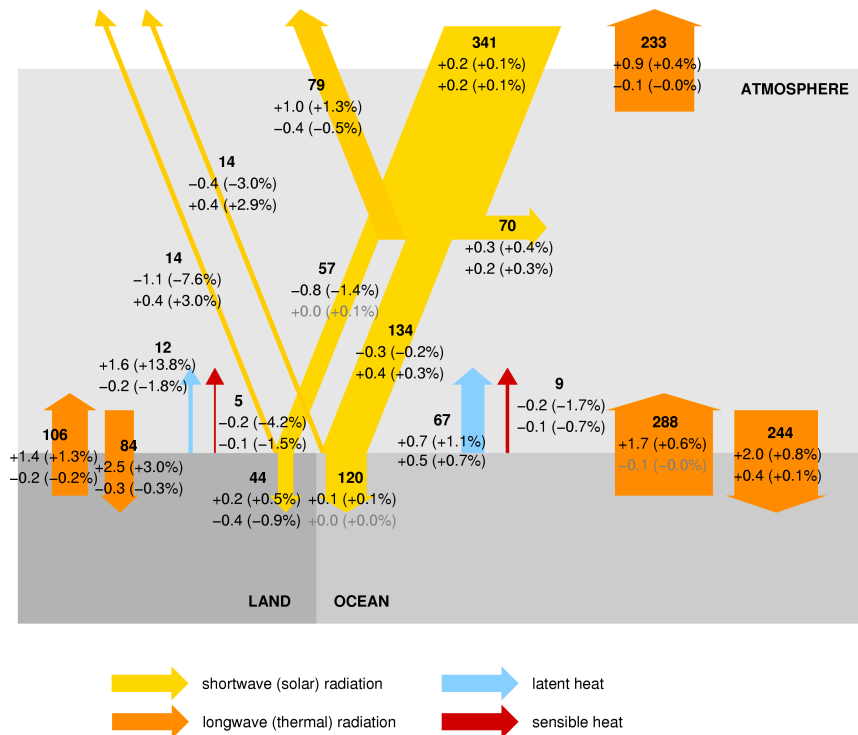
Figure 4.10: *Overview of the global energy balance for the control run CTL$^+$ and anomalies for 127–125 ky B.P. (upper value) and 116–114 ky B.P. (lower value) from the EEM$^+$ experiment. All fluxes are in W m^{-2}, the relative changes are given for 127–125 and 116–114 ky B.P. as well. Anomalies that are not significantly different from the control run ($\alpha = 0.01$) are printed in grey.*

The effects on the incoming radiation at the surface are in general much lower for the experiment without land surface coupling (AEEM$^-$) than for the experiment with land surface coupling (AEEM$^+$). Land surface changes are a significant amplifier of the energy balance effects due to changes in insolation for this time period, even on a global scale.
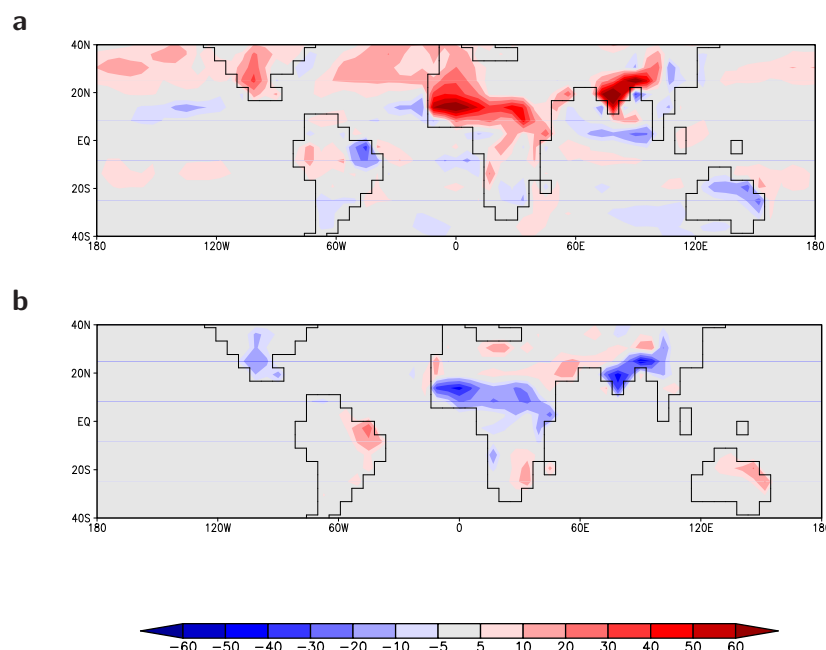
Figure 4.11: *127-125 ky B.P.: Anomalies of (a) latent heat loss and (b) sensible heat loss (W m^{-2}) for the coupled experiments (EEM$^+$-CTL$^+$).*

4.4   Conclusions and discussion

Climate change during the Eemian was forced by changes in the spatial and temporal patterns of incoming solar radiation. It caused clear changes in the land surface cover, especially in the high latitudes of the northern hemisphere, and in the monsoon regions in the subtropics of the northern hemisphere.

For the period from 128 to 120 ky B.P., the simulated forest fraction in the high latitudes is larger than in the control run, with a maximum around 126 ky B.P. and a gradual decrease afterwards. Due to the positive feedback between temperature, forest growth and albedo, this growth caused a decrease of the surface albedo and enhanced the temperature change in the high latitudes. A comparison between experiments with fixed land surface and experiments with interactive land surface shows that roughly two third of this enhancement is due to the effect of forest presence on snow albedo, and one third is due to the difference in background albedo between trees and grasses and due to synergetic effects between these two processes.

The enhanced monsoon circulation between 128 and 122 ky B.P. over north Africa and southeast Asia caused an increase in transport of water vapour to north Africa. The enhanced vegetation growth and increase in

soil moisture amplified this effect, which was caused by changes in the surface albedo, rather than changes in the other land surface parameters.

Overall, these changes in the land surface, in both cases related to changes in the surface albedo, have global implications, and tend to intensify climate change as induced by changes in the earth's orbit. This intensification was simulated for key climate factors, such as temperature and precipitation. The simulations presented here show no areas with a clear negative feedback on land surface albedo. The amplification due to albedo changes was simulated for the Eemian before by Kubatzki et al. (2000) and Crucifix and Loutre (2002). Together with albedo changes from ice sheet and sea ice changes, land surface albedo could play a major role in the difference between glacial and interglacial climate, and might be an important factor in triggering the transition from an interglacial to a glacial, as was suggested before by De Noblet et al. (1996), Gallimore and Kutzbach (1996) and Yoshimori et al. (2002). Calov et al. (2005) however showed for the CLIMBER-2 model that vegetation dynamics are amplifying the feedback, but that changes in insolation, together with the feedback between ice cover, surface albedo and temperature, are capable of starting glaciation without vegetation dynamics, ocean dynamics or CO_2 decrease as essential trigger.

Probably the largest drawback of the experiment setup applied in this chapter for a realistic reconstruction of Eemian climate is the absence of dynamical continental ice sheets. Over the time covered by the experiments (128-113 ky B.P.), the ice sheets are known to have changed (Tarasov and Peltier, 2003), with a clear onset of glaciation towards the end of the covered period. Experiments with the ice sheet model SICOPOLIS (Greve, 1997) are planned with an improved version of the coupled earth system model as presented in Winguth et al. (2005) and Mikolajewicz et al. (submitted). Ice sheet changes are expected to enhance the albedo effect in high latitudes. In this way, the albedo changes due to ice sheets and vegetation changes might be an important factor for glaciation.

The acceleration of 8 times, as used in the accelerated experiments, seems to be reasonable for assessing the effect of biogeophysical land surface changes, and much smaller differences were simulated between the experiments with and without acceleration of the insolation changes (AEEM$^+$ and EEM$^+$) than between the experiments with and without interactive land surface (AEEM$^+$ and AEEM$^-$). This indicates that the acceleration effect is much smaller than the effect of an interactive land surface. However, the use of the acceleration technique would not be appropriate for slower processes. e.g. carbon storage in soils or in the ocean. The acceleration would cause an artificial delay in the response, thereby mixing this delayed response with the timely signal of faster processes. For these purposes unaccelerated experiments need to be performed.

Chapter 5

Changes in terrestrial carbon storage during interglacials: a comparison between Eemian and Holocene

Abstract

The changes in terrestrial carbon storage in transient simulations of two interglacial sections (Eemian, 128–113 ky B.P., and Holocene, 9 ky B.P.–present), performed with the earth system model, were studied with respect to changes in the earth's orbit. The driving climate factors for these changes were studied in offline experiments in which the vegetation model was forced with only temperature, hydrological parameters, radiation, or CO_2 concentration from the transient runs.

Although temperature caused the largest anomalies in terrestrial carbon storage, the positive effect of forest expansion and increased photosynthesis in the high latitudes are nearly balanced by the negative effect of increased respiration. Large positive effects came from an enhanced monsoon circulation in the subtropics between 128 and 121 ky B.P. and between 9 and 6 ky B.P., and from increases in incoming radiation during summer for 45° to 70°N.

Compared to a control run with present-day insolation, the net effect of these changes was a positive carbon storage anomaly of about 200 Pg C for 125 ky B.P. and 7 ky B.P., and a negative anomaly around 150 Pg C for 116 ky B.P. Although the net increases for Eemian and Holocene were rather similar, the causes of this differ substantially. The decrease in terrestrial carbon storage during the experiments was the main driver of an increase in atmospheric CO_2 concentration for both the Eemian and the Holocene.

5.1 Introduction

The historical CO_2 concentration in the atmosphere, as was derived from ice cores (Indermühle et al., 1999), shows a rising trend for the last 8 000 years, from around 260 ppm at 8 ky B.P. to around 280 ppm for the pre-industrial era. Many different factors were proposed as cause or contributor to this rise such as natural changes in carbon storage on land and in the ocean due to changes in temperatures and changes by mankind such as land use change (Ruddiman, 2003).

A few transient simulations were performed for the Holocene to reconstruct the course of atmospheric CO_2. Brovkin et al. (2002) performed simulations with the intermediate complexity model CLIMBER, and Joos et al. (2004) performed simulations with the dynamic global vegetation model LPJ coupled to an impulse-response function model for the ocean carbon cycle based on the HILDA ocean model.

Brovkin et al. (2002) and Joos et al. (2004) both obtain a reasonable reconstruction of the atmospheric CO_2 concentration, covering the increase over the last 8000 years. However, the causes for the increase in the atmospheric CO_2 concentration differed between these studies. In the study of Brovkin et al. (2002) the increase of the CO_2 concentration is caused by a decrease of terrestrial carbon storage of about 100 Pg C over the last 9000 years, while in the study by Joos et al. (2004) by a decrease of oceanic carbon due to compensation of terrestrial uptake by sediments and ocean surface heating. In the last study, the terrestrial biosphere shows no clear uptake or release of carbon for the last 8000 years. A reconstruction of terrestrial carbon storage for the Holocene by Kaplan et al. (2002) had similar results as the study by Joos et al. (2004): the terrestrial carbon storage increased clearly during the early Holocene, from 8 ky B.P. a slight increase was simulated.

Reconstructions of the global vegetation distribution for the Holocene were provided by the BIOME 6000 project (Prentice and Webb III, 1998; Prentice et al., 2000) for 6 ky B.P., based on pollen data, and by Adams and Faure (1997). Consistent features of mid-Holocene vegetation distribution in these and other studies is a northward expansion of the boreal forest zone in the northern hemisphere, and an increase of vegetation in monsoon areas in the subtropics of the northern hemisphere.

In the study presented here, the complex earth system model presented in chapter 2 was applied to reconstruct the carbon cycle for the Eemian and the Holocene. Carbon storage in the terrestrial biosphere and its contribution to the atmospheric CO_2 concentration were analysed. The changes in terrestrial carbon storage were traced back to certain climatic factors.

5.2 Method

The complex earth system model, as described in chapter 2, was applied with components for atmosphere and ocean dynamics, ocean biogeochemistry, and vegetation, to two interglacial periods. Long integrations were performed for the Eemian (128 ky B.P. – 113 ky B.P.) and the Holocene (9 ky B.P. – present) with the coupled earth system model, for which insolation changes were prescribed according to Berger (1978). A control run of 10 000 years was performed with present-day insolation. CO_2 was treated prognostically in the earth system model, changes in carbon storage on land and in the ocean influence the atmospheric CO_2 concentration. Ice sheets were fixed at their present-day state. Both experiments were started from a pre-industrial control run, followed by a 1000 year spinup with insolation according to 129–128 ky B.P. (Eemian) and 10–9 ky B.P. (Holocene).

Besides these two coupled integrations, the climate data of these experiments were used to perform experiments with the offline vegetation model. Experiments were performed based on control run climate, with temperatures, radiation, hydrological parameters or pCO_2 from the Eemian or Holocene experiments, to determine which parameters influence the distribution and carbon storage of vegetation most. An overview of the experiments is given in table 5.1.

Table 5.1: *Overview of the experiments.*

CTL	coupled control run with present-day insolation
EEM	coupled run with transient Eemian insolation (128–113 ky B.P.)
HOL	coupled run with transient Holocene insolation (9 ky B.P.– present)
EEM_tem	vegetation run with control run climate and Eemian temperatures (air, surface and soil temperatures)
EEM_hyd	vegetation run with control run climate and Eemian hydrological parameters (soil moisture, precipitation)
EEM_rad	vegetation run with control run climate and Eemian radiation
EEM_co2	vegetation run with control run climate and Eemian atmospheric CO_2 concentration
HOL_tem	vegetation run with control run climate and Holocene temperatures (air, surface and soil temperatures)
HOL_hyd	vegetation run with control run climate and Holocene hydrological parameters (soil moisture, precipitation)
HOL_rad	vegetation run with control run climate and Holocene radiation
HOL_co2	vegetation run with control run climate and Holocene atmospheric CO_2 concentration

5.3   Results

A general overview of climate change in the experiments will be given. It will be discussed how changes in the climate affect variations in the carbon storage. The shifts in the distribution of vegetation will be discussed using the classification described above, and will be compared to observations and reconstructions. The influence of these shifts and of changed climate on terrestrial carbon storage will be discussed.

5.3.1   Climate change

Due to changes in the incoming solar radiation, climate changes both in its annual cycle, and in its yearly mean state. For the beginning of both the Eemian and the Holocene experiment, global temperatures were higher than the control experiment by 0.5 K for 128 ky B.P. and 0.2 K for 9 ky B.P. (fig. 5.1a). During the two interglacials, global temperature decreased towards the pre-industrial control run average. For the Eemian from 117 ky B.P. onwards, global temperature was lower than for the control run. The increased temperatures are accompanied by increased evaporation, with a maximum of 0.015×10^6 km^3 y^{-1} for the Eemian and 0.006×10^6 km^3 y^{-1} for the Holocene over the control run value (fig. 5.1b). Global ice cover shows a course consistent with the global temperature: for the beginning of the insolation experiments ice cover is lower than for the control run by 2 to 3×10^6 km^2, and ice cover increases during the experiments (fig. 5.1c).

5.3.2   Vegetation distribution

Simulated changes

The distribution of vegetation for selected time slices in these periods is shown in figure 5.2, using the biome description presented in paragraph 2.4. For present-day (fig. 5.2d), the pattern matches quite well with what is considered as 'potential' vegetation for most parts of the world. Remarkable deviations were simulated for the Amazon region, which is dominated by savanna in the simulation, Europe, which is too much dominated by boreal forest rather than temperate forest, and Australia, which lacks large desert areas.

For 6 ky B.P. (fig. 5.2c), both at the northern and the southern boundary of the Sahara desert, as well as of the South Asian deserts, vegetation expands compared to the control run, thereby decreasing the deserted area. At the high latitudes of North America, and to a lesser extent the high latitudes of east Asia, boreal forest expands compared to the control run. For 126 ky B.P. (fig. 5.2a), these effects are even larger. The western part of the Sahara is covered with temperate grassland in the simulation, tropical forests in northern Africa and southeast Asia expand, and the boreal forests
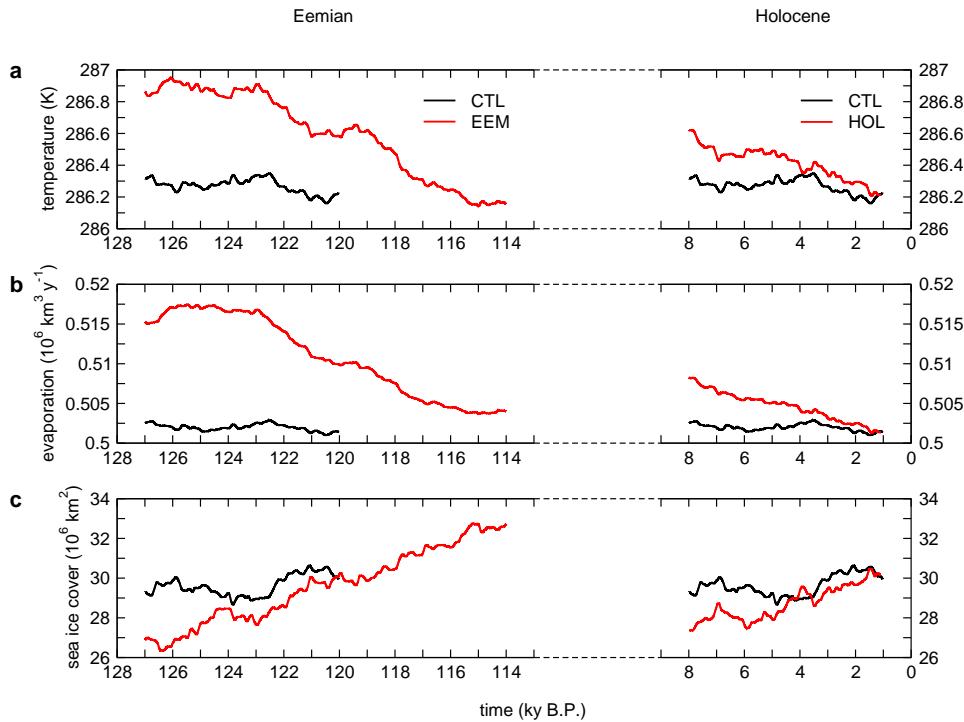
Figure 5.1: *Time series of (a) globally averaged near-surface air temperature, (b) global evaporation, and (c) global sea ice cover for the Eemian and the Holocene experiments (EEM and HOL) and the control run (CTL). Shown are 2 ky running means.*

expand northward up to the Arctic Ocean in many places. In the southern hemisphere a slight retreat of forests was simulated for Africa. For 115 ky B.P. (fig. 5.2b), the opposite can be seen: boreal forests in the northern hemisphere show a clear southward retreat and the vegetation cover in the monsoon areas decreases slightly, in most other regions vegetation patterns are very similar to simulated present-day conditions.

Comparison with vegetation data

Global data sets of vegetation for paleoclimatic times are rare, and provided only for selected time slices. The Holocene has been studied more often than the Eemian, which is related with the obtainability of pollen data.

For the last interglacial optimum, a reconstruction of northern hemisphere vegetation was provided by Grichuk (1992). For the high latitudes it shows a decreased tundra area, coniferous forests expand northward up to the Arctic Ocean. Some tundra areas remain in northeast Asia and the northeastern part of North America. This is consistent with the simulated distribution of tundra from the Eemian experiment (fig. 5.2a). The forest
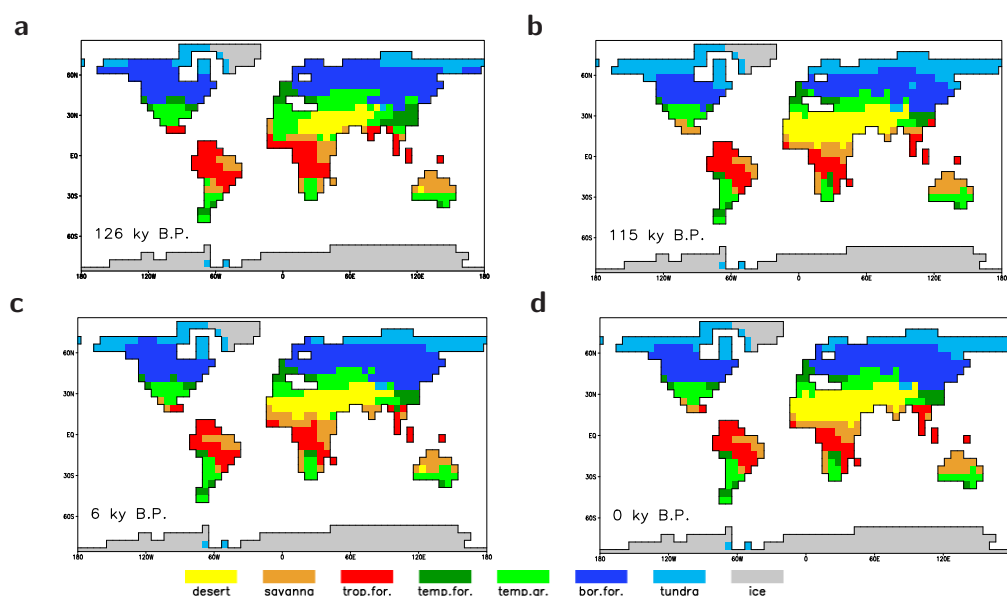
Figure 5.2: *Global distribution of biomes as calculated from LPJ, for (a) 126 ky B.P. (EEM), (b) 115 ky B.P. (EEM), (c) 6 ky B.P. (HOL), and (d) present (CTL). All plots show an average over 1000 years around the indicated time (present is an average over the complete CTL experiment, 10 000 years), for description of the biome calculation, see text and table 2.4.*

zone shifts northward, especially for North America. In the simulation, the border between temperate and boreal forest is too far south compared to the reconstruction. The subtropical trees and bushes occupy a larger area: large parts of northern Africa are covered with savanna-type vegetation. This was found in the Eemian experiment as well, although the simulated area is restricted to the western part of Africa (fig. 5.2a).

A large set of pollen data for central Asia during the Eemian was provided by Tarasov et al. (2005), revealing an increase of taiga till 125 ky B.P., followed by a period with relatively high taiga cover. At the end of the interglacial, steppe and tundra become more dominant again.

Reconstructions from the Holocene are less rare: global pollen reconstructions are provided by Prentice et al. (2000) for 6 ky B.P., and global vegetation maps based on fossils, pollen data and other sources for 8 and 5 ky B.P. are provided by Adams and Faure (1997). Detailed comparison studies between data sets and model output were performed for the Mid-Holocene (6 ky B.P.) on a global scale (Harrison and Prentice, 2003) as well as in more detail for 55°-90°N (Kaplan et al., 2003). For 6000 year B.P., Hoelzmann et al. (1998) provided reconstructions for northern Africa, indicating that roughly the northern half of north Africa was mainly covered with steppe, and the southern half was mainly covered with savanna. The main features

of vegetation changes in these studies were obtained in the simulation as well: a gradual southward retreat of the taiga-tundra boundary in the high latitudes of the northern hemisphere, as well as a southward retreat of the border between boreal and temperate forest, and a decrease of vegetation in monsoon areas.

5.3.3   Terrestrial carbon storage

The atmospheric CO_2 concentration increased during both the Eemian and the Holocene experiment (fig. 5.3a), starting around 270 ppm. For the Eemian experiment, a CO_2 concentration of 280 ppm (which corresponds to the pre-industrial level) is reached around 123 ky B.P., for the Holocene experiment, pre-industrial concentration is reached at the end (0 ky B.P.). The natural variability is remarkably large for the CTL experiment, the standard deviation is 3.6 ppm.
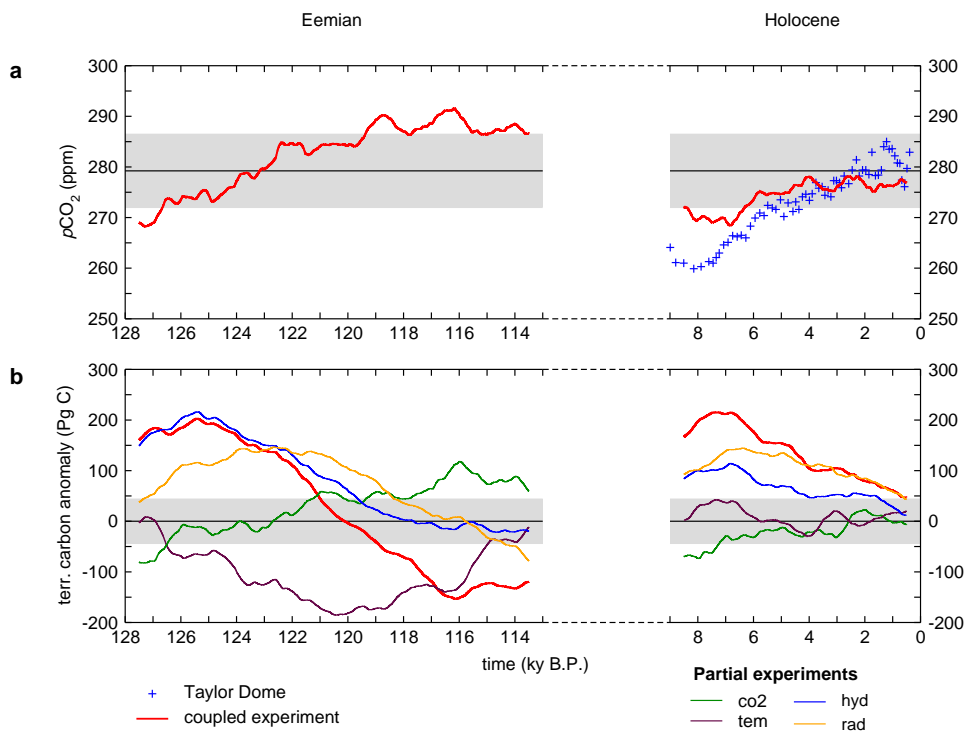
Figure 5.3: *Time series of (a) atmospheric CO_2 concentration for the HOL and EEM experiment, with average of the CTL experiments, and (b) total carbon storage anomaly in the terrestrial biosphere for all experiments. Shown are 1000 year running means, the grey areas indicate $\pm$ 2 standard deviations of the CTL experiment. For the Holocene, proxy data from Taylor Dome CO_2 concentration (Indermühle et al., 1999) are shown.*

For both interglacials, CO_2 concentration and terrestrial carbon storage

show an opposite tendency, with the amplitude of the atmospheric CO_2 concentration about 40 Pg C for the Eemian and 20 Pg C for the Holocene, and the amplitude of the terrestrial biosphere about 350 Pg C for the Eemian and 200 Pg C for the Holocene (fig. 5.3). The increase in CO_2 concentration is the result of release of terrestrial carbon (fig. 5.3b), the remaining carbon released from the terrestrial biosphere is taken up by the ocean. The decrease of terrestrial carbon storage was simulated for both the Eemian and the Holocene, with a rather similar maximum (around 205 Pg C and 215 Pg C for 125 ky B.P. and 7 ky B.P., compared to the control run). After 120 ky B.P., the terrestrial carbon storage is smaller than in the control run, with a minimum of -150 Pg C for 116 ky B.P.

The spatial pattern for carbon storage shows that particular regions play a dominant role in the changes during the interglacials (fig. 5.4): The high latitudes north of 60°N show an increase for 126 ky B.P. and 6 ky B.P. compared to the control run, for 115 ky B.P. this latitude band shows a decrease. The mid-latitudes, between 30°N and 60°N, show the opposite signal: a decrease of carbon storage for 126 ky B.P. and 6 ky B.P., and an increase for 115 ky B.P. The monsoon regions in northern Africa and southeast Asia show a clear increase for 126 ky B.P., and a small effect for 6 ky B.P. as well. The southern hemisphere shows some small changes, but no clear pattern can be observed here.

Carbon storage anomalies for the Eemian and the Holocene can not be explained from a single climate parameter (fig. 5.3). All parameters analysed here (temperature, radiation, hydrology and CO_2) show effects on the total carbon storage that are larger than two standard deviations of the control run storage. These parameters were analysed in detail, and are discussed below.

The evolution of terrestrial carbon storage in time (fig. 5.5a) shows the main features from the selected period in figure 5.4. The bands of increased and decreased storage in the high latitudes show a remarkable swap around 120 ky B.P. From 128 to 120 ky B.P., an increase was simulated for 60°–75°N, a decrease for 40°–60°N, and again an increase for 0°–30°N. After 120 ky B.P. the pattern shifts: a decrease was simulated for 55°–65°N, and an increase is seen for 45°–55°N.

Temperature

Temperature changes during the interglacials (fig. 5.6) are a direct effect of changes in the earth's orbit. Due to a summer perihelion at 127 ky B.P., combined with a large eccentricity of the earth orbit, summer insolation for the northern hemisphere is enhanced compared to present-day for the first half of the Eemian experiment. This causes positive temperature anomalies in summer (fig. 5.6). For the second half of the Eemian experiment, the perihelion occurs in winter for 116 ky B.P., causing a relatively low incoming
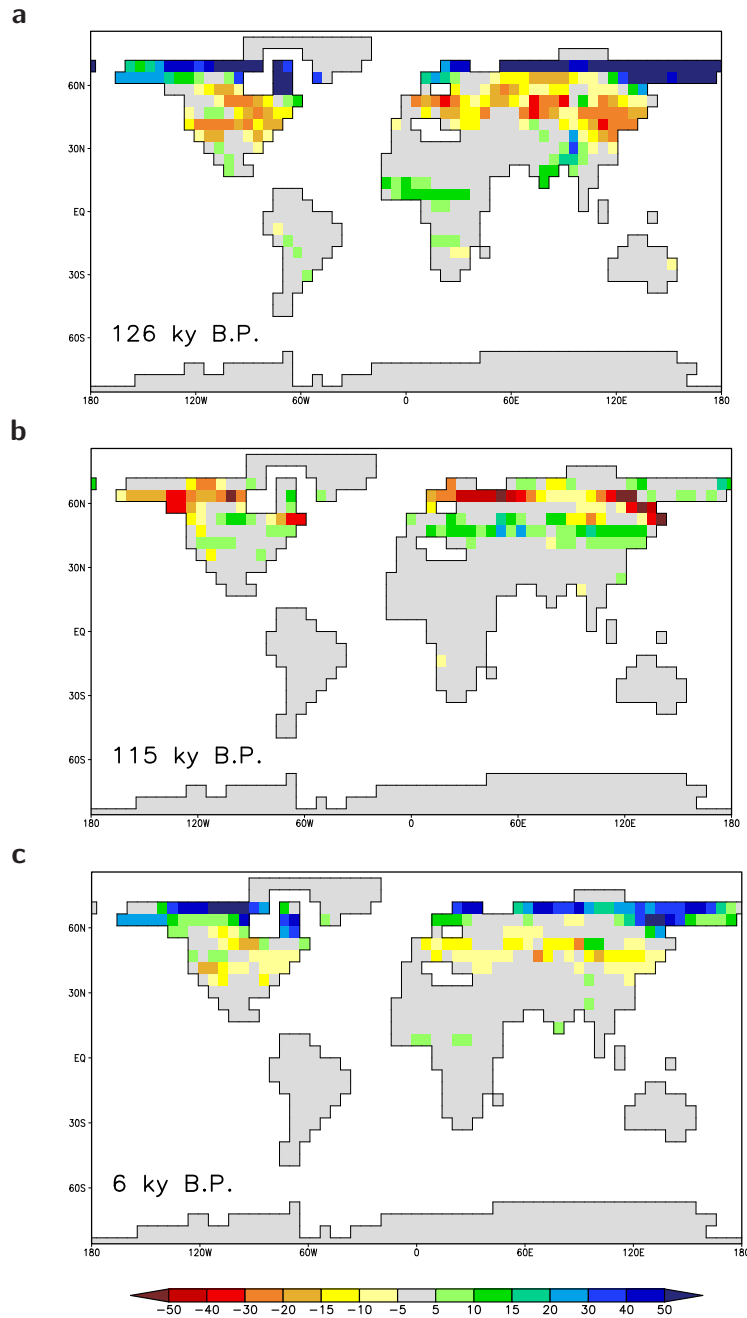
Figure 5.4: *Total terrestrial carbon storage anomalies (kg C m^{-2}) for selected periods from the interglacial experiments: (a) 126 ky B.P. (EEM), (b) 115 ky B.P. (EEM), and (c) 6 ky B.P. (HOL). Anomalies from the control run (CTRL) are shown for 2000 year periods around the given time.*
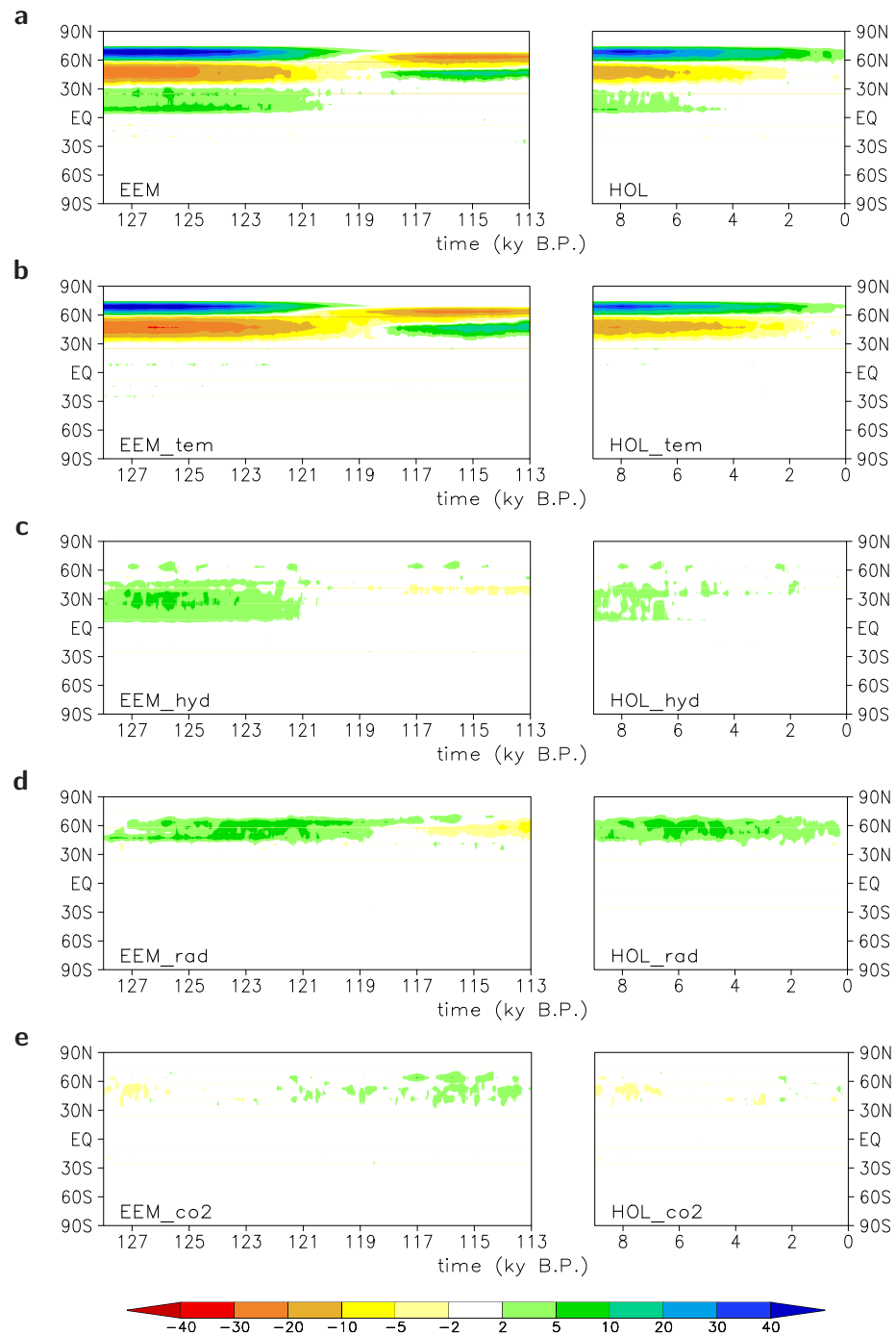
Figure 5.5: *Zonal anomalies of total carbon storage per latitude (Pg C per degree latitude) for the Eemian and the Holocene with full climate forcing (a), as well as for the temperature only (b), hydrology only (c), radiation only (d) and CO$_2$ only (e) experiments.*

radiation in summer, and an increase in insolation in winter (fig. 5.6). For the Holocene, the effect is slightly less: although perihelion occurs in summer as well, the eccentricity is roughly half of the Eemian eccentricity, thereby reducing the differences between summer and winter (Berger, 1978).
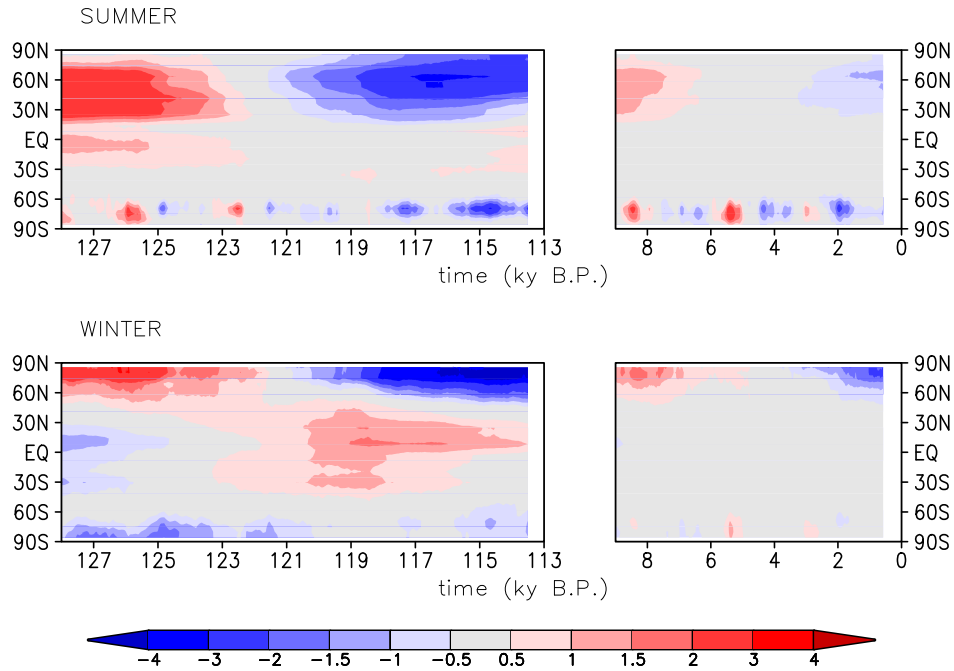
Figure 5.6: *Zonal mean temperature anomalies for Northern Hemisphere summer (JJA) and winter (DJF) for the insolation experiments (EEM and HOL). Shown are 1000 year running means.*

For the beginning of both Eemian and Holocene, the Northern Hemisphere summer is warmer, with a larger anomaly for the Eemian than for the Holocene. For the Eemian, warming occurs as well around the equator, the monsoon areas in the Northern Hemisphere are relatively cool due to increased evaporation and increased cloud cover, related to an enhancement of the monsoon precipitation. For the Eemian, a cooling up to 4 K occurs after 120 ky B.P. for the Northern Hemisphere north of 20°N. A slight cooling (up to 1.5 K) was simulated for the last 2000 years of the Holocene as well, which is remarkable, and which shows that a steady-state control run does not necessarily provide the state that would be reached at the end of a transient run. For the Northern Hemisphere winter, the latitudes north of 60°N show a clear positive temperature anomaly for the beginning of both experiments. This positive anomaly changes to a negative anomaly after 120 ky B.P. A similar pattern can be seen for the Holocene, although the mag-

nitude is slightly smaller. Again a cooling was simulated for the last 2000 years of the Holocene. The tropics and subtropics show a clear warming for winters between 122 and 114 ky B.P. In the Southern Ocean, variability is high, and positive and negative temperature anomalies for summer and winter are mainly related to changes in the convection.

Temperature-induced changes in terrestrial carbon storage show the most prominent signal of all climate parameters for the mid- and high latitudes in the partial experiments (fig. 5.5). For the beginning of the Eemian and Holocene experiments, an increased storage of carbon is simulated in the latitudes north of 60°N compared to the present-day situation, and a decreased storage is simulated between 40°N and 60°N. The anomalies become smaller with time, and for the Eemian the situation swaps around 119 ky B.P.: the high latitudes have a decreased storage and the mid-latitudes an increased storage compared to present-day. Despite the large anomalies, the net effect on carbon storage is rather small and even negative for the Eemian experiment (fig. 5.3b).
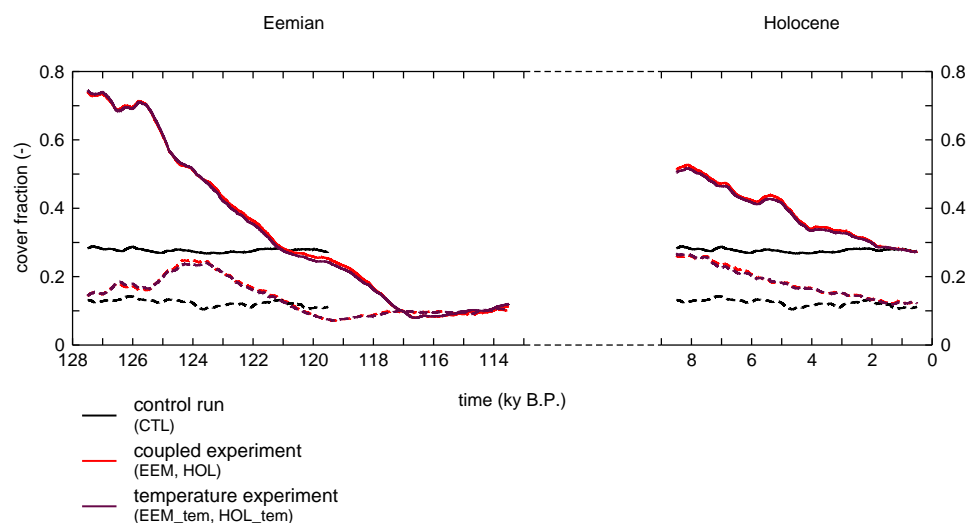
Figure 5.7: *Fractions of the land area between 60° N and 90° N covered with boreal trees (full line) and grasses (dashed line), for the control run (CTL), the coupled experiments (EEM and HOL) and the experiments forced with temperature only (EEM_tem and HOL_tem). Shown are 1000 year running means.*

For the area north of 60°N, temperature increase causes the region to become more favourable for forest growth, grasses are there replaced by trees. Between 128 and 121 ky B.P., the boreal forests cover a larger area than in the control run (fig. 5.7). In the beginning of the experiment, the cover is over 70% of the surface. After 125 ky B.P., it declines sharply, thereby enabling a slight increase of grass cover. A decline for both boreal

trees and grasses causes the covers to become lower than the control run around 121 ky B.P., with a minimum forest cover of about 10% (around 117 ky B.P.). For the Holocene, a decrease of forest fraction is simulated as well, although the maximum is not as high as for the Eemian. The increase in grass cover after retreat of the forests is not seen for the Holocene, and the covers of both trees and grasses are roughly equal to the control run values at the end of the Holocene experiment.

In the experiments forced with temperature of the coupled experiments only (EEM_tem and HOL_tem) the covers of boreal forests and grasses have a very similar behaviour for the area north of 60°N (fig. 5.7), indicating that temperature is the main driver for the changes in cover fractions. These changes cause the carbon storage effect north of 60°N. The area between 30°N and 60°N does not show large changes in the cover fraction. The changes in carbon storage here compared to the control run are related to changes in autotrophic and heterotrophic respiration. Due to higher temperatures, decay of carbon goes faster, which causes a reduction of the residence time of carbon. Especially soil carbon pools become smaller due to the faster turnover.

Hydrology

The climate change caused by variations in the orbital forcing includes changes in the hydrological cycle. Due to increased temperatures on land a stronger temperature gradient between the land surface and the ocean occurs and monsoon cells are strengthened, thereby bringing more moist air to the continents and causing more convection. This results in an increase of precipitation over land and a decrease over the ocean, especially in the tropics and subtropics (fig. 5.8a).

Most important changes in carbon storage due to changes in the hydrological cycle take place between 10°N and 40°N (fig. 5.5c), where water availability is a limiting factor for plant growth. Although local changes in carbon storage are smaller than the changes caused by temperature in the higher latitudes, the latitude band being influenced is rather large, and the changes in the hydrological cycle cause a spatially constant positive effect on carbon storage between 128 and 121 ky B.P. and between 9 and 6 ky B.P. In contrast to temperature, there are no regional decreases in carbon storage due to hydrological changes for these periods, making hydrology one of the most important net effects of the anomalies seen for these periods in total carbon storage (fig. 5.3b).

Figure 5.8a shows the positive anomaly of precipitation over the continents and the negative anomaly over the ocean between 128 and 121 ky B.P. and between 9 and 6 ky B.P. In northwest Africa, precipitation increased up to 500 mm per year compared to the pre-industrial control run. A strong increase of precipitation occurred as well in the southeast Asian

monsoon area around India, and at the west coast of North America. The most pronounced decrease of precipitation is found over the Atlantic Ocean, and to a lesser extend over the tropical Pacific. After 118 ky B.P., the north African as well as the North American subtropical and tropical parts of the continent become dryer than the control run.

Vegetation growth reacted strongly to the changes in precipitation for most regions. The most sensitive regions are northwest Africa, southeast Asia around India, and western North America, with in general strong positive anomalies in vegetation cover between 128 and 121 ky B.P. and 9 and 6 ky B.P., and smaller negative anomalies from 118 ky B.P. onwards (fig. 5.8b). Especially for Northwest Africa and Southeast Asia, vegetation cover was higher than present-day at the beginning of both experiments. The Eemian shows a gradual decrease of the vegetation cover in the western Sahara region from about 40% to practically 0% from 124 ky B.P. to 118 ky B.P. (chapter 4). For the Holocene, maximum vegetation cover is roughly half of the Eemian cover, with a decrease from 9 ky B.P. to 4 ky B.P.

The increase in vegetation cover, as well as the conversion of grass-covered areas into forests, causes an increase in carbon storage for these regions (fig. 5.8c). The patterns of carbon storage are very similar to those shown for vegetation cover, with again stronger anomalies for the Eemian than for the Holocene simulation. The maximum increase in global carbon storage due to hydrological changes (from the EEM_hyd and HOL_hyd experiments) was roughly twice as large for the Eemian than for the Holocene (fig. 5.3b). This difference is directly related to the strength of the monsoon, which is mainly determined by the contrast in heating between the ocean and the land surface. Due to a decrease of the surface albedo, this contrast is enhanced. This enhancement is larger for the Eemian than for the Holocene, because of the more eccentric earth orbit for the Eemian. Besides that, the positive feedback between presence of vegetation and precipitation (see chapter 4 for a more detailed analysis) enhances this contrast.
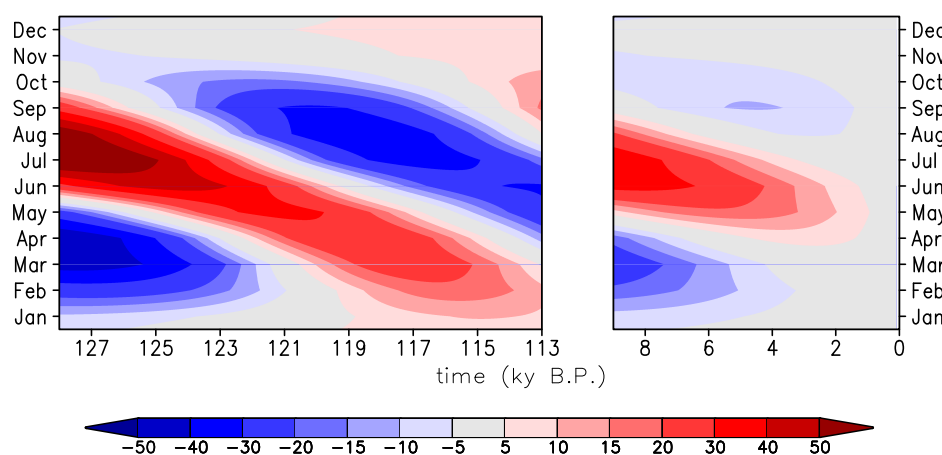
Radiation

Incoming solar radiation had both for the Eemian and for the Holocene a remarkably positive direct influence on carbon storage for the latitudes between 45°N and 70°N during the warm phase (fig. 5.5). The reason for this increase is an increase in photosynthesis for these latitudes, caused by an increase in absorbed shortwave radiation. The radiation anomaly for these latitudes (fig. 5.9) shows an increase of incoming radiation for the summer months and the largest decrease for spring at the beginning of the experiment. Both the positive and the negative anomaly are moving to earlier occurrence in the year, which causes the amplitude in the annual cycle of incoming radiation to become smaller, and both anomalies weaken during the experiments. The incoming radiation at the surface shows a
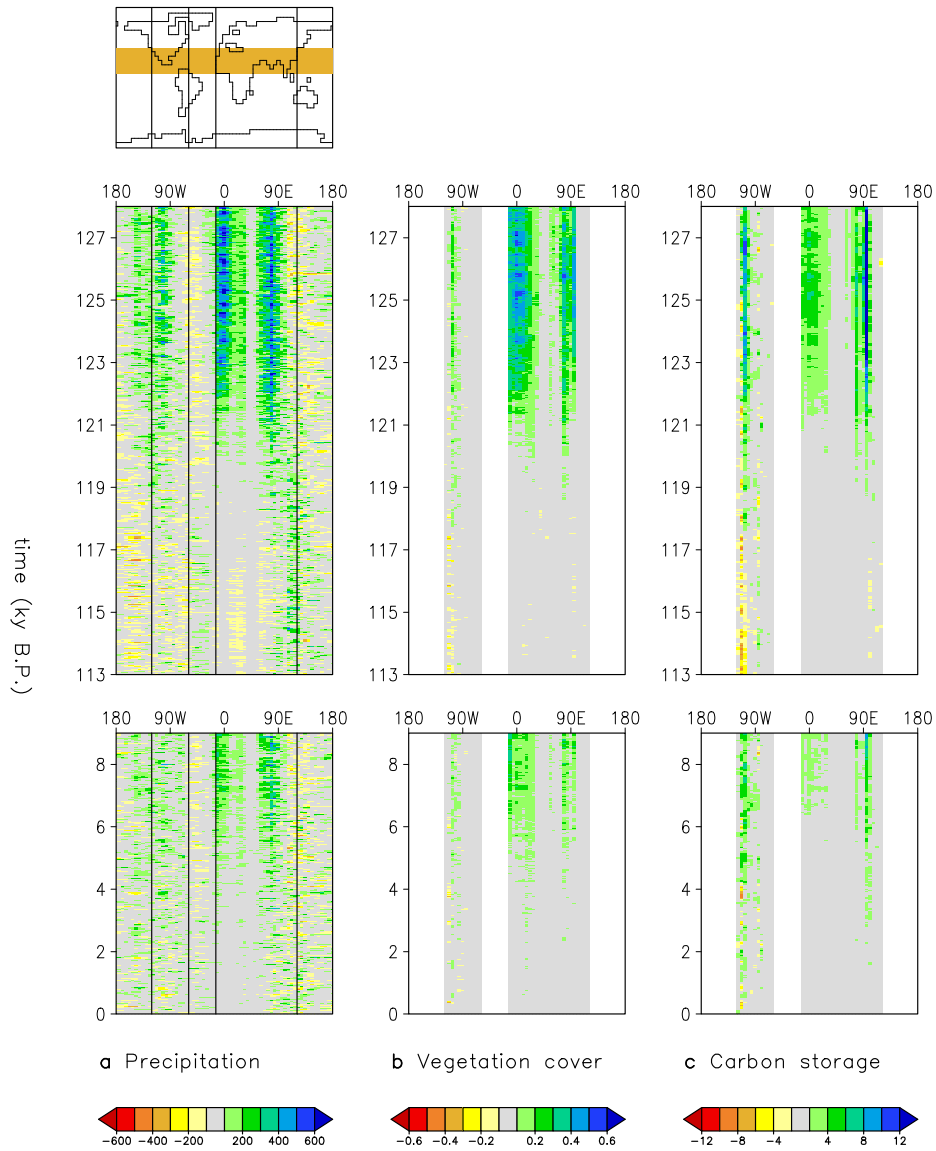
Figure 5.8: *Meridional anomalies of (a) precipitation (mm y^{-1}) from the fully coupled experiments (EEM and HOL), and (b) vegetation cover (-) and (c) carbon storage (kg m^{-2}) on land from the experiments with hydrological forcing only (EEM_hyd and HOL_hyd), all shown for the region 6°–34° N (see figure).*

similar pattern as the incoming radiation at the top of the atmosphere, but with a smaller amplitude (not shown). Maximum increase in incoming radiation at the surface is around 40 W m^{-2} for summer around 127 ky B.P., maximum decrease is around -30 W m^{-2} for spring 127 ky B.P. In general, the amplitude at the surface is roughly 30 to 50 % of the amplitude at the top of the atmosphere.

Figure 5.9: *Anomaly of the annual cycle of incoming shortwave radiation (W m^{-2}) at the top of the atmosphere for 60° N for the Eemian and Holocene.*

The influence of changes in the radiation on photosynthesis is shown in figure 5.10a. From 127 ky B.P. onwards, the maximum rate of photosynthesis decreased, and the peak in photosynthesis shifted later in summer. The anomalies of gross primary production (GPP) compared to the control run (fig. 5.10b) are a result of radiation and temperature changes (fig. 5.10c and 5.10d). The positive temperature anomaly both in summer and in winter for the beginning of the Eemian experiment (fig. 5.6) causes the growth and development of the vegetation to start earlier in the season, resulting in an increase of radiation absorption due to a faster leaf development and thereby in an increase of photosynthesis, especially in the first two months of the growing season (fig. 5.10d). This effect is enhanced by a positive radiation anomaly for the summer months (fig. 5.9), which results in additional photosynthesis (fig. 5.10c). After 122 ky B.P. the temperature anomaly became negative for the region north of 60°N, and the development of vegetation in spring becomes slower than in the control run. Due to the high radiation anomaly, the EEM_rad experiment had initially a slightly positive anomaly in GPP later in the season for 121 ky B.P. (fig. 5.10c), but this vanished afterwards, when the radiation anomaly decreased.
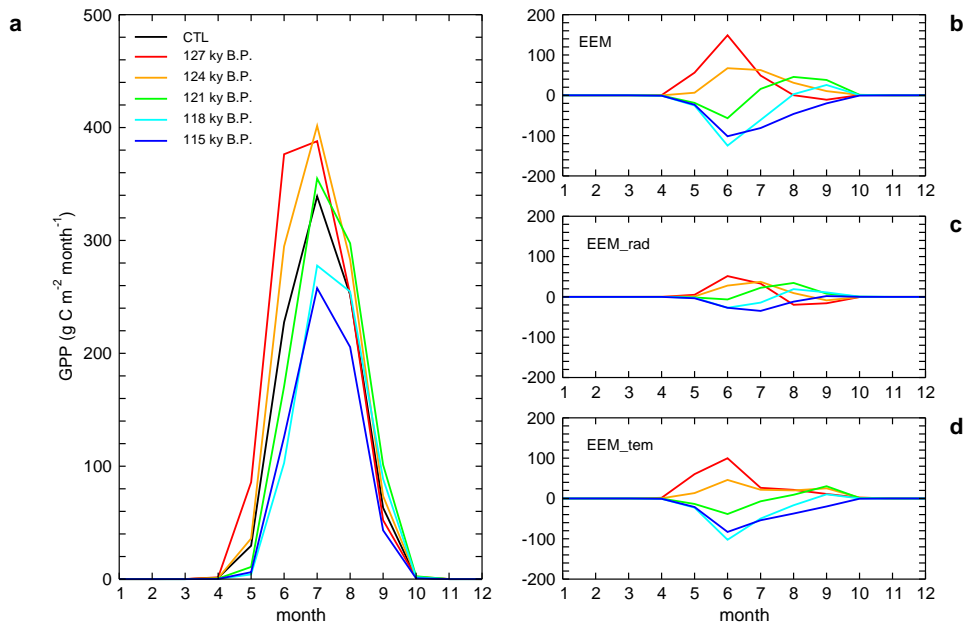
Figure 5.10: *(a) Anual cycle of photosynthesis around 60° N for selected periods (2000 year averages) from the Eemian coupled run (EEM) and the control run (CTL), and anomalies of the fully coupled experiment (b, EEM), the radiation only experiment (c, EEM_rad), and the temperature only experiment (d, EEM_tem), all compared to the control run (CTL).*

CO_2

Total terrestrial carbon storage in the experiments with CO_2 as varying forcing show most clearly a first-order reaction to the atmospheric CO_2 concentration (fig. 5.3). In these experiments, the amplitude of global net primary production (NPP) is roughly 4.5 Pg C y^{-1} (EEM_co2) and 2 Pg C y^{-1} (HOL_co2), compared to a standard deviation of 1.7 Pg C y^{-1} for the control run (CTL). These changes are small compared to changes from other factors, and work in the opposite direction of the CO_2 signal of the coupled experiments (fig. 5.11).

The effect of changes in the atmospheric CO_2 concentration are small on primary production and small on carbon storage, which was to be expected because the terrestrial biosphere was the driver of these atmospheric CO_2 changes. A terrestrial biosphere very sensitive to these changes would inevitably have led to a much smaller signal in the atmospheric CO_2 concentration.
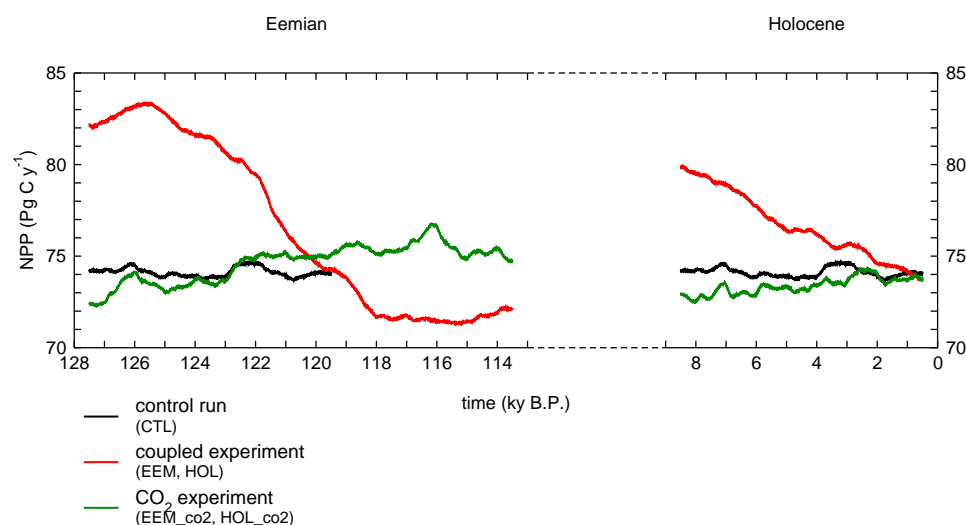
Figure 5.11: *Global net primary production (NPP) for the control run (CTL), the coupled experiments (EEM and HOL) and the experiments forced with CO_2 only (EEM_co2 and HOL_co2). Shown are 1000 year running means.*

5.4   Conclusions and discussion

The earth system model was used to study carbon storage during two interglacials, the Holocene and the Eemian. Under pre-industrial conditions, the model gives a reasonable distribution of the major vegetation zones, with some remarkable exceptions. In the Amazon region, large areas are covered with savanna type vegetation, because the simulated climate is too dry here. The border between temperate and boreal forests was situated too far south, due to too cold temperatures in the Northern Hemisphere mid and high latitudes.

For the beginning of the Eemian and Holocene simulations, enhanced vegetation growth in north Africa and Asia around India caused a decrease of the desert area and an increase in savanna and temperate grassland. This is in agreement with proxy data and reconstructions (e.g. Prentice et al., 2000).

The cover of forests in the high latitudes of the northern hemisphere decreased during both experiments due to a gradual cooling. This causes a southward retreat of the treeline, which agrees with observations (Adams and Faure, 1997; Prentice et al., 2000).

The changes in the distribution of vegetation, together with changes in photosynthesis rates, and changes in climatic circumstances, cause changes in the storage of carbon in the terrestrial biosphere. These were the main cause for a gradual increase of the atmospheric CO_2 concentration during

both interglacial experiments. For both the Eemian and the Holocene, terrestrial carbon storage was high in the beginning of the experiments, and gradually decreased from 125 ky B.P. and 8 ky B.P. onwards. These changes can be explained by the following relations between climate and the terrestrial carbon cycle.

Temperature affected carbon storage dominantly, but its global net effect is small: the increase in summer temperature of the mid and high latitudes around 125 ky B.P. and around 9 ky B.P. caused an increase in forest growth and in photosynthesis and thereby an increase in carbon storage for the high latitudes. Autotrophic and heterotrophic respiration increased as well due to the temperature increase, which in turn decreased carbon storage for the mid latitudes. The anomalies become smaller and for the Eemian experiment the pattern swaps after 120 ky B.P. Overall, these two opposing processes caused the global temperature effect on terrestrial carbon storage to be small in the coupled experiments that were performed here. From the size of the positive and negative anomalies, it is clear that this outcome is sensitive to changes in the sensitivity of both photosynthesis and autotrophic and heterotrophic respiration to temperature. Changes in the hydrological cycle were a main cause for increased carbon storage in the subtropics. The region between 10°N and 40°N showed an increase in storage from 128 to 121 ky B.P. and from 9 to 6 ky B.P. Although the local changes were much smaller than those caused by temperature effects, the effect was positive for all regions for the beginning of the experiment, which caused the globally averaged maximum storage increase due to hydrological changes to be around 200 Pg C for the Eemian and around 100 Pg C for the Holocene. Radiation changes were causing another important part of the increased carbon storage. Due to higher insolation in summer compared to the control run, photosynthesis increased for the land surface between 40° and 70°N for 128 to 119 ky B.P., resulting in more carbon storage. Maximum anomalies due to radiation changes were roughly 150 Pg C for both the Eemian and the Holocene. The CO_2 concentration had minor influence on the terrestrial carbon storage.Terrestrial carbon storage was a main driver of the changes in atmospheric CO_2. This indicates that the negative feedback between terrestrial carbon storage and CO_2 concentration is rather weak, and that changes in the orbital forcing are of much larger importance for carbon storage.

An estimate of terrestrial carbon storage for the Holocene for 8 ky B.P., based on a reconstructions of the vegetation distribution combined with estimates of carbon storage in selected ecosystems was derived by Adams and Faure (1998). They calculate a negative anomaly of terrestrial carbon storage compared to present-day of 170 Pg C. Kaplan et al. (2002) and Joos et al. (2004) both show an increase in terrestrial carbon storage for the Holocene from the last glacial maximum onwards, both performed with the LPJ model. In the study presented here, the opposite effect was observed:

for the last 9000 years it showed a decrease in terrestrial carbon storage. A similar effect was obtained by Brovkin et al. (2002), with a magnitude of 100 Pg C. Differences could occur from uncertainties in the temperature effect: the simulations showed that the temperature effect is caused by two opposing effects, of which the net outcome might be climate- and model-dependent. Besides that, Kaplan et al. (2002) state that they might have underestimated the carbon loss due to changes in the monsoon.

The changes in the CO_2 concentration for the interglacials was shown to be caused by changes in terrestrial carbon storage in these simulations. However, this is not at all indicative for carbon storage during glacials, or for interglacial-to-glacial transitions. During glacials, terrestrial carbon storage is supposed to be rather low due to low temperatures and a weak hydrological cycle. The CO_2 concentrations were relatively low during glacials (Petit et al., 1999), the explanation for this does not come from the mechanisms described here. Moreover, most likely carbon storage in other sinks will have to compensate another few hundred petagrams of carbon that are lost by the terrestrial biosphere.

Chapter 6

A general analysis of the interactions between vegetation and climate for the interglacial simulations

Abstract

The results from the studies on biogeophysics (chapter 4) and biogeochemistry (chapter 5) of the interglacial experiments are summarized. The biogeophysical and biogeochemical effects were compared, and the influence of biogeophysically induced climate change on terrestrial carbon storage was determined.

6.1   Introduction

The quantitative understanding about the interactions between vegetation and climate gained in the previous chapters will be used here to give a general analysis on the stability of the system.

Chapter 4 showed the biogeophysical interactions between the land surface and the atmosphere. These interactions caused mainly positive feedbacks, thereby enhancing the effects caused by changes in the earth orbit. Two regions showed largest effects: the high latitudes of the northern hemisphere, where the interactions between albedo, temperature and forest growth cause the positive feedback, and the monsoon region in the low latitudes, mainly northern Africa, where the interactions between albedo, precipitation and vegetation growth cause the positive feedback.

Chapter 5 showed the biogeochemical role of the terrestrial biosphere. The terrestrial biosphere was causing changes in the atmospheric CO_2 concentration, thereby acting as a driver of these changes. The terrestrial biogeochemistry is mainly causing a weak negative feedback. Several climatic factors were causing the changes in terrestrial carbon storage, with radiation and hydrology changes as positive contributors, and temperature changes as indeterminate effect.

Combination of the two studies brings us two important feedback loops: a positive feedback between climate change and land surface changes, and a negative loop between climate change, terrestrial carbon storage and atmospheric CO_2 concentration. In this chapter, these two feedback loops will be combined.

The results from the interglacial experiments in chapters 4 and 5 will be summarized, using key parameters for the biogeochemical and biogeophysical effects. Table 6.1 gives an overview of the experiments used in this chapter, table 6.2 provides a short overview with selected parameters that can be used to represent the strength of the feedback mechanisms. Summer insolation for 65°N is often used as an indicator for the insolation effect in paleoclimatic experiments.

6.2   Biogeophysical feedbacks

The biogeophysics of the interglacial simulations, as discussed in chapter 4, showed mainly positive feedbacks between land surface and climate. For 126 ky B.P., northern hemisphere summer temperatures were 2.2 K warmer than present for the EEM experiment, and 2.1 K for the AEEM$^+$ experiment (accelerated). A comparison of AEEM$^+$ and AEEM$^-$ reveals that 0.4 K of this summer warming for the northern hemisphere is caused by biogeophysical interactions between land surface and climate, leading to an enhanced global annual warming of 0.3 K. Largest effects for the Holocene

Table 6.1: *Overview of the experiments*

CTL$^+$	control run with present-day insolation and interactive land surface (10 000 years)
ACTL$^+$	control run with present-day insolation and interactive land surface, shorter asynchronous periods than CTL$^+$
ACTL$^-$	control run with present-day insolation and prescribed (present-day) land surface
EEM$^+$	insolation experiment (15 000 years)
AEEM$^+$	insolation experiment and interactive land surface (accelerated)
AEEM$^-$	insolation experiment and prescribed land surface (accelerated)
RAEEM$^+$	unaccelerated repetition of AEEM$^+$
RAEEM$^-$	unaccelerated repetition of AEEM$^-$

were found around 8 ky B.P. Summer temperatures for the northern hemisphere increased by 1.1 K, and global annual temperatures increased by 0.3 K.

Forests cover increased by 30% due to orbit induced climate change, and an extra 12% of the surface became afforested due to the enhanced warming related to the positive feedback in the high latitudes, which makes a total increase of 42% (table 6.2). For the Holocene, total increase in forest fraction was 23% for 8 ky B.P., and 12% for 5 ky B.P. Vegetation cover in the Sahara region increased by 41% for the Eemian (126 ky B.P.), and by 16% for the Holocene (8 ky B.P.).

The difference in biogeophysical effects for the Holocene and the Eemian is caused by the difference in changes in the earth's orbit. For both Eemian and Holocene, a summer perihelion caused the warming in summer. However, the eccentricity of the earth orbit for the Holocene was roughly half of the eccentricity for the Eemian. This difference is the main driver for the differences between biogephysical feedbacks for Eemian and Holocene, as discussed above, with a remarkably linear relation between orbital anomaly, climate anomaly, and vegetation anomaly.

6.3   Biogeochemical feedbacks

The biogeochemical role of the terrestrial biosphere was discussed in chapter 5. Despite the difference in forcing, a similar maximum increase of terrestrial carbon storage was simulated for both interglacials. The explanation for this is found in the effects of single climatic parameters (fig. 5.3b): the maximum effect of radiation on terrestrial carbon storage is slightly higher for the Eemian than for the Holocene, the maximum effect of hydrological changes is roughly twice as large. Only temperature plays a complex

Table 6.2: *Key biogeochemical and biogeophysical parameters from the insolation experiments in chapters 4 and 5: atmospheric CO_2 concentration; shortwave insolation in summer for 65° N; land surface albedo; planetary albedo; global temperature; summer (JJA) temperature of the Northern Hemisphere; forest fraction for the land surface 60°–90° N; vegetation cover in the western Sahara ($10° E$–$20° W$, $10°$–$30° N$); terrestrial carbon storage in the high latitudes (north of 30° N and south of 30° S); terrestrial carbon storage in the low latitudes (between 30° N and 30° S)*

Experiment		pCO_2 (ppm)	insolation 65°N, JJA (W m^{-2})	α_{land}	α_{plan}	T_{glob} (K)	T NH, JJA (K)	c_f 60°–90°N	c_v Sahara	C_{bios} high lat. (Pg C)	C_{bios} low lat. (Pg C)
CTL$^+$	pre-industrial	279.2	446.5	0.231	0.314	286.3	291.4	0.28	0.01	2879.	816.
ACTL$^+$	pre-industrial	280.0	446.5	0.231	0.314	286.2	291.4	0.27	0.01	2861.	809.
ACTL $^-$	pre-industrial	279.4	446.5	0.246	0.315	286.2	291.3	0.28	0.00	2951.	813.
EEM$^+$	126 ky B.P.	273.7	483.3	0.208	0.313	287.0	293.6	0.69	0.42	2942.	940.
AEEM$^+$	126 ky B.P.	276.8	483.2	0.209	0.313	286.8	293.5	0.70	0.42	2833.	933.
AEEM$^-$	126 ky B.P.	275.9	484.0	0.243	0.314	286.5	293.1	0.58	0.17	2841.	922.
EEM	115 ky B.P.	287.0	418.0	0.245	0.315	286.2	290.6	0.09	0.00	2750.	813.
AEEM$^+$	115 ky B.P.	286.3	417.8	0.244	0.315	286.2	290.7	0.10	0.01	2833.	826.
AEEM$^-$	115 ky B.P.	282.8	417.6	0.249	0.315	286.2	290.6	0.13	0.10	2920.	818.
HOL	8 ky B.P.	270.5	480.1	0.218	0.313	286.6	292.5	0.51	0.17	3012.	871.
HOL	5 ky B.P.	275.5	471.6	0.224	0.313	286.5	291.8	0.40	0.07	3004.	836.
HOL	2 ky B.P.	277.1	455.2	0.229	0.314	286.3	291.4	0.30	0.02	2951.	824.

role, and due to the positive effects of temperature increase on both photosynthesis and autotrophic and heterotrophic respiration, its effect differs substantially between the two interglacial experiments. For the Eemian, the negative effect is dominating, with a maximum negative carbon storage anomaly of -180 Pg C around 120 ky B.P. For the Holocene the positive and negative anomalies counterbalance, and the net temperature effect is small. This difference causes the total effects in the coupled experiments to be of a similar size, although the causes for this differ. It causes as well a difference in distribution of the extra carbon storage: the largest part of the additional carbon was stored in the low latitudes (between 30°N and 30°S) for 126 ky B.P., the largest part was stored in the high latitudes for 8 ky B.P. (table 6.2).

6.4 Mutual influence of the biogeophysical and biogeochemical roles

The enhanced temperatures in the high latitudes due to the biogeophysical coupling are likely to affect the biogeochemistry of this region. Due to the acceleration for the $AEEM^+$ and $AEEM^-$ experiments (chapter 4), terrestrial carbon storage in these experiments is distorted. The climate data from these experiments were used to repeat these experiments unaccelerated as $RAEEM^+$ and $RAEEM^-$: for each year in the original experiments, eight years were performed here using the climate archive that was used to bridge asynchronous periods. The climate forcing from the accelerated experiments was added to the climate archive at the right moment in order to represent an unaccelerated carbon cycle from accelerated data. Atmospheric CO_2 concentration was fixed at 280 ppm.

Vegetation carbon storage anomalies showed a rather similar response for the three experiments, with slightly higher carbon storage for the two interactively coupled experiments (EEM^+ and $RAEEM^+$) than for the experiment with fixed land surface ($RAEEM^-$, fig.6.1a). The difference between EEM^+ and $RAEEM^+$ between 128 and 122 ky B.P. was caused by the difference in CO_2 concentration: whereas the repeated experiment ($RAEEM^+$) had a fixed CO_2 concentration of 280 ppm, the coupled experiment (EEM^+) had a prognostic CO_2 calculation, resulting in concentrations lower than 280 ppm for this period (fig. 5.3a). Litter and soil carbon storage (fig. 6.1b) show higher values for the experiment with fixed land surface than for the experiments with interactive land surface. Less abundant warming in the high latitudes contributes to a longer conservation of carbon in soils.
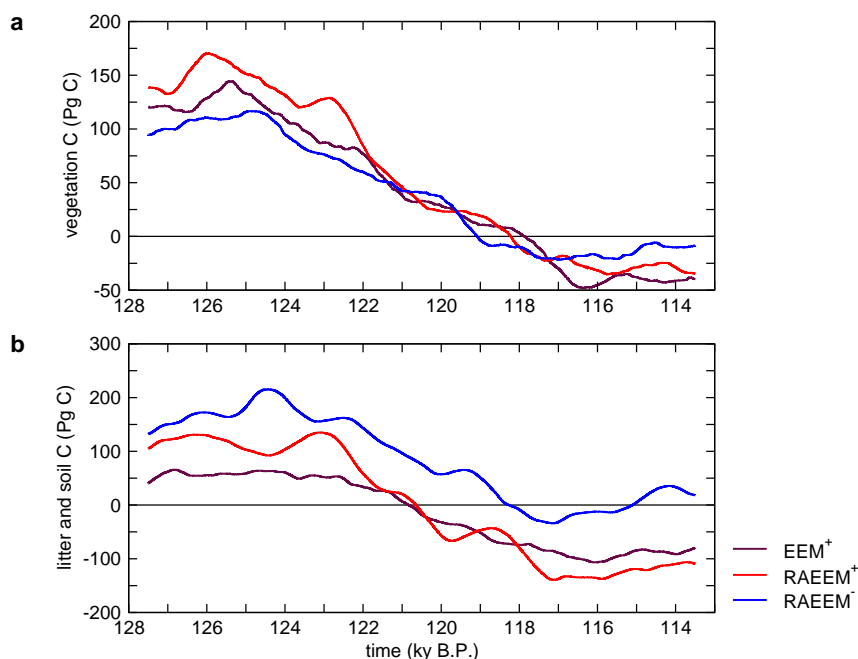
Figure 6.1: *Carbon storage anomalies for (a) vegetation and (b) litter and soil carbon, for the unaccelerated experiment (EEM$^+$) and the unaccelerated repetition of the accelerated experiments (RAEEM$^+$ and RAEEM$^-$). Shown are 1000 year running means.*

6.5   Conclusions and discussion

The Eemian and Holocene react both concerning the biogeophysical and the biogeochemical interactions rather similar. For the biogeophysical interactions, mainly causing positive feedbacks, the model responds rather linearly to the difference in forcing between Eemian and Holocene, causing the total anomalies for forest cover in the high latitudes and for vegetation cover in the western Sahara to be twice as large for the Eemian compared to the Holocene. For the biogeochemical interactions, with a weak negative feedback, the experiments for Eemian and Holocene show terrestrial carbon storage anomalies and atmospheric CO_2 concentration anomalies of roughly equal size, despite the difference in forcing. Two counteracting mechanisms caused by changes in temperature cause the outcome of the model to be sensitive to spatial differences in the temperature anomaly. This sensitivity makes the outcome of the biogeochemical effects more uncertain than that of the biogeophysical effects, and causes the outcome to depend strongly on parametrization of the vegetation model, and the climate model or climate data used for the simulation.

Chapter 7

Long-term effects of biogeophysical and biogeochemical interactions under anthropogenic climate change

Abstract

Feedbacks between the terrestrial biosphere and climate were studied with a set of long-term anthropogenic climate change simulations. CO_2 emissions were assigned according to historical data and the SRES IPCC scenarios B1, A1B and A2, followed by an exponential decay of the emissions for the period 2100–3000. The experiments give a reasonable reconstruction of the measured CO_2 concentrations between 1750 and 2000. Additional experiments were performed with CO_2 emissions and suppressed climate change, as well as with a prescribed land surface for one experiment. The biogeochemical and biogeophysical interactions between terrestrial biosphere and atmosphere were quantified and compared.

A decrease of albedo at high latitudes was the most important biogeophysical change. For the A2 scenario experiment, it caused an additional temperature increase of 1 to 2 K for some high latitude regions by the year 3000, but the changes are minor compared to the heating due to CO_2 increase.

The terrestrial biosphere takes up between 15 and 30 % of the CO_2 emissions, depending on the scenario and the period considered. Terrestrial carbon storage was responsible for a decrease of about 90 ppm in atmospheric CO_2 concentration, or a temperature decrease of about 0.8 K in global average temperature.

7.1　Introduction

Since the beginning of continuous measurements of the atmospheric CO_2 concentration at the end of the 1950s (Keeling, 1960), the CO_2 concentration is known to be rising, at the moment with roughly 1.5 ppm y^{-1} (Houghton et al., 2001). This increase, combined with the awareness of the fact that CO_2 is a greenhouse gas (Arrhenius, 1896), has given rise to numerous modelling studies trying to describe the uptake of carbon by the terrestrial biosphere and the ocean for the last centuries, and trying to predict the uptake for the centuries to come.

Early studies (e.g. Björkström, 1979; Goudriaan and Ketner, 1984) focussed on the role of the terrestrial biosphere as a part of the carbon cycle and as a potential sink for the emitted CO_2. In these studies interactions of the terrestrial biosphere with the global carbon cycle were investigated, but effects of climate change were not taken into account. Later, more detailed separate models of the ocean and the terrestrial biosphere were developed, driven with climate data from observations or from climate modelling studies. Many different models for the terrestrial biosphere exist, ranging from simple descriptions of the most important processes (e.g. Brovkin et al., 1997) to an explicit representation of the biogeographical distribution of plant types and detailed process descriptions (e.g. Foley et al., 1996; Sitch et al., 2003).

The biogeophysical effects of climate change due to changes in the CO_2 concentration were studied with climate models. Changes in the vegetation that were studied in relation to future climate change or as a consequence of other anthropogenic disturbances include climate-induced shifts of the boreal forest zone (Otterman et al., 1984; Brovkin et al., 2003), deforestation in the high latitudes of the northern hemisphere (Bonan et al., 1992; Douville and Royer, 1997) as well as in the tropics (Dickinson and Henderson-Sellers, 1988; Shukla et al., 1990), and natural or anthropogenic changes in the vegetation cover of the North African monsoon region (Charney, 1975; Wang and Eltahir, 2000; Claussen et al., 2003). These regions are either heavily influenced by mankind, or are likely to show an amplification of the primary forcing due to positive feedbacks between the land surface and the climate.

Coupled climate-vegetation models were used to study climate and vegetation as a coupled system, thereby taking both biogeochemical and biogeophysical effects into account. Experiments with intermediate complexity models were performed using future CO_2 scenarios (Petoukhov et al., 2005). These models are computationally efficient and can thus be used for longer coupled climate-carbon cycle simulations with anthropogenic perturbation (e.g. Lunt et al., 2004).

Experiments with complex earth system models (including cycles of terrestrial as well as marine carbon) were performed by Cox et al. (2000), Friedlingstein et al. (2001, 2003), Govindasamy et al. (2005), Fung et al.

(2005) and Friedlingstein et al. (accepted). Various types of anthropogenic forcing were applied, either prescribing the concentration of CO_2, or prescribing the emissions of CO_2 into the system. The complex model experiments are usually limited to a few hundred years, and do not include ice sheet dynamics.

In the study presented here, a complex, coupled earth system model including the cryosphere was used to predict the long term behaviour of the physical climate system and the carbon cycle under elevated atmospheric CO_2 concentrations, with several ensemble experiments for each scenario. The IPCC SRES scenarios (Nakićenović et al., 2000) were extended beyond 2100, to investigate how the climate system and the carbon cycle adapt to a continuation of the changes in radiative forcing and CO_2 concentration. Part of the experiments used here were described in Mikolajewicz et al. (submitted). Whereas they describe mainly the physical climate system and the general results, this study focusses on the role of the terrestrial biosphere in the climate system.

7.2 Method

The earth system model as presented in chapter 2 was used to study the effect of CO_2 emissions on climate and carbon cycle. All components of the model (atmosphere and ocean dynamics, ocean biogeochemistry, terrestrial biosphere and ice sheets) were included. A set of experiments with prescribed anthropogenic CO_2 emissions was carried out with the complex earth system model. Historical data from 1750 to 2000 were used for emissions from fossil fuel and cement production (Marland et al., 2005) and land use change (Houghton and Hackler, 2002). From 2000 to 2100, three different emissions ensembles according to IPCC SRES scenarios A1B, A2 and B1 (Nakićenović et al., 2000) were performed. Thereafter, emissions were reduced exponentially with a time constant of 150 years (fig. 7.1). A control run was performed without CO_2 emissions, with the atmospheric CO_2 concentration calculated prognostically. For the period 1750–2000, an ensemble of five experiments was performed, starting from different years of the control run. For the scenario period (2001–3000), five ensemble members were performed for the A1B scenario, for the A2 and B1 scenarios three ensemble members each were performed. The experiments were performed using a periodically synchronous coupling (Sausen and Voss, 1996), with an interval of 2 years in the fully coupled mode, followed by 8 years in which the atmosphere GCM was replaced by an energy balance scheme. Details on the coupling are given in Mikolajewicz et al. (submitted).

The sets of scenario experiments were accompanied by an experiment in which the biophysical effects of the terrestrial biosphere and the ice sheets were ignored: the atmosphere and ocean model were driven by the original
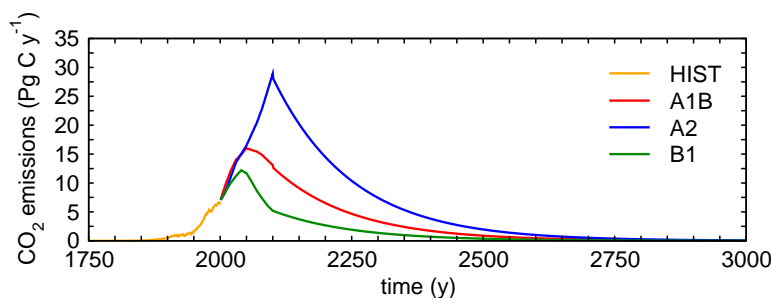
Figure 7.1: *Prescribed CO_2 emissions for the IPCC SRES scenario experiments.*

land surface parametrization and ice sheet conditions rather than the interactively calculated parameters from the terrestrial biosphere and ice sheet models. The carbon cycle effects from the terrestrial biosphere were taken into account, and both the ice sheet model and the biophysical part of the terrestrial biosphere were still included in the experiments for analysis purposes, although they were not allowed to affect the atmosphere and ocean model. In another set of experiments, climate change was suppressed by calculating the ratiative transfer in the atmosphere according to a pre-industrial CO_2 concentration of 280 ppm. However, the terrestrial and marine carbon cycle components reacted to the emissions of CO_2.

Offline experiments were performed for the period 2001–3000 with the terrestrial biosphere component only, in which the model was forced with control run climate and scenario run atmospheric CO_2 concentration (referred to as 'CO$_2$ only') or with scenario run climate and control run atmospheric CO_2 concentration (referred to as 'climate only'). These experiments are meant to determine the effects of CO_2 change and climate change separately. All experiments are summarized in table 7.1.

7.3   Results

The biogeophysical and biogeochemical interactions between the terrestrial biosphere and the atmosphere were analysed separately, as well as the mutual influence of biogeophysics and biogeochemistry. The focus is on the terrestrial biosphere here, with a short summary of the changes in the physical climate system. The changes in the atmosphere and the ocean are described in Mikolajewicz et al. (submitted).

7.3.1   Climate change and atmospheric CO_2 concentration

The simulated CO_2 concentration is shown in figure 7.2a. The maximum concentrations for the IPCC SRES scenarios are reached between year 2200

Table 7.1: *Overview of the experiments*

CTRL	coupled control run without CO_2 emissions
HIST	historical emissions 1750-2000 (5 ensemble members)
A1B	emissions according to IPCC SRES scenario A1B 2001-3000, exponential decay after 2100 (5 ensemble members)
A2	emissions according to IPCC SRES scenario A2 2001-3000, exponential decay after 2100 (3 ensemble members)
B1	emissions according to IPCC SRES scenario B1 2001-3000, exponential decay after 2100 (3 ensemble members)
. . .-280	atmosphere radiative forcing with 280 ppm (1 experiment for each scenario)
. . .-noland	with prescribed land surface and ice sheets (1 experiment for scenario A2, and 1 control run)
'CO$_2$ only'	offline run with the vegetation model, forced with CO_2 from the coupled experiment and control run climate
'climate change only'	offline run with the vegetation model, forced with climate from the coupled experiment and control run CO_2

and 2500, with values of about 520 ppm (B1), 860 ppm (A1B) and 1680 ppm (A2). At the end of the experiment, all scenario simulations show a slightly decreasing trend in the atmospheric CO_2 concentration, caused by the combination of negligible emissions and a continuing uptake of carbon by the ocean. A comparison with measured atmospheric CO_2 concentrations for the period up to 2000 (fig. 7.2b and 7.2c) shows that the model is able to capture the measured increase during the last century quite well. Most of the ensemble members stay within the range given by ± 2 standard deviations of the control run atmospheric CO_2 concentration. Between 1875 and 1950, two experiments get out of the range of the natural variability in the control run (fig. 7.2c), due to a larger uptake of carbon in the terrestrial biosphere. This takes place in several regions for both experiments.

Several other studies with coupled climate-carbon cycle models were performed in which the SRES scenarios were used (table 7.2). This study predicts CO_2 concentrations for the SRES scenarios around 2100 below the estimates from the IPCC Third Assessment Report (Houghton et al., 2001), but the concentrations agree reasonably with recent simulations from other earth system models (Dufresne et al., 2002; Govindasamy et al., 2005; Fung et al., 2005; Friedlingstein et al., accepted). Differences are caused by both changes in the uptake by the ocean and in the uptake by the terrestrial biosphere.

The increase in atmospheric CO_2 (fig. 7.2a) causes an increase in near-surface air temperature of 1.3 K (B1), 3.0 K (A1B) and 4.9 K (A2) for the period 2801-3000 compared to the pre-industrial control run average
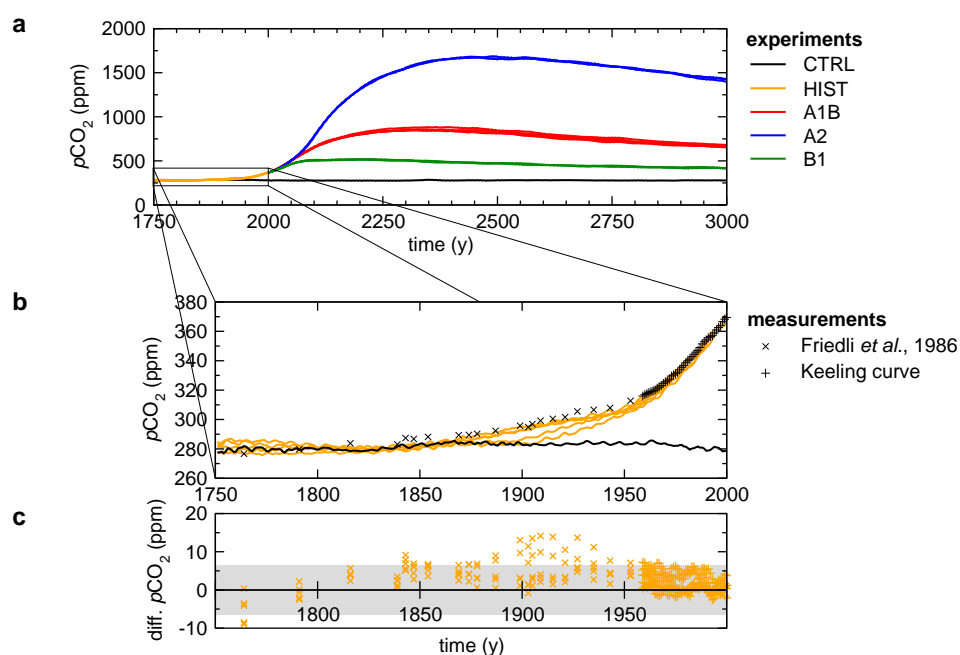
Figure 7.2: *(a) Simulated atmospheric CO_2 concentration for the control run and the IPCC SRES scenario experiments. (b) Close-up of the first 250 years of figure a, with measured CO_2 concentration from an ice core at Siple Station, Antarctica (Friedli et al., 1986) and from Mauna Loa, Hawaii (Keeling curve, Scripps Institution of Oceanography, University of California). (c) Difference between simulated and measured CO_2 concentration as in figure b. The grey area indicates the uncertainty (± 2 standard deviations) of the control run.*

Table 7.2: *Overview of modelled CO_2 concentrations (ppm) for 2100 for different studies with the IPCC SRES scenarios*

	B1	A1B	A2
ISAM[1]	549 (490–603[7])	717 (630–790[7])	856 (755–936[7])
Bern-CC[1,2]	540 (486–681[7])	703 (617–918[7])	836 (735–1080[7])
IPSL-CM2[3]			770
INCCA[4]			732
NCAR CSM1.4[5]		661	792
C4MIP[6]			730–1020
this study	506 (504–510[8])	656 (652–661[8])	778 (772–783[8])

[1] Houghton et al. (2001); [2] Joos et al. (2001); [3] Dufresne et al. (2002); Friedlingstein et al. (2003); [4] Govindasamy et al. (2005); [5] Fung et al. (2005); [6] Friedlingstein et al. (accepted), model intercomparison with 11 models; [7] range calculated with low and high CO_2 sensitivity of the atmosphere model; [8] range of the ensemble members

(fig. 7.3). Till 2100, all simulations show only a weak response of the meridional overturning to the changes in climate. However, after 2100 the meridional overturning in the North Atlantic reacts strongly to the changes in climate: ranging from a temporal decrease in strength for the B1 scenario experiments to a complete collapse for the A2 scenario experiments. The A1B scenario experiments appear to be close to a bifurcation point: two of the five ensemble experiments show a collapse between 2150 and 2250, one shows a collapse between 2600 and 2750, and two show only a temporal weakening as in the B1 experiments (see Mikolajewicz et al., submitted, for more details). The collapse of the meriodional overturning causes in general a massive cooling over the North Atlantic, thereby influencing the land surface as well. In cases where a clear distinction can be observed in the terrestrial biosphere response to these differences in the A1B experiments, the two experiments with an immediate collapse and the two without a collapse will be treated separately.
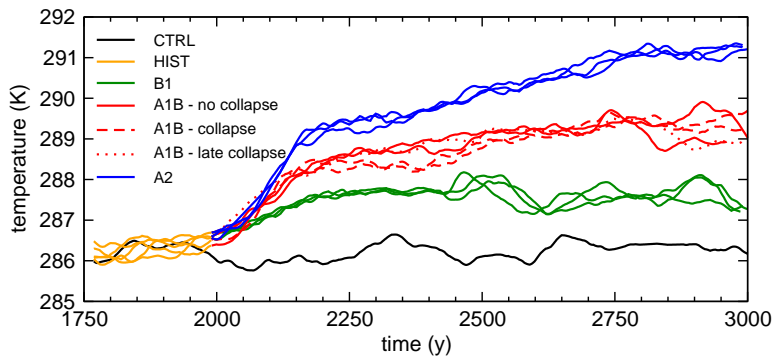
Figure 7.3: *Global mean near-surface temperature for the control run and the emission scenario experiments. Shown are 20-year running means.*

The major patterns of climate change are a direct response to the increasing CO_2 concentration. The magnitude of this response is partially determined by the terrestrial biosphere. It plays a role in the biogeochemistry of the earth, and changes in the land surface cause biogeophysical effects to the atmosphere. Each of these roles, as well as the combination of both roles, will be discussed below.

7.3.2   Land surface changes and biogeophysical interactions

The changes in climate related to an increase of the CO_2 concentration, as well as the changes in CO_2 concentration itself, favour shifts in the vegetation pattern (fig. 7.4). The simulated patterns in vegetation cover anomalies depend on the scenario, with largest anomalies for the A2 ensemble simulations. Tropical trees show an expansion in southern Africa and central South

America, where they oppress the temperate trees and C_3 herbs. Broadleaf summergreen trees in the temperate zone show a clear northward shift in North America and Eurasia, as do the needleleaf trees (evergreen and summergreen) in the boreal zone. Herbs increase mainly in the northern parts of North America and Eurasia, as well as in the dry regions in central Asia. The area of bare soil increases in northern Africa and the Middle East (fig. 7.4a).
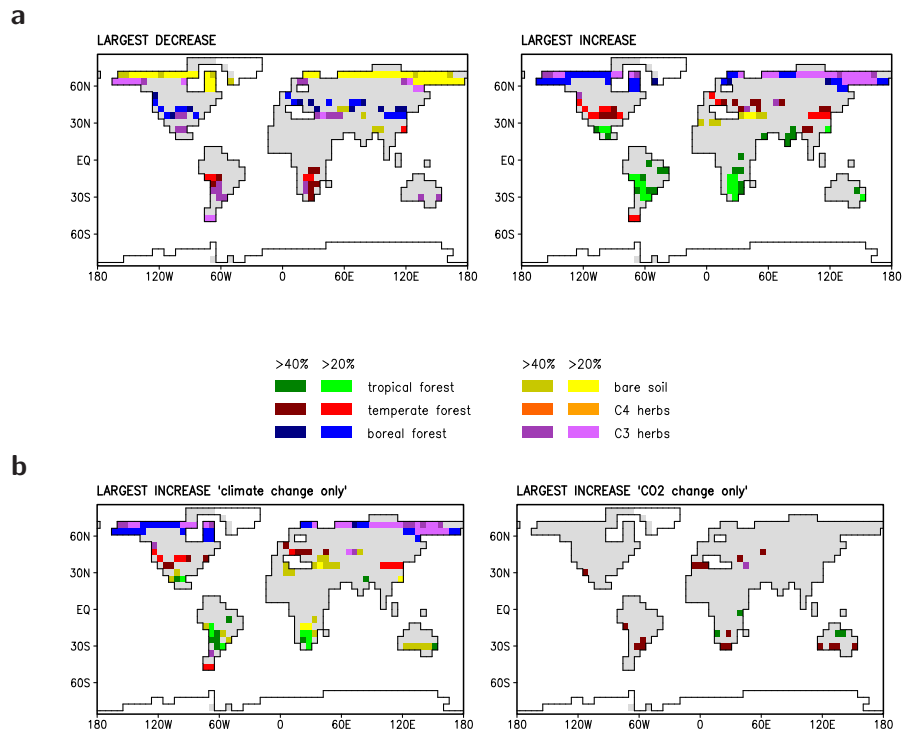
Figure 7.4: *(a) Principal shifts in the vegetation types for the A1B scenario (years 2801-3000 vs. control run average). Major decrease (left) and increase (right) are shown (dark colour: > 40% change of the grid-cell surface, light colour: > 20% change). (b) Major increase obtained in the 'climate change only' (left) and 'CO$_2$ change only' (right) experiments.*

Most of the changes in the mid and high latitudes are caused by changes in the climate, as can be deduced from the 'climate change only' experiments (fig. 7.4b). At lower latitudes, especially the dry regions around 30°N and 30°S, remarkable changes take place in the 'CO$_2$ only' simulations as well. Areas with mainly C_3 grasses in North and South America are replaced by

forest (fig. 7.4b). This effect is caused by an increase in water use efficiency due to the high CO_2 concentrations, which enables plants to grow in drier places due to a reduction of water loss. In the experiments with global warming, most of these changes due to CO_2 are counteracted by changes in the precipitation pattern.

The changes in the high latitudes take place very slowly. Boreal forest expansion and forest growth are slow processes, due to low temperatures and small rates of net primary production (NPP). Besides that, forest growth in the high latitudes shows a clear response to the collapse of the meridional overturning and the accompaning decrease in temperature in the related experiments (fig. 7.5): both the A1B experiments with a collapsing overturning and the A2 experiments show a decrease of forest fraction around 2250, with a recovery afterwards. For the A1B experiments, the collapse of the meridional overturning reduces forest fraction to pre-industrial levels. For the A2 experiment the response is less pronounced: due to the large global temperature increase the negative temperature anomaly over the Atlantic does not affect the increase in forest fraction as much as in the A1B scenario experiments. For the year 3000, forest fraction between 60° and 90°N increased from the pre-industrial level of 25% to 40% (B1), 50-55% (A1B) and 70% (A2).
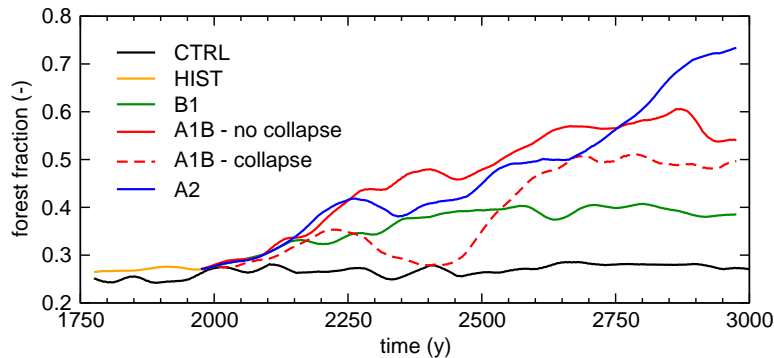
Figure 7.5: *Forest fraction for the land surface 60°-90° N (excluding ice sheets). Shown are 50 year running means.*

The changes in forest fraction in the high latitudes cause changes in the albedo of the surface, because forests are darker than grasses. Additionally, the albedo of snow-covered areas is influenced by the presence of forests: snow-covered forests have a lower albedo than snow-covered grasslands. These change in surface albedo are most likely the major biogeophysical feedback of natural vegetation changes to the atmosphere for warming climate in the future. Many studies were performed either afforesting or deforesting high latitudes in climate models. For example, Otterman et al.

(1984) performed experiments reducing the albedo of the high latitudes, thereby mimicking forest growth, and Bonan et al. (1992), Thomas and Rowntree (1992) and Douville and Royer (1997) performed experiments removing the forest in the high latitudes. They all showed that the climate of the high latitudes is sensitive to changes in the distribution of forests and tundra.

In the simulations, the effect of changes in vegetation distribution on climate can be analysed by comparing the A2 experiments with the A2-noland experiment. In the latter experiment, land surface properties were prescribed according to the original ECHAM3 parametrization, in order to have the climate not affected by biogeophysical feedbacks from land. Figure 7.6 shows the changes in albedo and changes in temperature for the high latitudes of the northern hemisphere. The albedo changes in the experiment without interactive land surface (A2-noland) are caused by changes in snow cover and sea ice cover. Due to higher temperatures (fig. 7.6b), both snow cover and sea ice cover decrease, thereby decreasing the surface albedo (fig. 7.6a). For the A2 simulations with interactive land surface (A2), albedo over land changes additionally due to shifts in the vegetation pattern. In the regions where bare soil was replaced by grasses and forests (fig. 7.4), albedo decreases up to 25 %.

This change in albedo causes an additional warming, up to 2 K (fig. 7.6c). The largest increase in temperature induced by land surface changes is simulated for northern Siberia, in the areas where albedo changes due to forest growth occur. This warming is restricted to the high latitudes of the northern hemisphere, resulting in a global average temperature increase of 0.26 K. A part of this global signal is caused by a slightly higher atmospheric CO_2 concentration in the A2 experiments compared to the A2-noland experiment, which will be discussed below. The patterns of temperature increase for both the A2 and the A2-noland experiments are dominated by a negative anomaly over the North Atlantic, caused by the decrease of the meriodional overturning, and an overall positive anomaly for the other regions, caused by the increased CO_2 concentration. The additional warming due to land surface changes in the A2 experiment in figure 7.6c is only a minor effect compared to the overall temperature increase (fig. 7.6b), with a global average of 4.9 K.

7.3.3   Carbon storage and biogeochemical interactions

A second effect of the terrestrial biosphere is related to its function in the global carbon cycle, influencing the atmospheric CO_2 concentration by uptake or release of carbon. The emissions of CO_2 lead to an increase in atmospheric concentration, followed by an uptake of CO_2 in the ocean and the terrestrial biosphere. Total increases of marine and terrestrial carbon storage are shown in figure 7.7. Whereas the ocean stays a sink for carbon
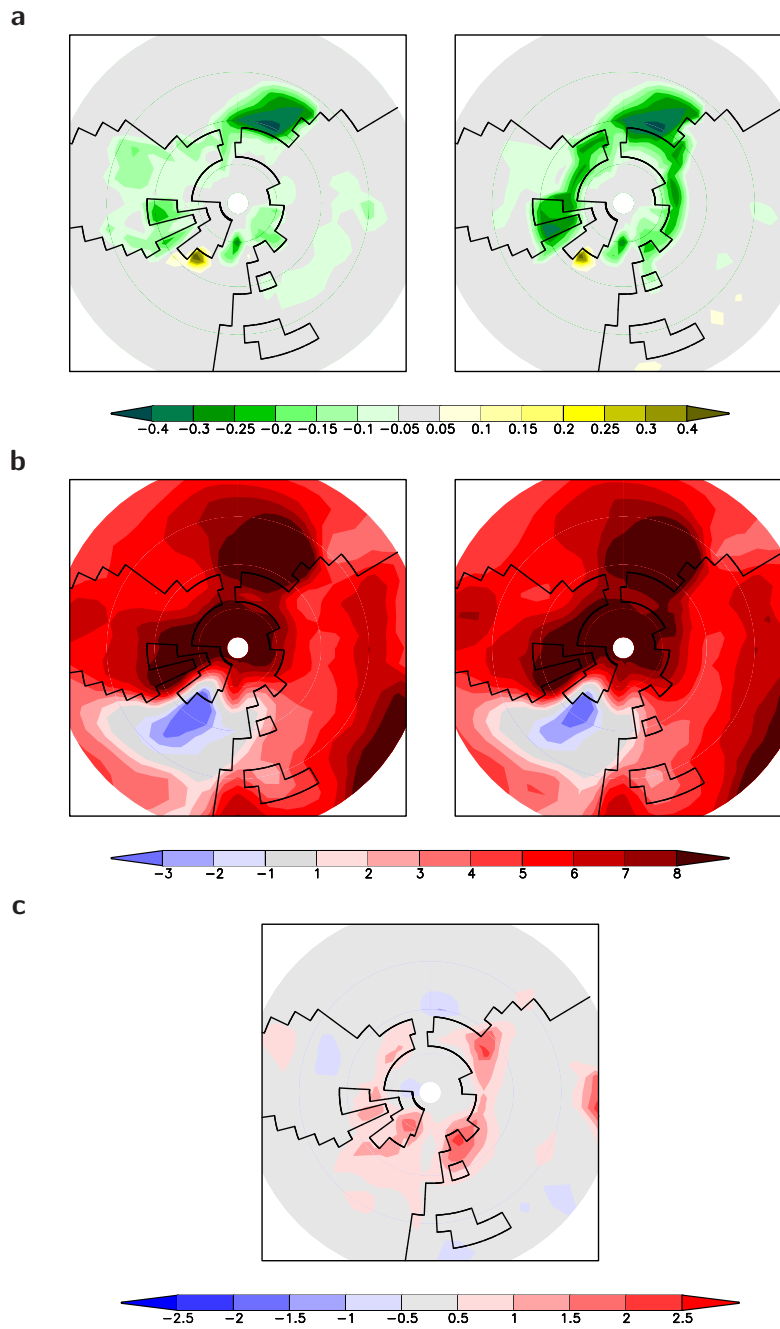
Figure 7.6: *Changes in annual means of (a) surface albedo, and (b) surface air tempe-rature (K), for the A2 experiments without (left, A2-noland−CTRL-noland) and with (right, A2−CTRL) interactive land surface for 2801–3000. (c) difference in temperature anomaly (K) for A2−A2-noland for 2801–3000.*

up to the year 3000, carbon storage in the terrestrial biosphere levels off after year 2300, and even declines slightly along with the atmospheric CO_2 concentration thereafter (fig. 7.2). By 3000, the total amounts of emitted CO_2 equal 1970 Pg (B1), 3810 Pg (A1B) and 6570 Pg (A2). The ocean has taken up 1260 Pg (B1), 2170 Pg (A1B) and 3010 Pg (A2), and the terrestrial biosphere has taken up 420 Pg (B1), 810 Pg (A1B) and 1130 Pg (A2) of these emissions. The relative uptake of carbon by the terrestrial biosphere and the ocean are lower for the A2 experiments than for the B1 and A1B experiments. The breakdown of the meridional overturning involves larger time constants for the ocean conveyor belt, which causes the A2 scenario to be further away from an equilibrium state (fig. 7.7), whereas the B1 and A1B experiments are much closer to a steady state.
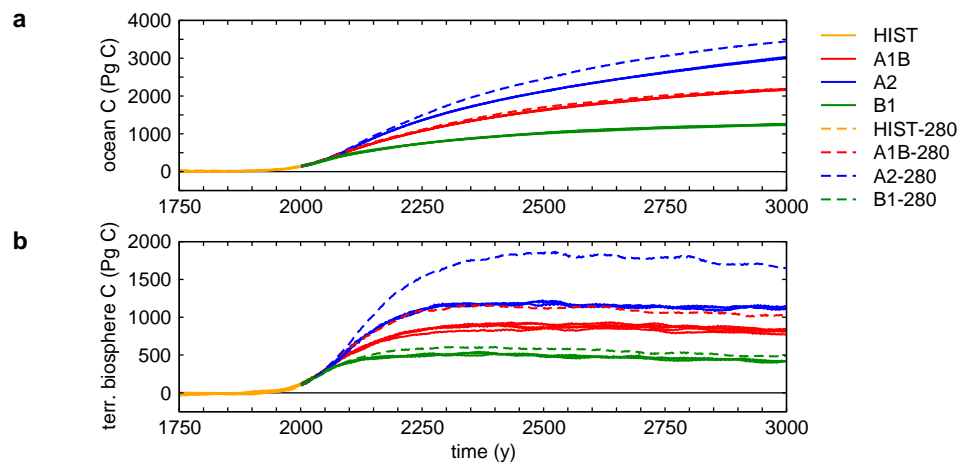
Figure 7.7: *(a) Total carbon storage in the ocean and (b) total carbon storage in the terrestrial biosphere for the historical experiments as well as the IPCC SRES scenario experiments and the scenario experiments in which the atmosphere was provided with a radiative forcing of 280 ppm CO_2.*

The increase in carbon storage on land due to CO_2 fertilization is partly counteracted by a decrease in storage due to climate change caused by atmospheric CO_2 increase. For both the marine and the terrestrial carbon storage, the effect of climate change depends on the scenario. In the emission scenarios B1-280, A1B-280 and A2-280 with pre-industrial radiative forcing and no climate feedback, carbon storage in the terrestrial biosphere is higher than in the experiments with feedbacks between climate and carbon cycle (fig. 7.7). Global warming causes a reduction of the extra carbon storage due to the fertilization with CO_2. This reduction can be calculated from the difference between the fully coupled experiments and the experiments without climate change. For the period 2801-3000, the reduction in carbon storage for the terrestrial biosphere was 16 % (B1), 22 % (A1B) and

34 % (A2). For the marine carbon storage, the situation changes from an increase in carbon storage of 5 % and 2 % for the B1 and A1B experiments respectively to a decrease of 9 % for the A2 scenario, all for the period 2801-3000. These values differ from those found by Winguth et al. (2005) for experiments with prescribed increase in CO_2 concentrations ($2\times CO_2$, $3\times CO_2$, $4\times CO_2$) performed with the same model. This is caused by a difference in setup: Winguth et al. (2005) used fixed CO_2 concentrations at the end of their experiments, which implies emissions roughly the size of the ocean uptake at the end, the emissions in the experiments presented here are negligible at the end of the experiments.

In the fully coupled experiment, carbon storage is enhanced almost everywhere on land, but the rate of increase differs greatly. Ten regions were defined for which carbon storage was calculated individually (fig. 7.8). The regions react differently to the combined effects of CO_2 and climate change. Fastest and largest increase was simulated for the tropical regions (northern and southern South America, southern Africa). The carbon storage in these regions tends to follow more or less the atmospheric CO_2 curve as shown in figure 7.2a. Northern North American and northern Asian carbon storage evolves differently, the amount of carbon increases steadily till the year 3000, reaching relatively high levels of carbon storage at the end. For these regions, the slow expansion of forests (fig. 7.5) is of major importance for carbon uptake. Grasslands or deserts (northern Africa and Arabia, Australia) have lowest absolute storage of carbon, they are relatively unimportant with respect to the biogeochemical role of the biosphere.

The offline experiments with the vegetation model driven with either increasing CO_2 concentration or changes in climate as forcing were used to determine the importance of CO_2 fertilization and climate change for the increase in carbon storage shown above. Figure 7.9 shows the fraction of the increase in carbon storage that is obtained in the 'CO$_2$ only' or 'climate change only' experiments relative to the change in the fully coupled experiments. Except for northern North America, climate change reduces the carbon uptake, and the increase of carbon storage for all regions, as was shown in figure 7.8, is due to CO_2 increase only. Largest ratios are obtained for northern Africa and Arabia. Climate change has a big reducing effect here, because the sparse vegetation present is suffering highly from the dryer conditions, whereas changes in CO_2 are helping them to stand these due to a higher water use efficiency. Relatively large negative effects of climate change are simulated for southern North America, Europe and northern Asia in the A2 scenario. For shorter time scales than those discussed here ($\sim$100 years), the importance of the high latitudes is usually smaller, because of the slow changes occurring here. Tropical effects are usually reported as the main change for future climate (e.g. Cox et al., 2000; Raddatz et al., submitted).

No experiments were performed to quantify the biogeochemical role of the terrestrial biosphere directly, but an estimate can be obtained from the
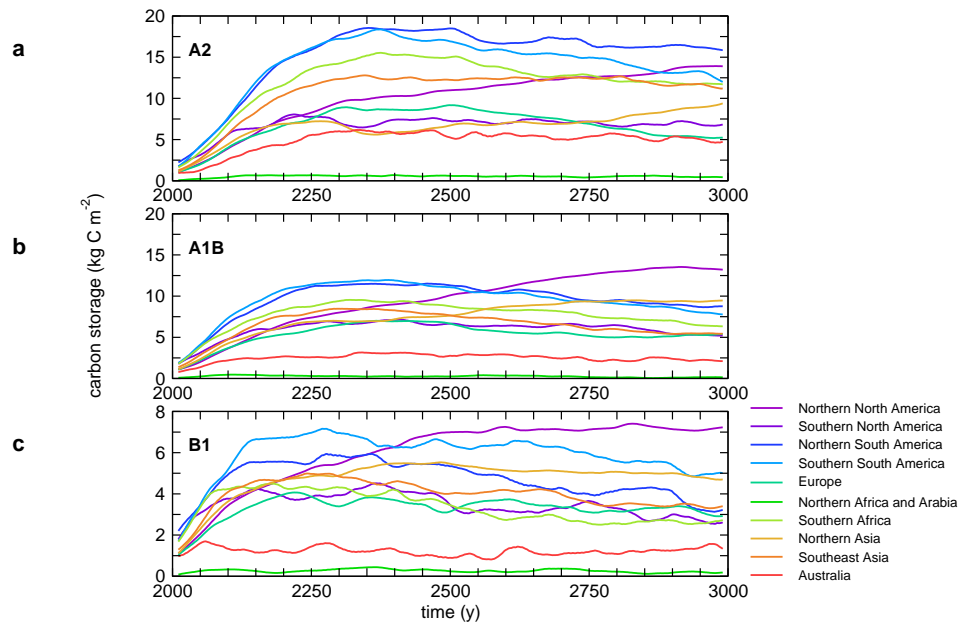
Figure 7.8: *Terrestrial carbon uptake for 10 regions, averaged for the (a) A2, (b) A1B and (c) B1 scenarios. The regions are defined as in the map.*
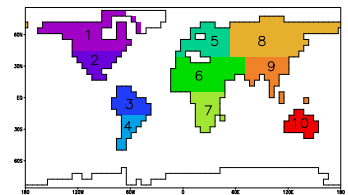
distribution of carbon over atmosphere, ocean and land (fig. 7.10), together with estimates of the temperature effect of CO_2 increase. In the beginning of the experiment, the terrestrial biosphere is responsible for storage of roughly 30% of the emitted carbon. This fraction decreases to below 20% during the experiment due to equilibration of the terrestrial biosphere with the atmospheric CO_2 concentration, while the ocean stays a sink for carbon (fig. 7.10). The ratio between total carbon increase in the terrestrial biosphere and in the atmosphere increases, due to a somewhat delayed response of the terrestrial biosphere to the strong increase in CO_2 during the period of high emissions (2050–2150).

One of the A2 simulations was continued till the year 9000, in order to obtain a state close to equilibrium. For the last 500 years of this experiment, the total amount of emitted carbon during the experiment was distributed over atmosphere, ocean and land in the fractions 18%, 66% and 16%. These ratios represent the integrated uptake over the whole experiment, and the incremental uptake of additional emissions at the state reached at the end of the experiment would be smaller for both the terrestrial biosphere and the ocean due to saturation, resulting in a relatively larger fraction for the
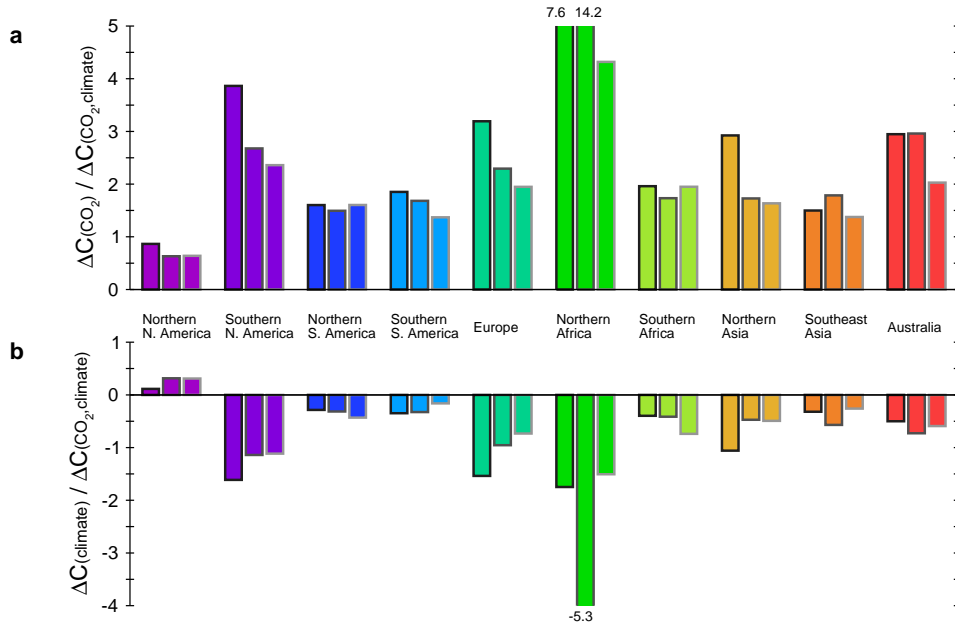
Figure 7.9: *Ratio between carbon uptake in the offline experiments and the experiments with full forcing, average for the period 2801–3000: (a) for the experiments with CO_2 change only, and (b) for the experiments with climate change only. Dark grey indicates the average for the A2 experiments, middle grey for the A1B experiments and light grey for the B1 experiments. The region are defined as in figure 7.8.*
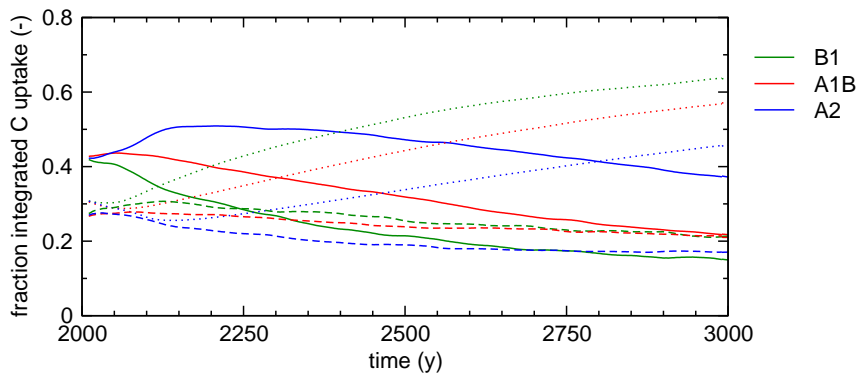
Figure 7.10: *Fraction of total emitted carbon stored in the atmosphere (full line), ocean (dotted line) and terrestrial biosphere (dashed line) for the scenario experiments.*

atmosphere. Using these fractions to determine a potential effect of the terrestrial uptake of CO_2 thus results in a minimum estimate for the atmospheric CO_2 decrease due to terrestrial carbon storage. According to these fractions, the ocean looses 0.81 Pg and the atmosphere looses 0.19 Pg eventually for every petagram of carbon stored in the terrestrial biosphere. If the total terrestrial carbon uptake for the A2 experiment, which was 1010 Pg by the year 9000, would not have been stored, the atmospheric CO_2 concentration would have been increased by at least 90 ppm.

The A2 experiment that was continued till 9000 reveals as well that the temperature increase has a large lag compared to the CO_2 increase (fig. 7.11). The increase of CO_2 up to its maximum concentration (close to year 2500) causes a somewhat linear reaction of the global mean temperature, with an increase around 0.26 K per 100 ppm (fig. 7.11), and a levelling off of the temperature increase shortly before the maximum concentration is reached, which is caused by the collapse of the meriodional overturning. However, from the CO_2 maximum onwards, the concentration starts decreasing for about 1500 years, whereas the global temperature still increases, and levels off by the year 4000. From 4000 onwards, both CO_2 concentration and temperature decrease with a rate of about 0.62 K per 100 ppm (fig. 7.11). This behaviour shows clearly that the ocean heating lags the CO_2 forcing by a few thousand years. At the end of the experiment, a state close to equilibrium is reached. Between years 7000 and 9000 there are no clear changes in either temperature or CO_2 concentration (fig. 7.11).

Warming caused by CO_2 increase has a relatively fast component, which is related to the atmosphere and the mixed layer of the ocean, and a slow component due to mixing to the deep ocean (Voss and Mikolajewicz, 2001). Therefore the effect of CO_2 increase will differ depending on the timescale of interest. The 'potential warming' effect of the terrestrial biosphere, the temperature increase that would occur when the terrestrial biosphere would not have taken up any additional carbon, can be calculated from the potential CO_2 increase of 90 ppm combined with the relation between temperature and CO_2 concentration from the end of the long A2 experiment. Linear regression over years 6000–9000 from this experiment reveals a gradient of 0.9 K per 100 ppm ($R^2 = 0.24$). This brings the 'potential warming' effect to roughly 0.8 K globally in case of equilibrium.

7.3.4 Mutual influence of the biogeophysical and biogeochemical roles

The interactions between land and atmosphere are complex, partly because the biogeophysical and biogeochemical effects shown above cause secondary effects, e.g. alteration of carbon storage caused by climate-related land surface changes, which in turn changes climate. These mutual influences are discussed below.
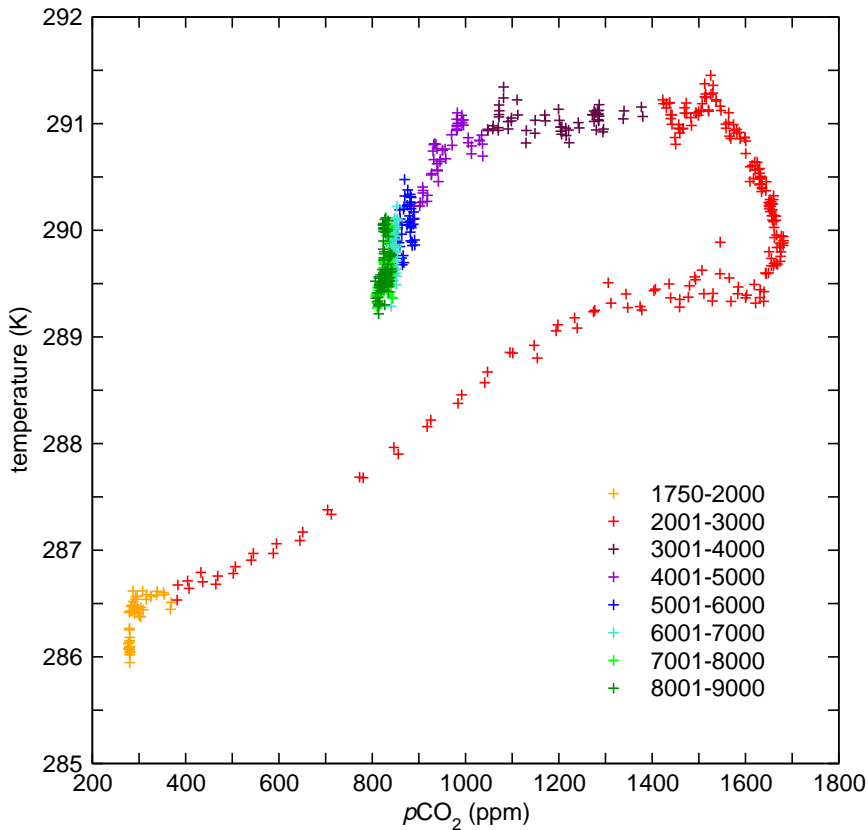
Figure 7.11: *Relation between global mean surface air temperature and CO_2 concentration for the historical experiment and the extended A2 experiment (1750–9000).*

The effect of interactive land surface changes on climate is ambiguous. On the one hand, positive feedbacks between temperature, albedo, and forest growth, as were shown in figure 7.6, cause an amplification of the temperature change caused by the rising CO_2 concentration. On the other hand, forest growth itself reduces this CO_2 concentration due to uptake of carbon, thereby causing an overall negative feedback on temperature. Besides these two processes, the effect of temperature rise on carbon storage in high latitudes is ambiguous itself, as it is the result of two counteracting mechanisms: it will increase forest growth, but it will accelerate carbon decay in soils as well.

Betts (2000) suggested that the biogeophysical effect (i.e. albedo change) of afforestation in the high latitudes is larger than the biogeochemical effect due to afforestation (i.e. temperature reduction due to reduction of atmospheric CO_2 concentration related to the uptake of carbon), for present-day circumstances. Claussen et al. (2001) compared biogeophysical and

biogeochemical feedbacks for tropical and boreal forests under present-day conditions, and found that the biogeochemical feedback is more important for the tropical forests, whereas the biogeophysical feedback is more important for the boreal forests. Note that the experiments differ widely in setup from each other and from the experiments we performed here. The rough estimate of 0.8 K as a cooling effect of additional carbon storage in the terrestrial biosphere is higher than the global warming of 0.26 K for the biogeophysical interactions, but for certain regions in the high latitudes the biogeophysical effect could be larger than the biogeochemical effect.

Figure 7.12 shows the evolution of carbon storage for the A2 experiments with and the A2-noland experiment without interactive land surface. The atmospheric CO_2 concentration was roughly 75 ppm higher for the A2 experiments with interactive land surface (A2) compared to the experiment with fixed land surface (A2-noland) experiment, and this difference stays roughly constant between 2300 and 3000. The decrease in carbon storage from the A2-noland experiment to the A2 experiments mainly took place in the areas which became warmer due to interactive land surface changes (fig. 7.6c).
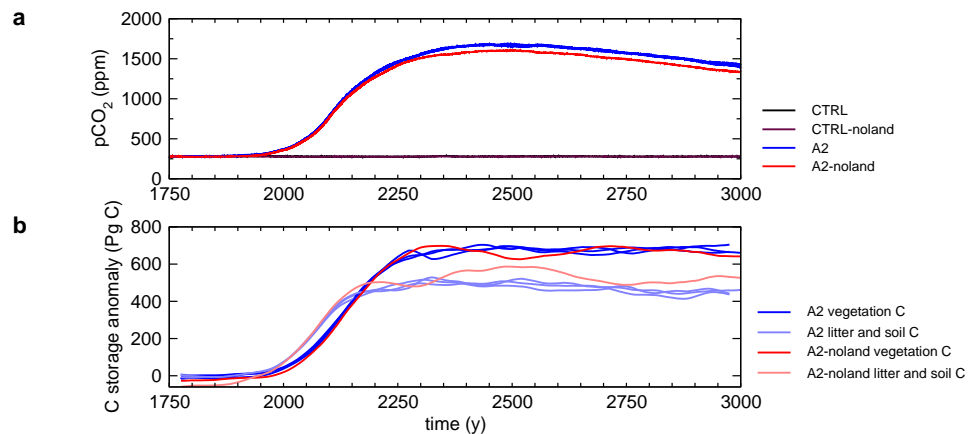
Figure 7.12: *Time series of (a) atmospheric CO_2 concentration, and (b) carbon storage in vegetation and litter and soil for the A2 experiments with and without interactive land surface (A2 and A2-noland).*

The heating effect of the 75 ppm increase is relatively large if it would persist till an equilibrium state (according to the estimates in the previous paragraph the temperature effect would be about 0.7 K). It is an important secondary effect compared to the estimated potential increase in atmospheric CO_2 concentration of 90 ppm if the terrestrial biosphere would not take up carbon.

7.4   Conclusions and discussion

The effect of biogeophysical and biogeochemical interactions between vegetation and climate were studied with the complex earth system model presented in chapter 2. For the period 1750-2000, the model simulations of atmospheric CO_2 concentration agree reasonably well with the observations from ice cores and direct air samples.

Shifts in vegetation were predicted for the northern hemisphere high latitudes, where bare soil was replaced by herbs and boreal trees, and the border between temperate and boreal forest moved northward. Furthermore, temperate forests in the southern hemisphere (South America, southern Africa) were replaced by tropical forests. The largest biogeophysical feedback from these changes in vegetation distribution occurs in the high latitudes, where land albedo was reduced up to 0.25. The positive feedback between temperature, forest growth and albedo results in a local warming up to 2 K for the period 2801-3000 in the A2 scenario compared to a similar experiment without land surface changes, or 0.26 K on global average. This change is relatively small compared to the 4.9 K global increase in surface air temperature, with an even stronger warming over land.

The increase in CO_2 concentration causes an increase in terrestrial carbon storage due to CO_2 fertilization. Climate change reduces this increase, mainly through rising temperatures, which cause an increase in turnover time of litter and soil carbon. Similar effects were obtained by Friedlingstein et al. (2003) and Govindasamy et al. (2005). Cox et al. (2000) simulated an even stronger decrease of carbon storage due to climate change for the IS92a scenario, exceeding the increase in carbon storage due to CO_2 fertilization. Although the general trend, especially in atmospheric CO_2 concentration, is rather similar between the experiments presented here and the A1B and A2 experiments performed by Friedlingstein et al. (2003), Govindasamy et al. (2005) and Fung et al. (2005), the distribution of carbon uptake between terrestrial biosphere and ocean differs greatly. Whereas carbon storage in the A2 experiment of Govindasamy et al. (2005) takes place mainly in the terrestrial biosphere (47% of the emissions by 2100, and 10% for the oceans), the other studies, as this study, have a more equal distribution of carbon over land and ocean. The land surface takes up 22% (Dufresne et al., 2002; Friedlingstein et al., 2003), 25% (Fung et al., 2005), and 20% (this study), the ocean takes up 31% (Dufresne et al., 2002; Friedlingstein et al., 2003), 21% (Fung et al., 2005), and 21% (this study). Large differences between the models rise from the sensitivity of the modelled climate to changes in the atmospheric CO_2 concentration. Although the studies mentioned before have roughly similar atmospheric CO_2 concentrations, the climate effects differ substantially. Warming for the A2 scenarios by 2100 obtained in the other studies is 3.0 K (Dufresne et al., 2002, 1860–2100) and 3.2 K (Govindasamy et al., 2005, 1900–2100), compared to 1.8 K (Fung et al., 2005, 1820–2100)

and 1.6 K (1750–2100) in the A2 experiment presented here.

The uptake of CO_2 by the terrestrial biosphere has lead to a (potential) decrease of the atmospheric CO_2 concentration of at least 90 ppm for the A2 experiment close to equilibrium, resulting in a cooling of about 0.8 K. This effect might look relatively small compared to the global temperature increase of 3.5 K, again close to equilibrium. Nevertheless it is not negligible, and this is a measure of the uncertainty due to carbon uptake for the situation with land use changes, as the role of the terrestrial biosphere for present and future as a source or sink of carbon is still unclear (Houghton et al., 2001).

The biogeochemical role of the terrestrial biosphere is more important than the biogeophysical role on a global scale for the future scenarios shown in this study. However, on a local scale the changes of the land surface might become more important, most likely in the high latitudes of the northern hemisphere. Both changes are significantly smaller than the direct effect of CO_2 increase on climate, but their effects are nevertheless substantial.

Chapter 8

General conclusions

Abstract

General conclusions from the studies in this thesis are drawn. The experiments with orbital forcing and the experiments with CO_2 emissions as forcing were compared with respect to the role of the terrestrial biosphere. The insight obtained from the experiments performed in this thesis was used to discuss other issues: the difference in storage of carbon and atmospheric CO_2 concentration between glacials and interglacials, and the potential effects of human-induced land use changes on the biogeophysical and biogeochemical roles.

8.1   Introduction

General conclusions about the role of the terrestrial biosphere in the earth system were drawn from the studies in the previous chapters. A comparison is made between experiments forced with changes in the earth orbit, and experiments forced with emissions of CO_2. The understanding obtained from the experiments in these chapters will be applied to some other themes: effects of terrestrial biosphere changes on glacial-interglacial transitions, and effects of land use changes on climate.

8.2   The influence of the terrestrial biosphere on climate

8.2.1   Biogeophysical influence

Biogeophysical feedbacks were simulated both in the paleoclimatic experiments in chapters 4, 5 and 6, and in the future anthropogenic climate change experiments in chapter 7. In both cases biogeophysical effects caused a positive feedback, enhancing the effects of changes in insolation for the paleoclimate experiments or changes in CO_2 concentration for the future climate change experiments.

For both types of experiments the positive 'taiga–tundra' feedback, the feedback between forest growth, albedo and temperatures, plays an important role. The high latitudes are sensitive to changes in insolation due to the presence of large land masses, the existence of other positive feedbacks between sea ice and snow presence, albedo and temperature, and in case of the paleoclimate experiments as well due to its latitudinal position, causing large fluctuations in the incoming radiation.

The largest biogeophysical feedback simulated in the low latitudes was the feedback between vegetation growth, albedo and precipitation in north Africa, and to a lesser extend in southeast Asia. A substantial increase of vegetation growth occurred only for the paleoclimate experiments (both Eemian and Holocene), for the anthropogenic climate change experiments there was no clear change simulated here. For both past and future, the high latitude feedback was recognised as important amplifier of climate change before (e.g. Otterman et al., 1984; Foley et al., 1994).

The low latitude feedback was recognised for the past, for the future however its importance is less pronounced. The anthropogenic climate change simulations performed with the earth system model presented in this thesis did not show a clear increase of vegetation in the western Sahara region, as was found for the paleoclimate experiments. The changes in atmospheric circulation needed to trigger the low latitude feedback, an increase of moisture transport into the monsoon areas, are best provided with an asymmetric warming of the continents.

James Lovelock's Gaia Hypothesis (Lovelock, 1979) stated that the earth behaves as a homeostatic creature, trying to maintain its conditions as favourable as possible for life. A conceptual model (Watson and Lovelock, 1983) was presented, using black and white daisies as analogy for plants with lower and higher albedoes, and shows a potential mechanism with which the plants would be able to do so. Although theoretically this might be a way of the terrestrial biosphere to maintain favourable temperatures, the simulations in this study do show rather a positive feedback than a negative feedback. One of the major shortcomings of the conceptual model by Watson and Lovelock (1983) to reach similar results is the lack of abiotic factors. The simulations performed in chapter 4 show a clear effect of soil colour of deserts and snow albedo, both lighter than vegetation, but there is no clear relation of this to any potential 'cooling' mechanism involving the terrestrial biosphere.

8.2.2   Biogeochemical influence

The biogeochemical role of the terrestrial biosphere is mainly featured by a negative feedback between atmospheric CO_2 and terrestrial carbon storage, and a positive feedback between atmospheric CO_2, temperature and terrestrial carbon storage. For the anthropogenic climate change experiments (chapter 7), the negative feedback was shown to be stronger than the positive one, thereby making the 'biogeochemical' biosphere to an overall stabiliser of the climate and carbon cycle. For the experiments with insolation changes (chapters 4, 5 and 6) the feedback is slightly more complicated: due to an asymmetric warming, a relatively undetermined impact of global temperature increase on carbon storage, and important other climatic factors (hydrology, radiation), the periods with global temperatures larger than in the control run were not associated with a large decrease of terrestrial carbon storage. On the contrary, terrestrial carbon storage was increased during the beginning of both the Eemian and the Holocene experiments caused by hydrological and radiative changes, and this increase caused a decrease of the atmospheric CO_2 concentration.

The large difference between the insolation-driven and emission-driven experiments for the biogeochemical role of the terrestrial biosphere is caused by the reaction of the physical climate system to these forcings. Whereas the emission-driven experiments show mainly a global temperature increase caused by the enhanced CO_2 concentration, the insolation-driven experiments show a zonally asymmetric warming, and a more important role for radiation changes and changes in the hydrological cycle.

8.3   The role of vegetation in shaping the glacial-interglacial CO_2 curve and the interglacial-to-glacial transition

The atmospheric CO_2 concentration, as recorded in ice cores, shows a clear distinction between interglacials, with CO_2 concentrations around 280 ppm, and glacials, with a gradual decrease of the CO_2 concentration to minimum levels of 200 ppm (Petit et al., 1999). Although the earth system model is able to capture the increase in atmospheric CO_2 concentration for the interglacials, it is unlikely that it will show the glacial minimum of 200 ppm. The processes responsible for the relatively low concentration in the beginning of interglacials are mainly driven by a relatively warm and moist climate, at least in the Northern Hemisphere. Under these conditions, the terrestrial biosphere stores more carbon than under present-day conditions, thereby lowering the atmospheric pCO_2. However, for glacials, the conditions are opposite to these in the beginning of the two studied interglacials: a cool and dry climate will cause a scarcer vegetation. Besides that, the land surface area available for vegetation growth is smaller due to the presence of large ice sheets, which is only partly compensated by a lowering of the sea level (sea level is supposed to be 120 m below present conditions (Ray and Adams, 2001)), and the negative feedback related to the low CO_2 concentration, as discussed in before, is opposing carbon storage as well.

Many hypotheses have been posed on mechanisms of carbon storage during glacials, both related to the land surface and to the ocean. Zeng (2003) come up with a glacial burial hypothesis: carbon produced in interglacials is stored under glaciers, and decomposes again after deglaciation. In this way, 547 Pg C can be stored (Zeng, 2003). Martin (1990) assumes additional carbon storage in the ocean by an increase in production due to iron fertilization of the oceans, which is supposed to have been much larger during glacial times. Munhoven (2002) contribute part of the glacial-interglacial changes of CO_2 to changes in rock weathering. They reach a maximum atmospheric CO_2 reduction of about 20 ppm. Up to now, none of these has been generally accepted as the cause of the glacial-interglacial changes in atmospheric CO_2 concentration.

8.4   The effect of human-induced changes in land cover

In the experiments with increased CO_2 concentrations, changes in land use were not taken into account. The studies in this thesis were primarily meant to gain understanding of the interactions between climate and natural vegetation. However, land use has large effects on both the biogeochemical

and the biogeophysical roles of the terrestrial biosphere. Both roles will be discussed briefly here, using the understanding of the interactions that was obtained from the studies in this thesis.

8.4.1   Land use change and biogeochemical interactions

The effect of land use change on carbon storage is poorly understood. In general, carbon storage will decrease in case of agriculture, especially when the area was deforested for this purpose. A large uncertainty is still the role of the soil as source or sink of carbon: soil cultivation will allow for a fast decomposition of organic carbon in the soils, but application of manure and crop residues will increase the carbon storage. Sitch et al. (2005) simulate an additional increase of the atmospheric CO_2 concentration due to land use changes between 20 ppm (B1) and 127 ppm (A2)by 2100 for SRES scenarios similar to those used in chapter 7.

8.4.2   Land use change and biogeophysical interactions

Land use change changes the biogeophysics of the land surface as well. The pronounced annual cycle of agriculture in the mid and high latitudes, with the soil being parts of the year uncovered, influences the annual albedo course and evaporation rates. Brovkin et al. (2004) simulated a slight cooling for the year 2000 caused by land use, compared to a control run without human influence. Claussen et al. (2001) simulated a cooling due to deforestation in the mid and high latitudes.

8.5   The terrestrial biosphere: cause, amplifier or damper of climate change?

In this thesis, two types of forcing were used to study the climate system and the role of the terrestrial biosphere herein. In chapters 4, 5 and 6, experiments were described in which changes in the earth's orbit were prescribed as driving force. In chapter 7 experiments were described in which climate and carbon cycle were forced with emissions of CO_2. These two types differ substantially: in the first type of experiments the terrestrial biosphere reacts mainly to changes in the climate (caused by the orbital changes), and causes changes in the atmospheric CO_2 as a side-effect. In the second type the terrestrial biosphere reacts more directly to changes in the CO_2 concentration, as well as to changes in climate caused by the CO_2 concentration.

Although CO_2 changes for the Eemian and Holocene were shown to be caused by changes in the terrestrial carbon storage (chapter 5), the amplitude of the climate change caused by the -relatively moderate- changes in atmospheric CO_2 is smaller than the changes in climate caused by changes in the earth's orbit, amplified by land surface changes and sea ice changes.

The atmospheric CO_2 changes are merely a weak negative feedback rather than a cause of climate change.

The man-made changes of climate and carbon cycle due to emissions of CO_2 cause a shift from a climate with the largest changes occurring due to orbital variations (on a scale of millennia) to a climate with the largest changes occuring due to emissions of greenhouse gasses. With this shift, the primary role of the terrestrial biosphere in the earth system shifts from a biogeophysical one to a biogeochemical one. As long as the biogeochemical role is dominated by a negative feedback, as was shown for the studies in this thesis, the effect will be ratable. Large uncertainties, not only about the terrestrial biosphere, but about the state of the earth system as a whole, will come up when this negative feedback would turn into a positive one, as was shown for other studies, e.g. due to a massive dieback of tropical forests (Cox et al., 2000). Enhanced by positive feedbacks from the 'biogeophysical' biosphere in the high latitudes, and the positive feedbacks from snow and sea ice cover, a situation could be created of a 'runaway-climate', of which state and implications can hardly be estimated at the moment.

Bibliography

Adams, J., Faure, H., 1997. Preliminary vegetation maps of the world since the last glacial maximum: an aid to archaeological understanding. Journal of Archaeological Science 24, 623–647.

Adams, J., Faure, H., 1998. A new estimate of changing carbon storage on land since the last glacial maximum, based on global land ecosystem reconstruction. Global and Planetary Change 16-17, 3–24.

Ainsworth, E., Long, S., 2005. What have we learned from 15 years of free-air CO_2 enrichment (FACE)? a meta-analytic review of the responses of photosynthesis, canopy properties and plant production to rising CO_2.

Arrhenius, S., 1896. On the influence of carbonic acid in the air upon the temperature of the ground. Philosophical Magazine 41, 237–276.

Berger, A., 1978. Long-term variations of daily insolation and Quaternary climate changes. Journal of the Atmospheric Sciences 35, 2362–2367.

Betts, R., 2000. Offset of the potential carbon sink from boreal forestation by decreases in surface albedo. Nature 408, 187–190.

Björkström, A., 1979. A model of CO_2 interaction between atmosphere, oceans, and land biota. In: Bolin, B., Degens, E., Kempe, S., Ketner, P. (Eds.), The global carbon cycle, SCOPE 13. John Wiley.

Bolin, B., Degens, E., Kempe, S., Ketner, P., 1979. The global carbon cycle. SCOPE 13. Wiley and Sons, Chichester.

Bonan, G., Pollard, D., Thompson, S., 1992. Effects of boreal forest vegetation on global climate. Nature 359, 716–718.

Braconnot, P., Joussaume, S., Marti, O., de Noblet, N., 1999. Synergistic feedbacks from ocean and vegetation on the African monsoon response to mid-Holocene insolation. Geophysical Research Letters 26 (16), 2481–2484.

Brovkin, V., Bendtsen, J., Claussen, M., Ganopolski, A., Kubatzki, C., Petoukhov, V., Andreev, A., 2002. Carbon cycle, vegetation, and climate dynamics in the Holocene: Experiments with the CLIMBER-2 model. Global Biogeochemical Cycles 16 (4), 1139, doi: 10.1029/2001GB001662.

Brovkin, V., Ganopolski, A., Svirezhev, Y., 1997. A continuous climate-vegetation classification for use in climate-biosphere studies. Ecological Modelling 101, 251–261.

Brovkin, V., Levis, S., Loutre, M.-F., Crucifix, M., Claussen, M., Ganopolsky, A., Kubatzki, C., Petoukhov, V., 2003. Stability analysis of the climate-vegetation system in the northern high lattitudes. Climatic Change 57, 119–138.

Brovkin, V., Sitch, S., Von Bloh, W., Claussen, M., Bauer, E., Cramer, W., 2004. Role of land cover changes for atmospheric CO_2 increase and climate change during the last 150 years. Global Change Biology 10, 1253–1266, doi: 10.1111/j.1365-2486.2004.00812.x.

Calov, R., Ganopolski, A., Petoukhov, V., Claussen, M., Brovkin, V., Kubatzki, C.,

2005. Transient simulation of the last glacial inception. part II: sensitivity and feedback analysis. Climate Dynamics 24, 563–576, doi: 10.1007/s00382-005-0008-5.

Campbell, J., Norman, J., 1998. An introduction to environmental biophysics. Springer.

Charney, J., 1975. Dynamics of deserts and droughts in the Sahel. Quarterly Journal of the Royal Meteorological Society 101 (428), 193–202.

Charney, J., Stone, P., Quirk, W., 1975. Drought in the Sahara: a biogeophysical feedback mechanism. Science 187, 434–435.

Charney, J., Stone, P., Quirk, W., 1976. Reply to Ripley, E.A., Drought in the Sahara: insufficient biogeophysical feedback. Science 191, 100–102.

Churkina, G., Running, S., 1998. Contrasting climatic controls on the estimated productivity of global terrestrial biomes. Ecosystems 1, 206–215.

Ciais, P., Reichstein, M., Viovy, N., Granier, A., Ogée, J., Allard, V., Aubinet, M., Buchmann, N., Bernhofer, C., Carrara, A., Chevallier, F., De Noblet, N., Friend, A., Friedlingstein, P., Grünwald, T., Heinesch, B., Keronen, P., Knohl, A., Krinner, G., Loustau, D., Manca, G., Matteucci, G., Miglietta, F., Ourcival, J., Papale, D., Pilegaard, K., Rambal, S., Seufert, G., Soussana, J., Sanz, M., Schulze, E., Vesala, T., Valentini, R., 2005. Europe-wide reduction in primary productivity caused by the heat and drought in 2003. Nature 437, 529–533, doi: 10.1038/nature03972.

Claussen, M., 1991. Estimation of areally-averaged surface fluxes. Boundary-Layer Meteorology 54, 387–410.

Claussen, M., 1994. On coupling global biome models with climate models. Climate Research 4, 203–221.

Claussen, M., 1997. Modelling bio-geophysical feedback in the African and Indian monsoon region. Climate Dynamics 13, 247–257.

Claussen, M., Brovkin, V., Ganopolski, A., 2001. Biogeophysical versus biogeochemical feedbacks of large-scale land cover change. Geophysical Research Letters 28 (6), 1011–1014.

Claussen, M., Brovkin, V., Ganopolski, A., Kubatzki, C., Petoukhov, V., 1998. Modelling global terrestrial vegetation-climate interaction. Philosophical Transactions of The Royal Society of London B 353, 53–63.

Claussen, M., Brovkin, V., Ganopolski, A., Kubatzki, C., Petoukhov, V., 2003. Climate change in Northern Africa: The past is not the future. Climatic Change 57 (1-2), 99–118.

Claussen, M., Gayler, V., 1997. The greening of the Sahara during the mid-Holocene: results of an interactive atmosphere-biome model. Global Ecology and Biogeography Letters 6, 369–377.

Claussen, M., Kubatzki, C., Brovnik, V., Ganopolski, A., Hoelzmann, P., Pachur, H., 1999. Simulation of an abrupt change in Saharan vegetation in the mid-Holocene. Geophysical Research Letters 24 (14), 2037–2040.

Claussen, M., Lohmann, U., Roeckner, E., Schulzweida, U., 1994. A global data set of land-surface parameters. Tech. Rep. 135, Max-Planck-Institut für Meteorologie, Hamburg.

Claussen, M., Mysak, L., Weaver, A., Crucifix, M., Fichefet, T., Loutre, M.-F., Weber, S., Alcamo, J., Alexeev, V., Berger, A., Calov, R., Ganopolski, A., Goosse, H., Lohmann, G., Lunkeit, F., Mokhov, I., Petoukhov, V., Stone, P., Wang, Z., 2002. Earth system models of intermediate complexity: closing the gap in the spectrum of climate system models. Climate Dynamics 18, 579–586.

Coe, M., Bonan, G., 1997. Feedbacks between climate and surface water in northern Africa during the middle Holocene. Journal of Geophysical Research 102 (D10), 11087–11101.

Cosgrove, B., Barron, E., Pollard, D., 2002. A simple interactive vegetation model coupled

to the GENESIS GCM. Global and Planetary Change 32, 253–278.

Cox, P., Betts, R., Jones, C., Spall, S., Totterdell, I., 2000. Acceleration of global warming due to carbon-cycle feedbacks in a coupled climate model. Nature 408, 184–187.

Cramer, W., Bondeau, A., Woodward, F., I.C., P., Betts, R., Brovkin, V., Cox, P., Fisher, V., Foley, J., Friend, A., Kucharik, C., Lomas, M., Ramankutty, N., Sitch, S., Smith, B., White, A., Young-Molling, C., 2001. Global response of terrestrial ecosystem structure and function to CO_2 and climate change: results from six dynamic global vegetation models. Global Change Biology 7, 357–373.

Cramer, W., Kicklighter, D., Bondeau, A., Moore III, B., Churkina, G., Nemry, B., Ruimy, A., Schloss, A., participants of the Potsdam NPP model intercomparison, 1999. Comparing global models of terrestrial net primary productivity (NPP): overview and key results. Global Change Biology 5 (Suppl. 1), 1–15.

Crowley, T., Baum, S., 1997. Effect of vegetation on an ice-age climate model simulation. Journal of Geophysical Research 102 (D14), 16463–16480.

Crucifix, M., Betts, R., Hewitt, C., 2005. Pre-industrial-potential and Last Glacial Maximum global vegetation simulated with a coupled climate-biosphere model: Diagnosis of bioclimatic relationships. Global and Planetary Change 45, 295–312.

Crucifix, M., Loutre, M., 2002. Transient simulations over the last interglacial period (126 - 115 kyr BP): feedback and forcing analysis. Climate Dynamics 19, 417–433.

De Noblet, N., Prentice, I., Joussaume, S., Texier, D., Botta, A., Haxelteine, A., 1996. Possible role of atmosphere-biosphere interactions in triggering the last glaciation. Geophysical Research Letters 23 (22), 3191–3194.

De Noblet-Ducoudré, N., Claussen, M., Prentice, C., 2000. Mid-Holocene greening of the Sahara: first results of the GAIM 6000 year BP experiment with two asynchronously coupled atmosphere/biome models. Climate Dynamics 16, 643–659.

Delire, C., Foley, J., Thompson, S., 2003. Evaluating the carbon cycle of a coupled atmosphere-biosphere model. Global Biogeochemical Cycles 17 (1), doi: 10.1029/2002GB001870.

Dickinson, R., Henderson-Sellers, A., 1988. Modelling tropical deforestation: A study of GCM land-surface parameterizations. Quarterly Journal of the Royal Meteorological Society 114, 439–462.

Diffenbaugh, N., Sloan, L., 2002. Global climate sensitivity to land surface change: The Mid Holocene revisited. Geophysical Research Letters 29 (10), 114, DOI 10.1029/2002GL014880.

DKRZ, 1993. The ECHAM3 Atmospheric General Circulation Model. Tech. Rep. 6, Deutsches Klimarechenzentrum, Hamburg.

Doherty, R., Kutzbach, J., Foley, J., Pollard, D., 2000. Fully coupled climate/dynamical vegetation model simulations over Northern Africa during the mid-Holocene. Climate Dynamics 16, 561–573.

Douville, H., Royer, J.-F., 1997. Influence of the temperate and boreal forests on the northern hemisphere climate in the Météo-France climate model. Climate Dynamics 13, 57–74.

Dufresne, J.-L., Friedlingstein, P., Berthelot, M., Bopp, L., Ciais, P., Fairhead, L., Le Treut, H., Monfray, P., 2002. On the magnitude of positive feedback between future climate change and the carbon cycle. Geophysical Research Letters 29, doi: 10.1029/2001GL013777.

Eltahir, E., 1996. Role of vegetation in sustaining large-scale atmospheric circulations in the tropics. Journal of Geophysical Research 101 (D2), 4255–4268.

Foley, J., Kutzbach, J., Coe, M., Levis, S., 1994. Feedbacks between climate and boreal

forests during the Holocene epoch. Nature 371, 52–54.

Foley, J., Prentice, I., Ramankutty, N., Levis, S., Pollard, D., Sitch, S., Haxeltine, A., 1996. An integrated biosphere model of land surface processes, terrestrial carbon balance, and vegetation dynamics. Global Biogeochemical Cycles 10 (4), 603–628.

Fraedrich, K., Kleidon, A., Lunkeit, F., 1999. A green planet versus a desert world: estimating the effect of vegetation extremes on the atmosphere. Journal of Climate 12, 3156–3163.

François, L., Delire, C., Warnant, P., Munhoven, G., 1998. Modelling the glacial-interglacial changes in the continental biosphere. Global and Planetary Change 16-17, 37–52.

Friedli, H., Lötscher, H., Oeschger, H., Siegenthaler, U., Stauffer, B., 1986. Ice core record of the $^{13}C/^{12}C$ ratio of atmospheric CO_2 in the past two centuries. Nature 324, 237–238.

Friedlingstein, P., Bopp, L., Ciais, P., Dufresne, J.-L., Fairhead, L., LeTreut, H., Monfray, P., Orr, J., 2001. Positive feedback between future climate change and the carbon cycle. Geophysical Research Letters 28 (8), 1543–1546.

Friedlingstein, P., Cox, P., Betts, R., Bopp, L., Von Bloh, W., Brovkin, V., Cadule, P., Doney, S., Eby, M., Fung, I., Bala, G., John, J., Jones, C., Joos, F., Kato, T., Kawamiya, M., Knorr, W., Lindsay, K., Matthews, H., Raddatz, T., Rayner, P., Reick, C., Roeckner, E., Schnitzler, K.-G., Schnur, R., Strassmann, K., Weaver, A., Yoshikawa, C., Zeng, N. Climate-carbon cycle feedback analysis, results from the C^4MIP model intercomparison. Accepted by Journal of Climate.

Friedlingstein, P., Delire, C., Müller, J., Gérard, J., 1992. The climate induces variation of the continental biosphere: a model simulation of the Last Glacial Maximum. Geophysical Research Letters 19 (9), 897–900.

Friedlingstein, P., Dufresne, J.-L., Cox, P., Rayner, P., 2003. How positive is the feedback between climate change and carbon? Tellus 55B, 692–700.

Fung, I., Doney, S., Lindsay, K., John, J., 2005. Evolution of carbon sinks in a changing climate. Proceedings of the National Academy of Sciences 102 (32), 11201–11206.

Gallimore, R., Jacob, R., Kutzbach, J., 2005. Coupled atmosphere-ocean-vegetation simulations for modern and mid-Holocene climates: role of extratropical vegetation cover feedbacks. Climate Dynamics 25, 755–776, doi: 10.1007/s00382-005-0054-z.

Gallimore, R., Kutzbach, J., 1996. Role of orbitally induced changes in tundra area in the onset of glaciation. Nature 381, 503–505.

Ganopolski, A., Kubatzki, C., Claussen, M., Brovkin, V., Petoukhov, V., 1998. The influence of vgetation-atmosphere-ocean interactions on climate during the mid-holocene. Science 280, 1916–1919.

Gerber, S., Joos, F., Prentice, I., 2004. Sensitivity of a dynamic global vegetation model to climate and atmospheric CO_2. Global Change Biology 10, 1223–1239, doi: 10.1111/j.1365-2486.2004.00807.x.

Goudriaan, J., Ketner, P., 1984. A simulation study for the global carbon cycle, including man's impact on the biosphere. Climatic change 6, 167–192.

Govindasamy, B., Thompson, S., Mirin, A., Wickett, M., Caldeira, K., 2005. Increase of carbon cycle feedback with climate sensitivity: results from a coupled climate and carbon cycle model. Tellus 57B, 153–163.

Greve, R., 1997. Application of a polythermal three-dimensional ice sheet model to the greenland ice sheet: Response to steady-state and transient climate scenarios. Journal of Climate 10 (5), 901–918.

Grichuk, V., 1992. Vegetation during the last interglacial. In: Frenzel, B., Pécsi, M., Velichko, A. (Eds.), Atlas of paleoclimates and paleoenvironments of the Northern

Hemisphere. Gustav Fischer Verlag, Stuttgart.

Gu, L., Baldocchi, D., Wofsy, S., Munger, W., Michalsky, J., Urbanski, S., Boden, T., 2003. Response of a deciduous forest to the Mount Pinatubo eruption: enhanced photosynthesis. Science 299, 2035–2038.

Hagemann, S., Botzet, M., Dümenil, L., Machenhauer, B., 1999. Derivation of global gcm boundary conditions from 1 km land use satellite data. Tech. Rep. 289, Max-Planck-Institut für Meteorologie, Hamburg.

Harrison, S., Jolly, D., Laarif, F., Abe-Ouchi, A., Dong, B., Herterich, K., Hewitt, C., Joussaume, S., Kutzbach, J., Mitchell, J., De Noblet, N., Valdes, P., 1998. Intercomparison of simulated global vegetation distributions in response to 6 kyr BP orbital forcing. Journal of Climate 11, 2721–2742.

Harrison, S., Kutzbach, J., Prentice, I., Behling, P., Sykes, M., 1995. The response of northern hemisphere extratropical climate and vegetation to orbitally induced changes in insolation during the last interglacial. Quaternary Research 43, 174–184.

Harrison, S., Prentice, C., 2003. Climate and CO_2 controls on global vegetation distribution at the Last Glacial Maximum: analysis based on paleovegetation data, biome modelling and paleoclimate simulations. Global Change Biology 9, 983–1004.

Henderson-Sellers, A., McGuffie, K., 1995. Global climate models and 'dynamic' vegetation changes. Global Change Biology 1, 63–75.

Hilbert, D., Roulet, N., Moore, T., 2000. Modelling and analysis of peatlands as dynamical systems. Journal of Ecology 88, 230–242.

Hoelzmann, P., Jolly, D., Harrison, S., Laarif, F., Bonnefille, R., Pachur, H.-J., 1998. Mid-Holocene land-surface conditions in northern Africa and the Arabian peninsula: A data set for the analysis of biogephysical feedbacks in the climate system. Global Biogeochemical Cycles 12 (1), 35–51.

Houghton, J., Ding, Y., Griggs, D., Noguer, M., Van der Linden, P., Dai, X., Maskell, K., Johnson, C., 2001. Climate Change 2001: the scientific basis. Contribution of Working Group I to the Third Assessment Report of the IPCC. Cambridge University Press, Cambridge, United Kingdom.

Houghton, R., Hackler, J., 2002. Carbon flux to the atmosphere from land-use changes. In: Trends: A compendium of data on global change. Carbon Dioxide Information Analysis Center, Oak Ridge National Laboratory, U.S. Department of Energy, Oak Ridge, USA.

Indermühle, A., Stocker, T., Joos, F., Fischer, H., Smith, H., Wahlen, M., Deck, B., Mastroianni, D., Tschumi, J., Blunier, T., Meyer, R., Stauffer, B., 1999. Holocene carbon-cycle dynamics based on CO_2 trapped in ice at Taylor Dome, Antarctica. Nature 398, 121–126.

Joos, F., Gerber, S., Prentice, I., Otto-Bliesner, B., Valdes, P., 2004. Transient simulations of Holocene atmospheric carbon dioxide and terrestrial carbon since the Last Glacial Maximum. Global Biogeochemical Cycles 18, doi: 10.1029/2003GB002156.

Joos, F., Prentice, I., Sitch, S., Meyer, R., Hooss, G., Plattner, G.-K., Gerber, S., Hasselmann, K., 2001. Global warming feedbacks on terrestrial carbon uptake under the Intergovernmental Panel on Climate Change (IPCC) emission scenarios. Global Biogeochemical Cycles 15 (4), 891–907.

Kanamitsu, M., Ebisuzaki, W., Woollen, J., Yang, S.-K., Hnilo, J., Fiorino, M., Potter, G., 2002. NCEP-DOE AMIP-II Reanalysis (R-2). Bulletin of the American Meteorological Society 83, 1631–1643, doi: 10.1175/BAMS-83-11-1631.

Kaplan, J., Bigelow, N., Prentice, I., Harisson, S., Bartlein, P., Christensen, T., Cramer, W., Matveyeva, N., McGuire, A., Murray, D., Razzhivin, V., Smith, B., Walker, D., Anderson, P., Andreev, A., Brubaker, L., Edwards, M., Lozhkin, A., 2003. Climate change and Arctic ecosystems: 2. Modelling, paleodata-model comparisons, and future

projections. Journal of Geophysical Research 108 (D19), doi: 10.1029/2002JD002559.

Kaplan, J., Prentice, I., Knorr, W., Valdes, P., 2002. Modeling the dynamics of terrestrial carbon storage since the Last Glacial Maximum. Geophysical Research Letters 29 (22), 2074, doi: 10.1029/2002GL015230.

Keeling, C., 1960. The concentration and isotopic abundance of carbon dioxide in the atmosphere. Tellus 12, 200–203.

Kleidon, A., Fraedrich, K., Heimann, M., 2000. A green planet versus a desert world: estimating the maximum effect of vegetation on the land surface climate. Climatic Change 44, 471–493.

Klinger, L., Taylor, J., Franzen, L., 1996. The potential role of peatland dynamics in ice-age initiation. Quaternary Research 45, 89–92.

Knorr, W., Prentice, I., House, J., Holland, E., 2005. Long-term sensitivity of soil carbon turnover to warming. Nature 433, 298–301.

Köhler, P., Fischer, H., 2004. Simulating changes in the terrestrial biosphere during the last glacial/interglacial transition. Global and Planetary Change 43, 33–55.

Köppen, W., 1931. Grundriss der Klimakunde. Walter de Gruyter & Co, Berlin/Leipzig, Germany.

Krinner, G., Viovy, N., de Noblet-Ducoudré, N., Ogée, J., Polcher, J., Friedlingstein, P., Ciais, P., Sitch, S., Prentice, I., 2005. A dynamic global vegetation model for studies of the coupled atmosphere-biosphere system. Global Biogeochemical Cycles 19, gB1015, doi: 10.1029/2003GB002199.

Kubatzki, C., Claussen, M., 1998. Simulation of the global bio-geophysical interactions during the Last Glacial Maximum. Climate Dynamics 14, 461–471.

Kubatzki, C., Montoya, M., Rahmstorf, S., Ganopolski, A., Claussen, M., 2000. Comparison of the last interglacial climate simulated by a coupled global model of intermediate complexity and an AOGCM. Climate Dynamics 16, 799–814.

Kukla, G., Robinson, D., 1980. Annual cycle of surface albedo. Monthly Weather Review 108, 56–68.

Leemans, R., 1991. Sensitivity analysis of a forest succession model. Ecological Modelling 53, 247–262.

Leffelaar, P., 1999. Basic elements of dynamic simulation. In: Leffelaar, P. (Ed.), On systems analysis and simulation of ecological processes with examples in CSMP, FST and FORTRAN. Kluwer Academic Publishers, Dordrecht, The Netherlands.

Levis, S., Foley, J., Pollard, D., 1999. CO_2, climate, and vegetation feedbacks at the Last Glacial Maximum. Journal of Geophysical Research - Atmosphere D24, 31191–31198.

Levis, S., Foley, J., Pollard, D., 2000. Large-scale vegetation feedbacks on a doubled CO_2 climate. Journal of Climate 13 (7), 1313–1325.

Lorenz, S., Lohmann, G., 2004. Acceleration technique for Milankovitch type forcing in a coupled atmosphere-ocean circulation model: method and application for the Holocene. Climate Dynamics 23, 727–743, doi: 10.1007/s00382-0040469-y.

Lovelock, J., 1979. Gaia - a new look at life on earth. Oxford University Press, Oxford.

Lüdeke, M., Badeck, F.-W., Otto, R., Häger, C., Dönges, S., Kindermann, J., Würth, G., Lang, T., Jäkel, U., Klaudius, A., Ramge, P., Habermehl, S., Kohlmaier, G., 1994. The Frankfurt Biosphere Model: a global process-oriented model of seasonal and long-term CO_2 exchange between terrestrial ecosystems and the atmosphere. i. Model description and illustrative results for cold deciduous and boreal forests. Climate Research 4, 143–166.

Lunt, D., de Noblet-Ducoudré, N., Charbit, S., 2004. Effects of a melted Greenland ice sheet on climate, vegetation, and the cryosphere. Climate Dynamics 23, 679–694, doi:

10.1007/s00382-004-0463-4.

Lynch, A., Rivers, A., Bartlein, P., 2003. An assessment of the influence of land cover uncertainties on the simulation of global climate in the early Holocene. Climate Dynamics 21, 243–256.

Maier-Reimer, E., 1993. Geochemical cycles in an ocean general circulation model. preindustrial tracer distributions. Global Biogeochemical Cycles 7 (3), 645–677.

Maier-Reimer, E., Mikolajewicz, U., Hasselmann, K., 1993. Mean circulation of the Hamburg LSG OGCM and its sensitivity to the thermohaline forcing. Journal of Physical Oceanography 23, 731–757.

Marland, G., Boden, T., Andres, R., 2005. Global, regional, and national fossil fuel CO_2 emissions. In: Trends: A compendium of data on global change. Carbon Dioxide Information Analysis Center, Oak Ridge National Laboratory, U.S. Department of Energy, Oak Ridge, USA.

Martin, J., 1990. Glacial-interglacial CO_2 change: the iron hypothesis. Paleoceanography 5 (1), 1–13.

Mikolajewicz, U., Gröger, M., Maier-Reimer, E., Schurgers, G., Vizcaíno, M., Winguth, A. Long-term effects of anthropogenic CO_2 emissions simulated with a complex earth system model. Submitted to Climate Dynamics.

Milly, P., Shmakin, A., 2002. Global modeling of land water and energy balances. part I: The Land Dynamics (LaD) model. Journal of Hydrometeorology 3, 283–299.

Mooney, H., Roy, J., Saugier, B., 2001. Terrestrial Global Productivity: Past, Present and Future. Academic Press, San Diego.

Munhoven, G., 2002. Glacial-interglacial changes of continental weathering: estimates of the related CO_2 and HCO_3^- flux variations and their uncertainties. Global and Planetary Change 33, 155–176.

Nakićenović, N., Alcamo, J., Davis, G., De Vries, B., Fenhann, J., Gaffin, S., Gregory, K., Grübler, A., Jung, T., Kram, T., Lebre La Rovere, E., Michaelis, L., Mori, S., Morita, T., Pepper, W., Pitcher, H., Price, L., Riahi, K., Roehrl, A., Rogner, H.-H., Sankovski, A., Schlesinger, M., Shukla, P., Smith, S., Swart, R., Van Rooijen, S., Victor, N., Dadi, Z., 2000. Special Report on Emissions Scenarios. A special report of Working Group III of the Intergovernmental Panel on Climate Change. Cambridge University Press, Cambridge, United Kingdom.

Otterman, J., Chou, M.-D., Arking, A., 1984. Effects of nontropical forest cover on climate. Journal of Climate and Applied Meteorology 23, 762–767.

Otto, D., Rasse, D., Kaplan, J., Warnant, P., Franois, L., 2002. Biospheric carbon stocks reconstructed at the Last Glacial Maximum: comparison between general circulation models using prescribed and computed sea surface temperatures. Global and Planetary Change 33, 117–138.

Petit, J., Jouzel, J., Raynaud, D., Barkov, N., Barnola, J.-M., Basile, I., Bender, M., Chappelaz, J., Davis, M., Delaygue, G., Delmotte, M., Kotlyakov, V., Legrand, M., Lipenkov, V., Lorius, C., Pépin, L., Ritz, C., Saltzman, E., Stievenard, M., 1999. Climate and atmospheric history of the past 420,000 years from the Vostok ice core, Antarctica. Nature 399, 429–436.

Petoukhov, V., Claussen, M., Berger, A., Crucifix, M., Eby, M., Eliseev, A., Fichefet, T., Ganopolski, A., Goosse, H., Kamenkovich, I., Mokhov, I., Montoya, M., Mysak, L., Sokolov, A., Stone, P., Wang, Z., Weaver, A., 2005. EMIC Intercomparison Project (EMIC-CO_2): comparative analysis of EMIC simulations of climate, and of equilibrium and transient responses to atmospheric CO_2 doubling. Climate Dynamics 25, 363–385, doi: 10.100/s00382-005-0042-3.

Prentice, I., Cramer, W., Harrison, S., Leemans, R., Monserud, R., Solomon, A., 1992.

A global biome model based on plant physiology and dominance, soil properties and climate. Journal of Biogeography 19, 117–134.

Prentice, I., Jolly, D., BIOME 6000 participants, 2000. Mid-Holocene and glacial-maximum vegetation geography of the northern continents and Africa. Journal of Biogeography 27, 507–519.

Prentice, I., Leemans, R., 1990. Pattern and process and the dynamics of forest structure: a simulation approach. Journal of Ecology 78, 340–355.

Prentice, I., Sykes, M., Cramer, W., 1993a. A simulation model for the transient effects of climate change on forest landscapes. Ecological Modelling 65, 51–70.

Prentice, I., Sykes, M., Lautenschlager, M., Harrison, S., Denissenko, O., Bartlein, P., 1993b. Modelling global vegetation patterns and terrestrial carbon storage at the Last Glacial Maximum. Global Ecology and Biogeography Letters 3, 67–76.

Prentice, I., Webb III, T., 1998. BIOME 6000: reconstructing global mid-Holocene vegetation patterns from palaeoecological records. Journal of Biogeography 25, 997–1005.

Raddatz, T., Reick, C., Knorr, W., Kattge, J., Roeckner, E., Schnur, E., Schnitzler, K.-G., Wetzel, P., Jungclaus, J. Will the tropical land biosphere dominate the climate-carbon cycle feedback during the 21st century? Submitted to Climate Dynamics.

Ray, N., Adams, J., 2001. A GIS-based vegetation map of the world at the last glacial maximum (25,000-15,000 BP). Internet Archaeology 11.

Reichstein, M., Subke, J.-A., Angeli, A., Tenhunen, J., 2005. Does the temperature sensitivity of deomposition of soil organic matter depend upon water content, soil horizon, or incubation time? Global Change Biology 11, 1754–1767, doi: 10.1111/j.1365-2486.2005.01010.x.

Roderick, M., Farquhar, G., Berry, S., Noble, I., 2001. On the direct effect of clouds and atmospheric particles on the productivity and structure of vegetation. Oecologia 129, 21–30, doi: 10.1007/s004420100760.

Ruddiman, W., 2003. The anthropogenic greenhouse era began thousands of years ago. Climatic Change 61, 261–293.

Sausen, R., Voss, R., 1996. Techniques for asynchronous and periodically synchronous coupling of atmosphere and ocean models. part I: general strategy and application to the cyclo-stationary case. Climate Dynamics 12, 313–323.

Schlesinger, W., 1991. Biogeochemistry: an analysis of global change. Academic Press, San Diego.

Scholze, M., Kaplan, J., Knorr, W., Heimann, M., 2003. Climate and interannual variability of the atmosphere-biosphere $^{13}CO_2$ flux. Geophysical Research Letters 30, 1097, doi:10.1029/2002GL015631.

Shukla, J., Nobre, C., Sellers, P., 1990. Amazon deforestation and climate change. Science 247, 1322–1325.

Sitch, S., Brovkin, V., Von Bloh, W., Van Vuuren, D., Eickhout, B., Ganopolski, A., 2005. Impacts of future land cover changes on atmospheric CO_2 and climate. Global Biogeochemical Cycles 19, doi: 10.1029/2004GB002311.

Sitch, S., Smith, B., Prentice, I., Arneth, A., Bondeau, A., Cramer, W., Kaplan, J., Levis, S., Lucht, W., Sykes, M., Thonicke, K., Venevsky, S., 2003. Evaluation of ecosystem dynamics, plant geography and terrestrial carbon cycling in the LPJ Dynamic Global Vegetation Model. Global Change Biology 9 (2), 161–185.

Tarasov, L., Peltier, W., 2003. Greenland glacial history, borehole constraints, and Eemian extent. Journal of Geophysical Research 108 (B3), 2143, doi: 10.1029/2001JB001731.

Tarasov, P., Granoszweski, W., Bezrukova, E., Brewer, S., Nita, M., Abzaeva, A., Oberhänsli, H., 2005. Quantitative reconstruction of the last interglacial vegetation

and climate based on pollen record from Lake Baikal, Russia. Climate Dynamics 25, 625–637, doi: 10.1007/s00382-005-0045-0.

TEMPO (Kutzbach, J., Bartlein, P., Foley, J., Harrison, S., Hostetler, S., Liu, Z., Prentice, I., Webb III, T.), 1996. Potential role of vegetation feedback in the climate sensitivity of high-latitude regions: A case study at 6000 years B.P. Global Biogeochemical Cycles 10 (4), 427–436.

Texier, D., de Noblet, N., Harrison, S., Haxeltine, A., Jolly, D., Joussaume, S., Laarif, F., Prentice, I., Tarasov, P., 1997. Quantifying the role of biosphere-atmosphere feedbacks in climate change: coupled model simulations for 6000 years BP and comparison with paleodata for northern Eurasia and northern Africa. Climate Dynamics 13, 865–882.

Thomas, G., Rowntree, P., 1992. The boreal forests and climate. Quarterly Journal of the Royal Meteorological Society 118, 469–497.

Voss, R., Mikolajewicz, U., 2001. Long-term climate changes due to increased CO_2 concentration in the coupled atmosphere-ocean general circulation model ECHAM3/LSG. Climate Dynamics 17, 45–60.

Wang, G., Eltahir, E., 2000. Biosphere-atmosphere interactions over west africa ii: Multiple climate equilibria. Quarterly Journal of the Royal Meteorological Society 126, 1261–1280.

Watson, A., Lovelock, J., 1983. Biological homeostasis of the global environment: the parable of daisyworld. Tellus 35B, 284–289.

WBGU, 1988. Die Anrechnung biolischer Quellen und Senken in Kyoto-Protokoll: Fortschritt oder Rückschlag für den globalen Umweltschutz, Sondergutachten 1988.

Wilson, M., Henderson-Sellers, A., 1985. A global archive of land cover and soils data for use in general circulation climate models. Journal of Climatology 5, 119–143.

Winguth, A., Mikolajewicz, U., Gröger, M., Maier-Reimer, E., Schurgers, G., Vizcaíno, M., 2005. CO_2 uptake of the marine biosphere: Feedbacks between the carbon cycle and climate change using a dynamic earth system model. Geophysical Research Letters 32, doi: 10.1029/2005GL023681.

Wyputta, U., McAvaney, B., 2001. Influence of vegetation changes during the Last Glacial Maximum using the BMRC atmospheric general circulation model. Climate Dynamics 17, 923–932.

Yoshimori, M., Reader, M., Weaver, A., McFarlane, N., 2002. On the causes of glacial inception at 116 kaBP. Climate Dynamics 18, 383–402.

Zeng, N., 2003. Glacial-interglacial atmospheric CO_2 change - the glacial burial hypothesis. Advances in Atmospheric Sciences 20 (5), 677–693.

Appendix A

Experiments

Table A.1: *Experiments used in this thesis*

experiment	chapter	time	years	components[a]		CO$_2$	description
control runs							
CTL, CTL$^+$	2, 4	1–10000	10 000	AOB	T	prognostic	
ACTL$^+$	2, 4	1–2000	2 000	AOB	T	prognostic	reduced length of asynchronous periods compared to CTL$^+$
ACTL$^-$	2, 4	1–2000	2 000	AOB	T	prognostic	
CTRL	7	1–2250	2 250	AOB	T I	prognostic	
sensitivity experiments							
–	2	1–2000	2 000		T	280 ppm	temperature sensitivity experiments (global anomalies applied of -5 K, -2 K, 0 K, +2 K, +5 K) with the old parametrization and hydrology, forced with 20 years of NCEP reanalysis data (1980–1999, Kanamitsu et al., 2002)
–	2	1–2000	2 000		T	5 levels	CO$_2$ sensitivity experiments (prescribed concentration of 200 ppm, 280 ppm, 360 ppm, 520 pm, 840 ppm) with the old parametrization and hydrology, forced with 20 years of NCEP reanalysis data (1980–1999, Kanamitsu et al., 2002)

[a] AOB atmosphere–ocean–ocean biogeochemistry; T terrestrial biosphere; I ice sheets

experiment	chapter	time	years	components[a]	CO$_2$	description
–	2	1–2000	2 000	T	280 ppm	temperature sensitivity experiments (global anomalies applied of -5 K, -2 K, 0 K, +2 K, +5 K) with the new parametrization and hydrology, forced with 20 years of the CTL experiment
–	2	1–2000	2 000	T	5 levels	CO$_2$ sensitivity experiments (prescribed concentration of 200 ppm, 280 ppm, 360 ppm, 520 pm, 840 ppm) with the new parametrization and hydrology, forced with 20 years of the CTL experiment
–	3	1–15000	15 000	T	2 levels	experiments to determine timescales, 1–5000 spinup phase with a CO$_2$ concentration of 280 ppm and climate from a control run, 5001–10000 reaction phase with CO$_2$ concentration of 840 ppm and/or climate from a 3×CO$_2$ experiment (Winguth et al., 2005), 10001–15000 reaction phase with CO$_2$ concentration of 280 ppm and climate from a control run
paleoclimate experiments						
EEM, EEM$^+$	4, 5, 6	128–113 ky B.P.	15 000	AOB T	prognostic	insolation forcing 8 times accelerated
AEEM$^+$	4, 6	128–113 ky B.P.	1 875	AOB T	prognostic	insolation forcing 8 times accelerated
AEEM$^-$	4, 6	128–113 ky B.P.	1 875	AOB T	prognostic	insolation forcing 8 times accelerated, prescribed land surface
HOL	5, 6	9–0 ky B.P.	9 000	AOB T	prognostic	

[a] AOB atmosphere–ocean–ocean biogeochemistry; T terrestrial biosphere; I ice sheets

experiment	chapter	time	years	components[a]	CO_2	description
EEM_tem	5	128–113 ky B.P.	15 000	T	as CTL	forced with temperatures of the EEM experiment and other parameters of the CTRL experiment
EEM_hyd	5	128–113 ky B.P.	15 000	T	as CTL	forced with hydrological parameters of the EEM experiment and other parameters of the CTRL experiment
EEM_rad	5	128–113 ky B.P.	15 000	T	as CTL	forced with radiation of the EEM experiment and other parameters of the CTRL experiment
EEM_co2	5	128–113 ky B.P.	15 000	T	as EEM	forced with CO_2 concentration of the EEM experiment and other parameters of the CTRL experiment
HOL_tem	5	9–0 ky B.P.	9 000	T	as CTL	forced with temperatures of the HOL experiment and other parameters of the CTRL experiment
HOL_hyd	5	9–0 ky B.P.	9 000	T	as CTL	forced with hydrological parameters of the HOL experiment and other parameters of the CTRL experiment
HOL_rad	5	9–0 ky B.P.	9 000	T	as CTL	forced with radiation of the HOL experiment and other parameters of the CTRL experiment
HOL_co2	5	9–0 ky B.P.	9 000	T	as HOL	forced with CO_2 concentration of the HOL experiment and other parameters of the CTRL experiment
RAEEM[+]	6	128–113 ky B.P.	15 000	T	280 ppm	unaccelerated repetition of AEEM[+] with the vegetation model only

[a] AOB atmosphere–ocean–ocean biogeochemistry; T terrestrial biosphere; I ice sheets

experiment	chapter	time	years	components[a]	CO$_2$	description
RAEEM$^-$	6	128–113 ky B.P.	15 000	T	280 ppm	unaccelerated repetition of AEEM$^-$ with the vegetation model only
IPCC SRES scenario experiments						
HIST	7	1750–2000	250	AOB T I	prognostic	reconstruction of historical emissions (5 ensembles)
B1	7	2001–3000	1 000	AOB T I	prognostic	IPCC SRES emission scenario B1 with exponential decay after 2100 (3 ensembles)
A1B	7	2001–3000	1 000	AOB T I	prognostic	IPCC SRES emission scenario A1B with exponential decay after 2100 (5 ensembles)
A2	7	2001–3000	1 000	AOB T I	prognostic	IPCC SRES emission scenario A2 with exponential decay after 2100 (3 ensembles)
B1-280	7	2001–3000	1 000	AOB T I	prognostic	IPCC SRES emission scenario B1 with exponential decay after 2100, radiative forcing calculated with 280 ppm CO$_2$
A1B-280	7	2001–3000	1 000	AOB T I	prognostic	IPCC SRES emission scenario A1B with exponential decay after 2100, radiative forcing calculated with 280 ppm CO$_2$
A2-280	7	2001–3000	1 000	AOB T I	prognostic	IPCC SRES emission scenario A2 with exponential decay after 2100, radiative forcing calculated with 280 ppm CO$_2$
A2-noland	7	2001–3000	1 000	AOB T I	prognostic	IPCC SRES emission scenario A2 with exponential decay after 2100, no effect of land surface changes or ice sheet changes

[a] AOB atmosphere–ocean–ocean biogeochemistry; T terrestrial biosphere; I ice sheets

Acknowledgements

Three and a half years of work resulted in the thesis eventually. This would not have been possible without the help of many.

I owe a big Thank You to Uwe, for the cooperation, his help, and his willingness to learn about terrestrial vegetation. And besides that for his desire to construct an earth system model, and the curiosity with which he did this. Thanks as well to Matthias and Miren, for all the answers to all the questions, and for the great cooperation, and to Arne and Ernst for their help, explanations and patience.

Thanks to Professor Grassl, for his support and his questions, to Martin Claussen, Thomas Raddatz, and others for their comments on manuscripts of parts of this thesis and for their discussions about the terrestrial biosphere, and to the colleagues of the MPI and the IMPRS for the great working environment and all help.

And many thanks to my friends and family, for the support, and for all good moments.

Beginn einer neuen Veröffentlichungsreihe des MPIM, welche die vorherigen Reihen "Reports" und "Examensarbeiten" weiterführt:

„Berichte zur Erdsystemforschung" , „*Reports on Earth System Science*", ISSN 1614-1199
Sie enthält wissenschaftliche und technische Beiträge, inklusive Dissertationen.

Berichte zur Erdsystemforschung Nr.14 August 2005	**The** HAM**burg** O**cean** C**arbon** C**ycle Model HAMOCC5.1 - Technical Description Release 1.1** Ernst Maier-Reimer, Iris Kriest, Joachim Segschneider, Patrick Wetzel
Berichte zur Erdsystemforschung Nr.15 Juli 2005	**Long-range Atmospheric Transport and Total Environmental Fate of Persistent Organic Pollutants - A Study using a General Circulation Model** Semeena Valiyaveetil Shamsudheen
Berichte zur Erdsystemforschung Nr.16 Oktober 2005	**Aerosol Indirect Effect in the Thermal Spectral Range as Seen from Satellites** Abhay Devasthale
Berichte zur Erdsystemforschung Nr.17 Dezember 2005	**Interactions between Climate and Land Cover Changes** Xuefeng Cui
Berichte zur Erdsystemforschung Nr.18 Januar 2006	**Rauchpartikel in der Atmosphäre: Modellstudien am Beispiel indonesischer Brände** Bärbel Langmann
Berichte zur Erdsystemforschung Nr.19 Februar 2006	**DMS cycle in the ocean-atmosphere system and its response to anthropogenic perturbations** Silvia Kloster
Berichte zur Erdsystemforschung Nr.20 Februar 2006	**Held-Suarez Test with ECHAM5** Hui Wan, Marco A. Giorgetta, Luca Bonaventura
Berichte zur Erdsystemforschung Nr.21 Februar 2006	**Assessing the Agricultural System and the Carbon Cycle under Climate Change in Europe using a Dynamic Global Vegetation Model** Luca Criscuolo
Berichte zur Erdsystemforschung Nr.22 März 2006	**More accurate areal preciption over land and sea, APOLAS Abschlussbericht** K. Bumke, M. Clemens, H. Graßl, S. Pang, G. Peters, J.E.E. Seltmann, T. Siebenborn, A. Wagner
Berichte zur Erdsystemforschung Nr.23 März 2006	**Modeling cold cloud processes with the regional climate model REMO** Susanne Pfeifer
Berichte zur Erdsystemforschung Nr.24 Mai 2006	**Regional Modeling of Inorganic and Organic Aerosol Distribution and Climate Impact over Europe** Elina Marmer
Berichte zur Erdsystemforschung Nr.25 Mai 2006	**Proceedings of the 2nd HyCARE meeting, Laxenburg, Austria, 19-20 Dec 2005** Edited by Martin G. Schultz and Malte Schwoon
Berichte zur Erdsystemforschung Nr.26 Juni 2006	**The global agricultural land-use model KLUM – A coupling tool for integrated assessment** Kerstin Ellen Ronneberger